

CHAPTER 5

STATIC AND FATIGUE DESIGN

Steven M. Tipton, Ph.D., P.E.

*Associate Professor of Mechanical Engineering
University of Tulsa
Tulsa, Okla.*

<p>SYMBOLS 5.1</p> <p>NOTATIONS 5.2</p> <p>5.1 INTRODUCTION 5.3</p> <p>5.2 ESTIMATION OF STRESSES AND STRAINS IN ENGINEERING COMPONENTS 5.4</p> <p style="padding-left: 20px;">5.2.1 Definition of Stress and Strain 5.4</p> <p style="padding-left: 20px;">5.2.2 Experimental 5.9</p> <p style="padding-left: 20px;">5.2.3 Strength of Materials 5.11</p> <p style="padding-left: 20px;">5.2.4 Elastic Stress-Concentration Factors 5.11</p> <p style="padding-left: 20px;">5.2.5 Finite-Element Analysis 5.13</p> <p>5.3 STRUCTURAL INTEGRITY DESIGN PHILOSOPHIES 5.14</p> <p style="padding-left: 20px;">5.3.1 Static Loading 5.15</p> <p style="padding-left: 20px;">5.3.2 Fatigue Loading 5.16</p> <p>5.4 STATIC STRENGTH ANALYSIS 5.18</p> <p style="padding-left: 20px;">5.4.1 Monotonic Tensile Data 5.19</p>	<p style="padding-left: 20px;">5.4.2 Multiaxial Yielding Theories (Ductile Materials) 5.20</p> <p style="padding-left: 20px;">5.4.3 Multiaxial Failure Theories (Brittle Materials) 5.21</p> <p style="padding-left: 20px;">5.4.4 Summary Design Algorithm 5.23</p> <p>5.5 FATIGUE STRENGTH ANALYSIS 5.24</p> <p style="padding-left: 20px;">5.5.1 Stress-Life Approaches (Constant-Amplitude Loading) 5.25</p> <p style="padding-left: 20px;">5.5.2 Strain-Life Approaches (Constant-Amplitude Loading) 5.37</p> <p style="padding-left: 20px;">5.5.3 Variable-Amplitude Loading 5.52</p> <p>5.6 DAMAGE-TOLERANT DESIGN 5.58</p> <p style="padding-left: 20px;">5.6.1 Stress-Intensity Factor 5.58</p> <p style="padding-left: 20px;">5.6.2 Static Loading 5.59</p> <p style="padding-left: 20px;">5.6.3 Fatigue Loading 5.60</p> <p>5.7 MULTIAXIAL FATIGUE LOADING 5.62</p> <p style="padding-left: 20px;">5.7.1 Proportional Loading 5.62</p> <p style="padding-left: 20px;">5.7.2 Nonproportional Loading 5.65</p>
---	---

SYMBOLS

<p>α = “characteristic length” (empirical curve-fit parameter)</p> <p>a = crack length</p> <p>a_f = final crack length</p> <p>a_i = initial crack length</p> <p>A = cross-sectional area</p> <p>A_f = Forman coefficient</p> <p>A_p = Paris coefficient</p> <p>A_w = Walker coefficient</p> <p>b = fatigue strength exponent</p> <p>b' = baseline fatigue exponent</p> <p>c = fatigue ductility exponent</p> <p>$C = 2\tau_{xy,a}/\sigma_{x,a}$ (during axial-torsional fatigue loading)</p> <p>C' = baseline fatigue coefficient</p>	<p>CM = Coulomb Mohr Theory</p> <p>d = diameter of tensile test specimen gauge section</p> <p>DAM_i = cumulative fatigue damage for a particular (i)th cycle</p> <p>Δ = range of (e.g., stress, strain, etc.) = maximum – minimum</p> <p>e = nominal axial strain</p> <p>e_{offset} = offset plastic strain at yield</p> <p>e_u = engineering strain at ultimate tensile strength</p> <p>E = modulus of elasticity</p> <p>E_c = Mohr’s circle center</p> <p>ϵ = normal strain</p> <p>ϵ_a = normal strain amplitude</p>
---	---

ϵ_f = true fracture ductility	S = stress amplitude during a fatigue test
ϵ'_f = fatigue ductility coefficient	S_e = endurance limit
ϵ_u = true strain at ultimate tensile strength	$S_{eq,a}$ = equivalent stress amplitude (multiaxial to uniaxial)
FS = factor of safety	$S_{eq,m}$ = equivalent mean stress (multiaxial to uniaxial)
G = elastic shear modulus	S_{nom} = nominal stress
γ = shear strain	$S_u = S_{ut}$ = ultimate tensile strength
K = monotonic strength coefficient	S_{uc} = ultimate compressive strength
K = stress intensity factor	S_y = yield strength
K' = cyclic strength coefficient	SALT = equivalent stress amplitude (based on Tresca for axial-torsional loading)
K_c = fracture toughness	SEQA = equivalent stress amplitude (based on von Mises for axial-torsional loading)
K_f = fatigue notch factor	σ = normal stress
K_{fc} = plane-strain fracture toughness	σ_a = normal stress amplitude
K_t = elastic stress-concentration factor	σ_{eq} = equivalent axial stress
MM = modified Mohr Theory	σ_f = true fracture strength
MN = maximum normal stress theory	σ'_f = fatigue strength coefficient
n = monotonic strain-hardening exponent	σ_m = mean stress during a fatigue cycle
n' = cyclic strain-hardening exponent	σ_{norm} = normal stress acting on plane of maximum shear stress
n_f = Forman exponent	σ_{notch} = elastically calculated notch stress
n_p = Paris exponent	σ_A = maximum principal stress
n_w and m_w = Walker exponents	σ_B = minimum principal stress
N = number of cycles to failure in a fatigue test	σ_u = true ultimate tensile strength
N_T = transition fatigue life	t = thickness of fracture mechanics specimen
P = axial load	τ = shear stress
ϕ = phase angle between σ_x and τ_{xy} stresses (during axial-torsional fatigue loading)	τ_{max} = maximum shear stress
r = notch root radius	θ_σ = orientation of maximum principal stress
R = cyclic load ratio (minimum load over maximum load)	θ_τ = orientation of maximum shear stress
R = Mohr's circle radius	ν = Poisson's ratio
RA = reduction in area	

NOTATIONS

1, 2, 3 = subscripts designating principal stress I, II, III = subscripts denoting crack loading mode

a_{eff} = subscript denoting effective stress amplitude (mean stress to fully reversed)	o = subscript referring to original dimensions of a tension test specimen
f = subscript referring to final dimensions of a tension test specimen	Tr = subscript referring to Tresca criterion
bend = subscript denoting bending loading	vM = subscript referring to von Mises criterion
max = subscript denotes maximum or peak during fatigue cycle	x, y, z = orthogonal coordinate axes labels
min = subscript denoting minimum or valley during fatigue cycle	

5.1 INTRODUCTION

The design of a component implies a design framework and a design process. A typical design framework requires consideration of the following factors: component function and performance, producibility and cost, safety, reliability, packaging, and operability and maintainability.

The designer should assess the consequences of failure and the normal and abnormal conditions, loads, and environments to which the component may be subjected during its operating life. On the basis of the requirements specified in the design framework, a design process is established which may include the following elements: conceptual design and synthesis, analysis and gathering of relevant data, optimization, design and test of prototypes, further optimization and revision, final design, and monitoring of component performance in the field.

Requirements for a successful design include consideration of data on the past performance of similar components, a good definition of the mechanical and thermal loads (monotonic and cyclic), a definition of the behavior of candidate materials as a function of temperature (with and without stress raisers), load and corrosive environments, a definition of the residual stresses and imperfections owing to processing, and an appreciation of the data which may be missing in the trade-offs among parameters such as cost, safety, and reliability. Designs are typically analyzed to examine the potential for fracture, excessive deformation (under load, creep), wear, corrosion, buckling, and jamming (due to deformation, thermal expansion, and wear). These may be caused by steady, cyclic, or shock loads, and temperatures under a number of environmental conditions and as a function of time. Reference 92 lists the following failures: ductile and brittle fractures, fatigue failures, distortion failures, wear failures, fretting failures, liquid-erosion failures, corrosion failures, stress-corrosion cracking, liquid-metal embrittlement, hydrogen-damage failures, corrosion-fatigue failures, and elevated-temperature failures.

In addition, property changes owing to other considerations, such as radiation, should be considered, as appropriate. The designer needs to decide early in the design process whether a component or system will be designed for infinite life, finite specified life, a fail-safe or damage-tolerant criterion, a required code, or a combination of the above.³

In the performance of design trade-offs, in addition to the standard computerized tools of stress analysis, such as the finite-element method, depending upon the complexity of the mathematical formulation of the design constraints and the function to be optimized, the mathematical programming tools of operations research may apply. Mathematical programming can be used to define the most desirable (optimum) behavior of a component as a function of other constraints. In addition, on a systems

level, by assigning relative weights to requirements, such as safety, cost, and life, design parameters can be optimized. Techniques such as linear programming, nonlinear programming, and dynamic programming may find greater application in the future in the area of mechanical design.⁹³

Numerous factors dictate the overall engineering specifications for mechanical design. This chapter concentrates on philosophies and methodologies for the design of components that must satisfy quantitative strength and endurance specifications. Only deterministic approaches are presented for statically and dynamically loaded components.

Although mechanical components can be susceptible to many modes of failure, approaches in this chapter concentrate on the comparison of the state of stress and/or strain in a component with the strength of candidate materials. For instance, buckling, vibration, wear, impact, corrosion, and other environmental factors are not considered. Means of calculating stress-strain states for complex geometries associated with real mechanical components are vast and wide-ranging in complexity. This topic will be addressed in a general sense only. Although some of the methodologies are presented in terms of general three-dimensional states of stress, the majority of the examples and approaches will be presented in terms of two-dimensional surface stress states. Stresses are generally maximum on the surface, constituting the vast majority of situations of concern to mechanical designers. [Notable exceptions are contact problems,¹⁻⁶ components which are surfaced processed (e.g., induction hardened or nitrided⁷), or components with substantial internal defects, such as pores or inclusions.]

In general, the approaches in this chapter are focused on isotropic metallic components, although they can also apply to homogeneous nonmetallics (such as glass, ceramics, or polymers). Complex failure mechanisms and material anisotropy associated with composite materials warrant the separate treatment of these topics.

Typically, prototype testing is relied upon as the ultimate measure of the structural integrity of an engineering component. However, costs associated with expensive and time consuming prototype testing iterations are becoming more and more intolerable. This increases the importance of modeling durability in everyday design situations. In this way, data from prototype tests can provide valuable feedback to enhance the reliability of analytical models for the next iteration and for future designs.

5.2 ESTIMATION OF STRESSES AND STRAINS IN ENGINEERING COMPONENTS

When loads are imposed on an engineering component, stresses and strains develop throughout. Many analytical techniques are available for estimating the state of stress and strain in a component. A comprehensive treatment of this subject is beyond the scope of this chapter. However, the topic is overviewed for engineering design situations.

5.2.1 Definition of Stress and Strain

An engineering definition of “stress” is the force acting over an infinitesimal area. “Strain” refers to the localized deformation associated with stress. There are several important practical aspects of stress in an engineering component:

1. A state of stress-strain must be associated with a particular location on a component.

2. A state of stress-strain is described by stress-strain components, acting over planes.
3. A well-defined coordinate system must be established to properly analyze stress-strain.
4. Stress components are either normal (pulling planes of atoms apart) or shear (sliding planes of atoms across each other).
5. A stress state can be uniaxial, but strains are usually multiaxial (due to the effect described by Poisson's ratio).

The most general three-dimensional state of stress can be represented by Fig. 5.1a. For most engineering analyses, designers are interested in a two-dimensional state of stress, as depicted in Fig. 5.1b. Each side of the square two-dimensional element in Fig. 5.1b represents an infinitesimal area that intersects the surface at 90°.

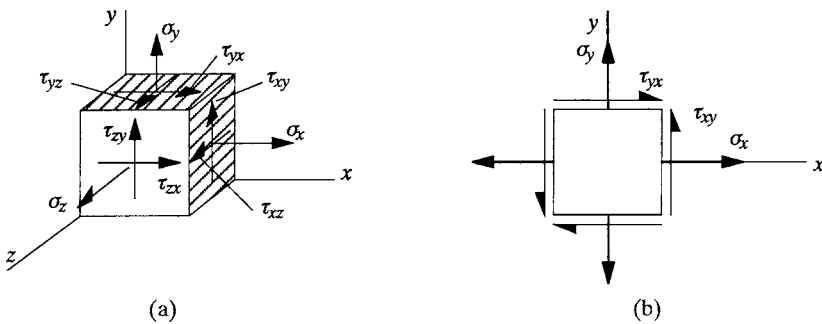


FIG. 5.1 The most general (a) three-dimensional and (b) two-dimensional stress states.

By slicing a section of the element in Fig. 5.1b, as shown in Fig. 5.2, and analytically establishing static equilibrium, an expression for the normal stress σ and the shear stress τ acting on any plane of orientation θ can be derived. This expression forms a circle when plotted on axes of *shear stress versus normal stress*. This circle is referred to as “Mohr's circle.”

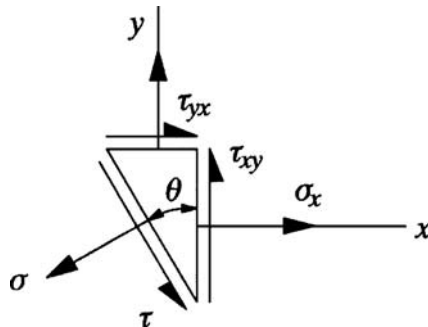


FIG. 5.2 Shear and normal stresses on a plane rotated θ from its original orientation.

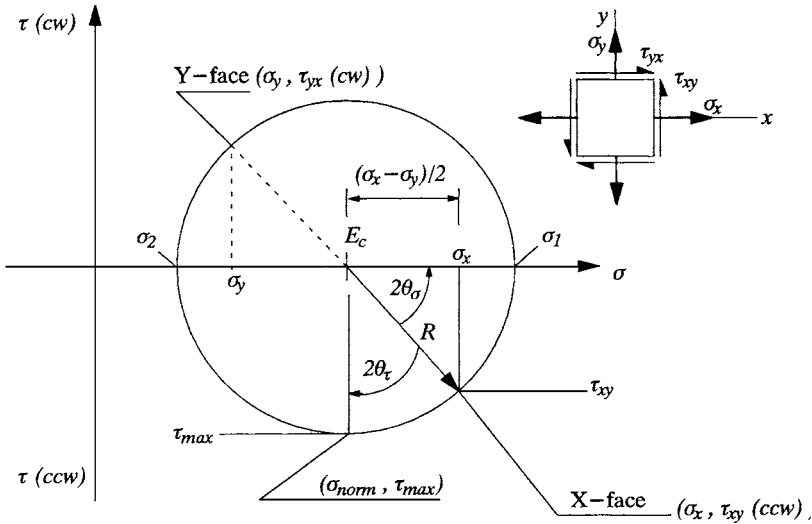


FIG. 5.3 Mohr's circle for a generic state of surface stress.

Mohr's circle is one of the most powerful analytical tools available to a design analyst. Here, the application of Mohr's circle is emphasized for two-dimensional stress states. From this understanding, it is a relatively simple step to extend the analysis to most three-dimensional engineering situations.

Consider the stress state depicted in Fig. 5.1*b* to lie in the surface of an engineering component. To draw the Mohr's circle for this situation (Fig. 5.3), three simple steps are required:

1. Draw the shear-normal axes [$\tau(\text{cw})$ positive vertical axis, σ tensile along horizontal axis].
2. Define the center of the circle E_c (which always lies on the σ axis):

$$E_c = (\sigma_x + \sigma_y)/2 \tag{5.1}$$

3. Use the point represented by the "X-face" of the stress element to define a point on the circle (σ_x, τ_{xy}). The X-face on the Mohr's circle refers to the plane whose normal lies in the X direction (or the plane with a normal and shear stress of σ_x and τ_{xy} , respectively).

That's all there is to it. The sense of the shear stress [clockwise (cw) or counter-clockwise (ccw)] refers to the direction that the shear stress attempts to rotate the element under consideration. For instance, in Figs. 5.1 and 5.2, τ_{yx} is ccw and τ_{xy} is cw. This is apparent in Fig. 5.3, a schematic Mohr's circle for this generic surface element.

The interpretation and use of Mohr's circle is as simple as its construction. Referring to Fig. 5.3, the radius of the circle R is given by Eq. (5.2).

$$R = \sqrt{\left(\frac{\sigma_x - \sigma_y}{2}\right)^2 + \tau_{xy}^2} \tag{5.2}$$

This could suggest an alternate step 3: that is, define the radius and draw the circle with the center and radius. The two approaches are equivalent. From the circle, the following important items can be composed: (1) the principal stresses, (2) the maximum shear stress, (3) the orientation of the principal stress planes, (4) the orientation of the maximum shear planes, and (5) the stress normal to and shear stress acting over a plane of any orientation.

1. *Principal Stresses.* It is apparent that

$$\sigma_1 = E_c + R \tag{5.3}$$

and

$$\sigma_2 = E_c - R \tag{5.4}$$

2. *Maximum Shear Stress.* The maximum in-plane shear stress at this location,

$$\tau_{\max} = R \tag{5.5}$$

3. *Orientation of Principal Stress Planes.* Remember only one rule: A rotation of 2θ around the Mohr's circle corresponds to a rotation of θ for the actual stress element. This means that the principal stresses are acting on faces of an element oriented as shown in Fig. 5.4. In this figure, a counterclockwise rotation from the X-face to σ_1 of $2\theta_\sigma$, means a ccw rotation of θ_σ on the surface of the component, where θ_σ is given by Eq. (5.6):

$$\theta_\sigma = 0.5 \tan^{-1} \left[\frac{2\tau_{xy}}{(\sigma_x - \sigma_y)} \right] \tag{5.6}$$

In Figs. 5.3 and 5.4, since the "X-face" refers to the plane whose normal lies in the x direction, it is associated with the x axis and serves as a reference point on the Mohr's circle for considering normal and shear stresses on any other plane.

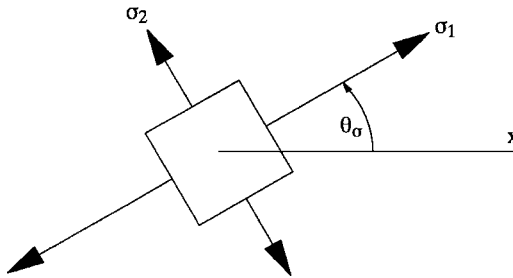


FIG. 5.4 Orientation of the maximum principal stress plane.

4. *Orientation of the Maximum Shear Planes.* Notice from Fig. 5.3 that the maximum shear stress is the radius of the circle $\tau_{\max} = R$. The orientation of the plane of maximum shear is thus defined by rotating through an angle $2\theta_\tau$ around the Mohr's circle, clockwise from the X-face reference point. This means that the plane oriented at an angle θ_τ (cw) from the x axis will feel the maximum shear stress, as shown in Fig. 5.5. Notice that the sum of θ_τ and θ_σ on the Mohr's circle is 90° ; this will always be the case. Therefore, the planes feeling the maximum principal (normal) stress and maximum shear stress always lie 45° apart, or

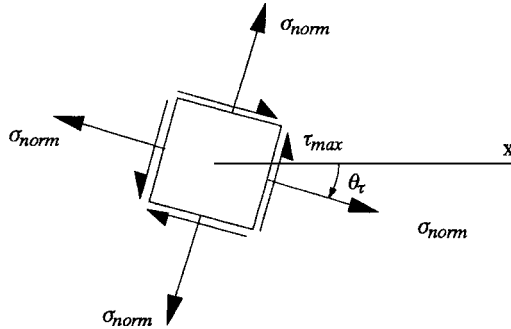


FIG. 5.5 Orientation of the planes feeling the maximum shear stress.

$$\theta_\tau = 45^\circ - \theta_\sigma \tag{5.7}$$

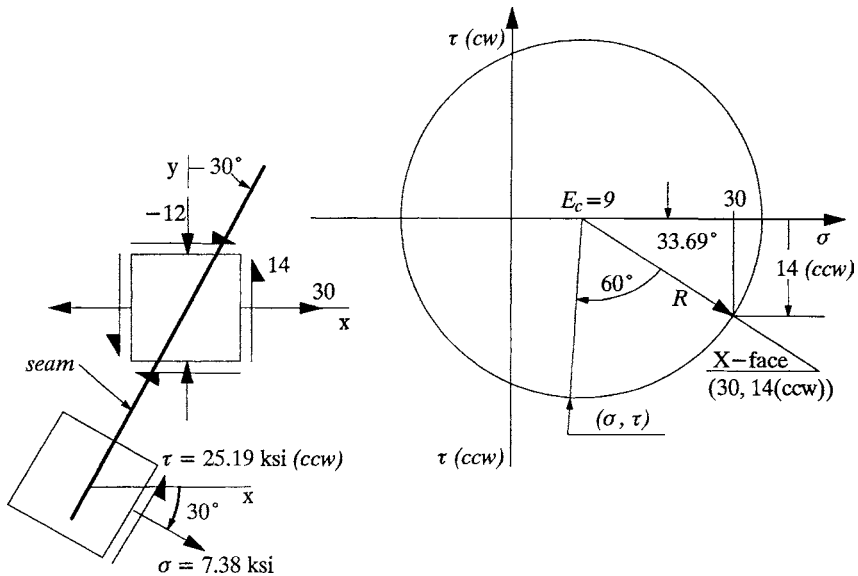
EXAMPLE 1 Suppose a state of stress is given by $\sigma_x = 30$ ksi, $\tau_{xy} = 14$ ksi (ccw) and $\sigma_y = -12$ ksi. If a seam runs through the material 30° from the vertical, as shown, compute the stress normal to the seam and the shear stress acting on the seam.

solution Construct the Mohr's circle by computing the center and radius:

$$E_c = \frac{[30 + (-12)]}{2} = 9 \text{ ksi} \quad R = \sqrt{\left(\frac{[30 - (-12)]}{2}\right)^2 + 14^2} = 25.24 \text{ ksi}$$

The normal stress σ and shear stress τ acting on the seam are obtained from inspection of the Mohr's circle and shown below:

$$\sigma = E_c + R \cos(33.69^\circ + 60^\circ) = 7.38 \text{ ksi}$$



$$\tau = R \sin(33.69^\circ + 60^\circ) = 25.19 \text{ ksi (ccw)}$$

The normal stress σ_{norm} is equal on each face of the maximum shear stress element and $\sigma_{\text{norm}} = E_c$, the Mohr's circle center. (This is always the case since the Mohr's circle is always centered on the normal stress axis.)

5. *Stress Normal to and Shear Stress on a Plane of Any Orientation.* Remember that the Mohr's circle is a collection of (σ, τ) points that represent the normal stress σ and the shear stress τ acting on a plane at any orientation in the material. The X-face reference point on the Mohr's circle is the point representing a plane whose stresses are (σ_x, τ_{xy}) . Moving an angle 2θ in either sense from the X-face around the Mohr's circle corresponds to a plane whose normal is oriented an angle θ in the same sense from the x axis. (See Example 1.)

More formal definitions for three-dimensional tensoral stress and strain are available.^{5,6,8-13} In the majority of engineering design situations, bulk plasticity is avoided. Therefore, the relation between stress and strain components is predominantly elastic, as given by the generalized Hooke's law (with ϵ and γ referring to normal and shear strain, respectively) in Eqs. (5.8) to (5.13):

$$\epsilon_x = \frac{1}{E}[\sigma_x - \nu(\sigma_y + \sigma_z)] \tag{5.8}$$

$$\epsilon_y = \frac{1}{E}[\sigma_y - \nu(\sigma_z + \sigma_x)] \tag{5.9}$$

$$\epsilon_z = \frac{1}{E}[\sigma_z - \nu(\sigma_x + \sigma_y)] \tag{5.10}$$

$$\gamma_{xy} = \frac{\tau_{xy}}{G} \tag{5.11}$$

$$\gamma_{yz} = \frac{\tau_{yz}}{G} \tag{5.12}$$

$$\gamma_{zx} = \frac{\tau_{zx}}{G} \tag{5.13}$$

where E is the modulus of elasticity, ν is Poisson's ratio, and G is the shear modulus, expressed as Eq. (5.14):

$$G = \frac{E}{2(1 + \nu)} \tag{5.14}$$

5.2.2 Experimental

Experimental stress analysis should probably be referred to as experimental strain analysis. Nearly all commercially available techniques are based on the detection of local states of strain, from which stresses are computed. For elastic situations, stress components are related to strain components by the generalized Hooke's law as shown in Eqs. (5.15) to (5.20):

$$\sigma_x = \frac{E}{1 + \nu} \epsilon_x + \frac{\nu E}{(1 + \nu)(1 - 2\nu)} (\epsilon_x + \epsilon_y + \epsilon_z) \tag{5.15}$$

$$\sigma_y = \frac{E}{1 + \nu} \epsilon_y + \frac{\nu E}{(1 + \nu)(1 - 2\nu)} (\epsilon_x + \epsilon_y + \epsilon_z) \tag{5.16}$$

$$\sigma_z = \frac{E}{1 + \nu} \epsilon_z + \frac{\nu E}{(1 + \nu)(1 - 2\nu)} (\epsilon_x + \epsilon_y + \epsilon_z) \tag{5.17}$$

$$\tau_{xy} = G\gamma_{xy} \tag{5.18}$$

$$\tau_{yz} = G\gamma_{yz} \tag{5.19}$$

$$\tau_{zx} = G\gamma_{zx} \tag{5.20}$$

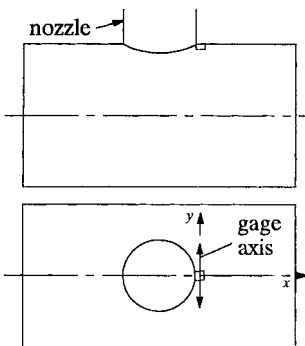
For strains measured on a stress-free surface where $\sigma_z = 0$; the in-plane normal stress relations simplify to Eqs. (5.21) and (5.22).

$$\sigma_x = \frac{E}{1 - \nu^2}[\epsilon_x + \nu\epsilon_y] \tag{5.21}$$

$$\sigma_y = \frac{E}{1 - \nu^2}[\epsilon_y + \nu\epsilon_x] \tag{5.22}$$

Several techniques exist for measuring local states of strain, including electro-mechanical extensometers, photoelasticity, brittle coatings, moiré methods, and holography.^{14,15} Other, more sophisticated approaches such as X-ray and neutron diffraction, can provide measurements of stress distributions below the surface. However, the vast majority of experimental strain data are recorded with electrical resistance strain gauges. Strain gauges are mounted directly to a carefully prepared surface using an adhesive. Instrumentation measures the change in resistance of the gauge as it deforms with the material adhered to its gauge section, and a strain is computed from the resistance change. Gauges are readily available in sizes from 0.015 to 0.5 inches in gauge length and can be applied in the roots of notches and other stress concentrations to measure severe strains that can be highly localized.

As implied by Eqs. (5.15) to (5.22), it can be important to measure strains in more than one direction. This is particularly true when the direction of principal stress is unknown. In these situations it is necessary to utilize three-axis rosettes (a pattern of three gauges in one, each oriented along a different direction). If the principal stress directions are known but not the magnitudes, two-axis (biaxial) rosettes can be oriented along principal stress directions and stresses computed with Eqs. (5.21) and (5.22) replacing σ_x and σ_y with σ_1 and σ_2 , respectively. These equations can be used to show that severe errors can result in calculated stresses if a biaxial stress state is assumed to be uniaxial. (See Example 2.)



EXAMPLE 2 This example demonstrates how stresses can be underestimated if strain is measured only along a single direction in a biaxial stress field. Compute the hoop stress at the base of the nozzle shown if (1) a hoop strain of 0.0023 is the only measurement taken and (2) an axial strain measurement of +0.0018 is also taken.

solution For a steel vessel ($E = 30,000$ ksi and $\nu = 0.3$), if the axial stress is neglected, the hoop stress is calculated to be

$$\sigma_y = E\epsilon_y = 69 \text{ ksi}$$

However, if the axial strain measurement of +0.0018 is used with Eq. (5.22), then the hoop stress is given by

$$\sigma_x = \frac{E}{1 - \nu^2}[0.0023 + 0.3(0.0018)] = 93.63 \text{ ksi}$$

In this example, measuring only the hoop strain caused the hoop stress to be underestimated by over 26 percent.

Obviously, in order to measure strains, prototype parts must be available, which is generally not the case in the early design stages. However, rapid prototyping techniques, such as computer numerically controlled machining equipment and stereolithography, can greatly facilitate prototype development. Data from strain-gauge testing of components in the final developmental stages should be compared to preliminary design estimates in order to provide feedback to the analysis.

5.2.3 Strength of Materials

Concise solutions have been developed for pressure vessels; beams in bending, tension and torsion; curved beams; etc.¹⁻⁶ These are usually based on considering a section through the point of interest, establishing static equilibrium with externally applied forces, and making assumptions about the distribution of stress or strain throughout the cross section.

Example 3 illustrates the use of traditional bending- and torsional-stress relations, showing how they can be used to improve the efficiency of an experimental strain measurement.

EXAMPLE 3 A steel component is welded to a solid base and loaded as shown. Identify the region of maximum stress. Show where to mount and how to orient a single-axis strain gauge to pick up the maximum signal. Compute the maximum principal stress and strain in the structure for a value of $P = 400,000$ lb.

solution The critical section is the cross section defined by $x = 0$, and the maximum stress can be expected at the origin of the coordinate system shown on page 5.14. The cross section feels bending about the centroidal y axis M_y , and a torque T . (Transverse shear is neglected since it is zero at the point of maximum stress.)

$$\sigma_x = \frac{M_y c}{I_y} = \frac{(1,800,000 \text{ in}\cdot\text{lb})(2.5 \text{ in})}{(11 \text{ in})(5 \text{ in})^3/12} = 39.27 \text{ ksi}$$

$$\tau_{xy} = \frac{4,760,000 \text{ in}\cdot\text{lb}}{(11 \text{ in})(5 \text{ in})^2} [3 + 1.8(\frac{5}{11})] = 66.09 \text{ ksi (from Ref. 1)}$$

Constructing a Mohr’s circle (as in Fig. 5.3) the orientations of the principal stresses and their magnitudes are given by

$$\theta = 36.7^\circ \text{ cw}$$

$$\sigma_1 = 88.58 \text{ ksi}$$

$$\sigma_2 = -49.3 \text{ ksi}$$

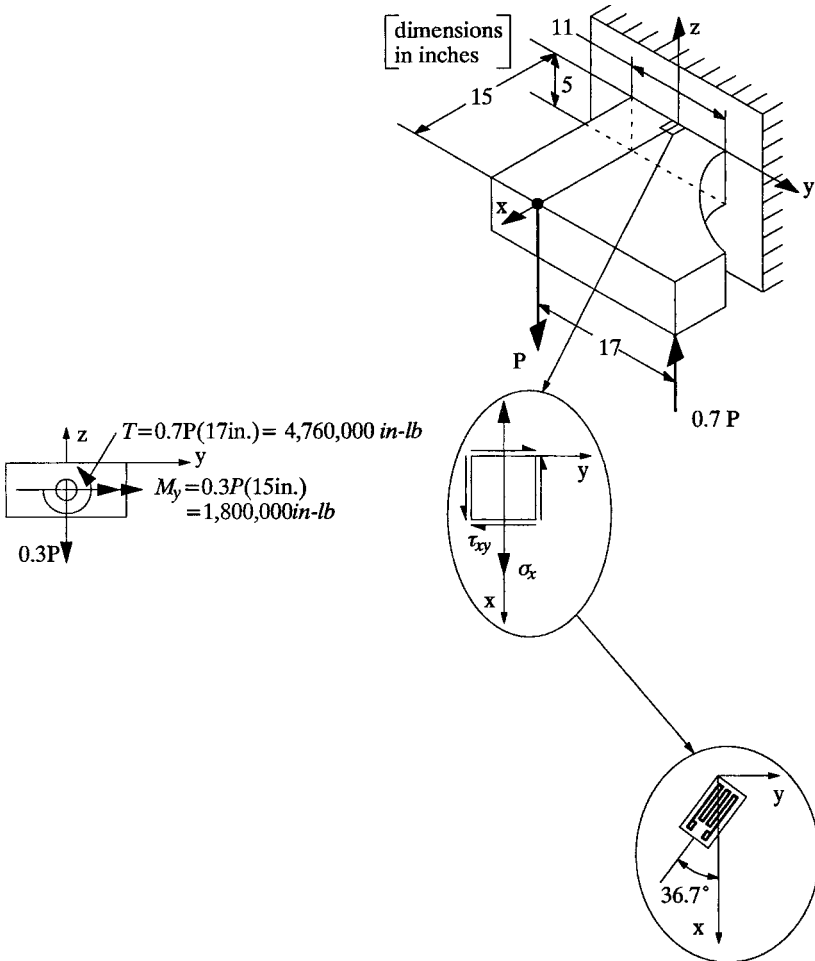
and Eqs. (5.21) and (5.22) yield

$$\epsilon_1 = 0.003446$$

$$\epsilon_2 = -0.002530$$

5.2.4 Elastic Stress-Concentration Factors

Most mechanical components are not smooth. Practical components typically include holes, keyways, notches, bends, fillets, steps, or other structural discontinuities. Stresses tend to become “concentrated” in such regions such that these stresses are



significantly greater than the nominally calculated stresses, based on the external forces and cross-sectional area. For instance, stress distributions are shown in Fig. 5.6 for a uniform rectangular plate in tension and through the identical cross section of a plate with a filleted step. Notice that the maximum elastically calculated stress at the root of the fillet, σ_{notch} , is greater than the nominal stress, S_{nom} . From this, the *stress-concentration factor* K_t is defined as the maximum stress divided by the nominal stress:

$$K_t = \frac{\sigma_{\text{notch}}}{S_{\text{nom}}} \tag{5.23}$$

Stress-concentration factors are found by a number of techniques including experimental, finite-element analysis, boundary-element analysis, closed-form elasticity solutions, and others. Fortunately, researchers have tabulated K_t values for many generalized geometries.^{16,17}

Reference 16, from Peterson, is a compendium of design charts. Reference 17, from Roark, provides useful empirical formulas that can be programmed into spreadsheets

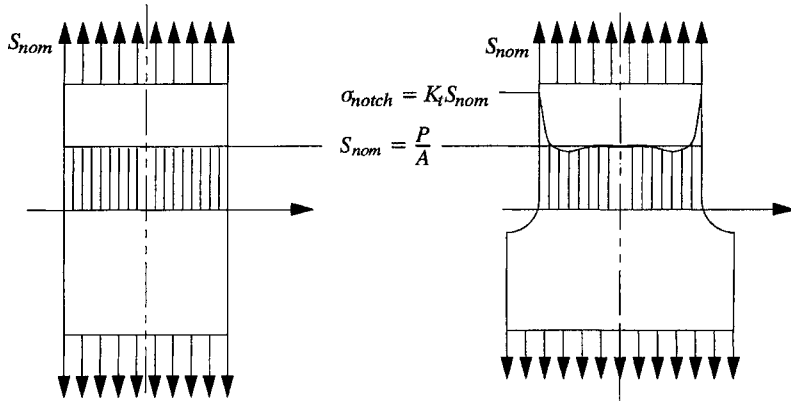


FIG. 5.6 Definition of elastic stress-concentration factor.

or computer routines for design optimization. There are several important points to remember about stress concentration factors:

1. They only apply to elastic states of stress-strain.
2. They are tabulated for a particular mode of loading (axial, bending, torsional, etc.).
3. Since they are elastic, they can be superimposed (i.e., computed separately, then added).

It has been shown that using the full value of stress-concentration factors for evaluating strength can be overly conservative, especially for static design situations. Shigley and Mischke¹ state that one can usually neglect the stress-concentration factor due to the fact that localized yielding can work-harden the material in the notch vicinity and relieve the stresses. On the other hand, neglecting stress-concentration factors can be nonconservative, especially if very brittle material or fatigue loading is involved. As safe design practice, stress-concentration factors should be considered for preliminary analysis. If the resulting solution is unacceptable from a weight, size, or cost standpoint, then reasonable reductions in K_t can be considered based on the potential for the material to deform and locally work-harden. Such decisions can be based on experimental data generated with the material of interest and notches with similar values of K_t . This type of testing can supplement analysis prior to the availability of fully designed prototype parts. Data from testing such as this should be carefully documented, since it can be used as a basis for future design decisions.

5.2.5 Finite-Element Analysis

The use of computers is increasing as rapidly in engineering design as in any other profession. Finite-element analysis (FEA),¹⁸⁻²¹ coupled with increasing computational capabilities, is providing increasing analytical power for use on everyday design situations. Commercially available software packages are enabling designers to evaluate states of stress in situations involving complex geometry and loading combinations. However, three important points should be considered when stresses are computed from FEA: (1) Elastic analysis can be straightforward, but the potential for error is great if the analyst has not assured mesh convergence, especially for sharp geometric

discontinuities or contact problems. (2) The specification of boundary conditions is critical to obtaining valid results that correlate with the physical stress-strain state in the component being modeled. (3) Elastic-plastic analysis is not yet simplified for everyday design use, particularly for cyclic loading conditions.²²

These three points are intended to remind the designer not to accept FEA results without an adequate awareness of the assumptions used to implement the analysis (most importantly, mesh density, boundary conditions, and material modeling). Most robust commercial FEA codes provide error estimates associated with their solutions. In high-stress-concentration regions, these errors can be substantial and a locally refined mesh could be called for (often not a simple task). A designer must be careful to avoid the tendency to simply marvel at appealing and colorful FEA output without fully understanding that the results are only as valid as the assumptions used to build the analytical model.

5.3 STRUCTURAL INTEGRITY DESIGN PHILOSOPHIES

An engineer must routinely assure that designs will endure anticipated loading histories with no significant change in geometry or loss in load-carrying capability. Anticipating service-load histories can require experience and/or testing. Techniques for load estimation are as diverse as any other aspect of the design process.²³

The *design* or *allowable* stress is generally defined as the tension or compressive stress (yield point or ultimate) depending on the type of loading divided by the safety factor. In fatigue the appropriate safety factor is used based on the number of cycles. Also when wear, creep, or deflections are to be limited to a prescribed value during the life of the machine element, the design stress can be based upon values different from above.

The magnitude of the design factor of safety, a number greater than unity, depends upon the application and the uncertainties associated with a particular design. In the determination of the factor of safety, the following should be considered:

1. The possibility that failure of the machine element may cause injury or loss of human life
2. The possibility that failure may result in costly repairs
3. The uncertainty of the loads encountered in service
4. The uncertainty of material properties
5. The assumptions made in the analysis and the uncertainties in the determination of the stress-concentration factors and stresses induced by sudden impact and repeated loads
6. The knowledge of the environmental conditions to which the part will be subjected
7. The knowledge of stresses which will be introduced during fabrication (e.g., residual stresses), assembly, and shipping of the part
8. The extent to which the part can be weakened by corrosion

Many other factors obviously exist. Typical values of design safety factors range from 1.0 (against yield) in the case of aircraft, to 3 in typical machine-design applications, to approximately 10 in the case of some pressure vessels. It is to be noted that these safety factors allow us to compute the allowable stresses given and are not in lieu of the stress-concentration factors which are used to compute stresses in service.

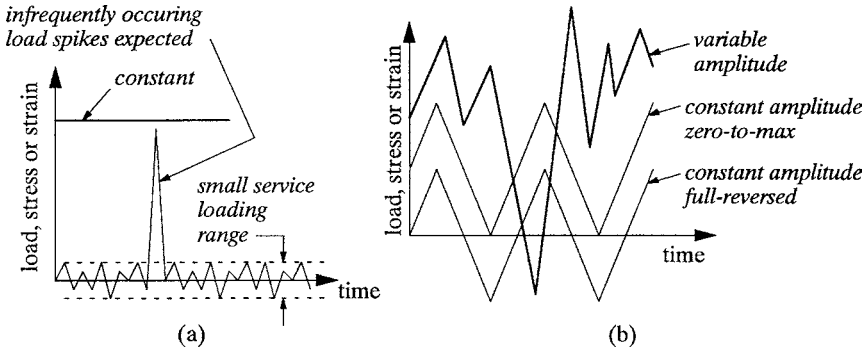


FIG. 5.7 Examples of (a) static and (b) dynamic, or fatigue, loading.

If the uncertainties are great enough to cause severe weight, volume, or economic penalties, testing and/or more thorough analyses should be performed rather than relying upon very large factors of safety. Factors of safety to be used with standard, commercially available design elements should be those recommended for them by reliable manufacturers and/or by established codes for design of machines.

In probabilistic approaches to design, in terms of stress (or actual load) and strength (or load capability) the safety factor is related to reliability. When a failure may cause injury or otherwise be disastrous, the probability density curves representing the strength of the part and the stress to be sustained should not overlap, and the factor of safety equals the ratio of the mean strength to the mean stress. If the tails of the two curves overlap, a possibility for failure exists.

The “true factor of safety,” which may be defined in terms of load, stress, deflection, creep, wear, etc., is the ratio of the magnitude of any of the above parameters resulting in damage to its actual value in service. For example:

$$\text{True factor of safety} = \frac{\text{maximum load part can sustain without damage}}{\text{maximum load part sustains in service}}$$

The true factor of safety is determined after a part is built and tested under service conditions.

In this chapter, loading is classified as “static” or “dynamic.” Static loading could be formally defined as loading that remains constant over the life of the component, as depicted in Fig. 5.7a. Under this type of loading, the primary concern is avoiding failure by yielding or fracture. Also shown in Fig. 5.7a is another type of loading that can be considered “static,” from a structural integrity viewpoint. This refers to situations where only a few, *infrequently occurring* load spikes can be expected in service. Dynamic loading fluctuates significantly during the life of the component, as shown in Fig. 5.7b. Although peak stresses can remain well below levels associated with yielding, this type of loading can lead to failure by fatigue.

5.3.1 Static Loading

Loading on a mechanical component is rarely steady. However, in many cases, safety factors and service load ratings are used in order to keep in-service load fluctuations small relative to the maximum load the component can sustain. Often this is assured by proof loading a component as the final step in its manufacturing process. Proof

loads usually exceed the rated service load by a factor of 2 to 3.5. Examples of this include chains, other lifting hardware, and pressure vessels. Proof loading not only ensures the structural integrity of the part, but can also serve to impart residual stresses that increase the functional elastic limit and increase fatigue life.^{24–26}

When a component is designed for static strength, it must be assured that service loads indeed remain well below the strength of the component. Unfortunately, the user, more than the designer, often dictates the maximum load level a component will experience. Users tend to push designs over the limit at every available opportunity. For safety-critical components, designers should consider mechanisms to ensure that loadings do not exceed safe operating levels. For instance, rupture disks are effective “weak links” in the design of pressure systems. Should the operating pressure be exceeded, the rupture disk fails by design, into a discharge tank. Another example would be the use of redundant, or backup, elements. When a specimen begins to deform under too great a load, it gains support when it encounters a backup element, thus avoiding complete fracture (and possibly alerting the end user).

Care must be taken when the loading on a component is classified as “static” for design purposes. The approach is only safe when the static limit is rarely seen in service, as depicted by the load spike in Fig. 5.7a. For example, suppose a nozzle discharges under a constant internal pressure. There is a tendency to utilize that pressure for static design (the constant loading line in Fig. 5.7a). However, if the nozzle discharges for 30 minutes, drains, then repeats, on a regular basis, then fatigue could be important.

5.3.2 Fatigue Loading

Under fatigue loading, cracks develop in high-stress regions which were initially free of any macroscopic defect. A component can endure numerous cycles of loading before the crack is detectable. Once this occurs, a dominant crack usually propagates progressively to fracture. The relative life spent in developing a crack of “engineering size” (usually defined as 1–2 mm in surface length) and then propagating the crack to fracture can define the fatigue design philosophy, as overviewed below.

Infinite-Life Design. This philosophy is based on the concept of the *fatigue limit*, or the stress amplitude below which fatigue will not occur. For high-cycle components like valve springs, turbo machinery, and other high-speed rotating equipment, this is still a very widely utilized concept. However, the approach is going out of style due to cost- and weight-reduction requirements. There are also problems pertaining to the definition of a fatigue limit for a particular material, since numerous factors have proven influential. These factors include heat treatment, surface condition, residual stresses, temperature, environment, etc. (Furthermore, aluminum and other nonferrous alloys do not exhibit a fatigue limit.) One final cautionary note: Intermittent overloads can reduce or eliminate the fatigue limit.¹³

Finite-Life (Safe-Life) Design. Instead of designing a component to never fail, parts are designed for a specified life deemed “safe,” or unlikely to occur during the rated life of the machine, except in cases of abusive loading. For instance, even a safety-critical automobile suspension component might be designed to sustain only 1000 of the most severe impact loads corresponding to the worst high-speed curb strike on the proving ground. However, the vast majority of automobiles will experience nowhere near this many occurrences. Pressure vessels are sometimes designed to lives on the order of a few hundred cycles, corresponding to cleanout cycles that will occur only a few times annually. Ball joints in automobiles and landing-gear parts in aircraft are other examples of finite-life design situations.

Fail-Safe Design. This strategy, developed primarily in the aircraft industry, should be implemented whenever possible. The approach invokes measures to ensure that, if cracks initiate, they will grow in a controlled manner. Then, measures are taken to ensure that catastrophic failure is avoided, including the use of redundant elements, backup elements, crack-arrest holes positioned at strategic locations, and the use of multiple load paths. This approach is referred to as “leak before burst” in the pressure-vessel industry.

Damage-Tolerant Design. Also developed in the aircraft industry, this philosophy assumes that cracks exist *before* a component is put into service. For instance, cracks are assumed to exist underneath rivet heads or behind a seam, anywhere that they might be concealed during routine inspection. Then, the behavior of the crack is predicted from flight-loading spectra anticipated for the aircraft. Analyses of many key locations on an aircraft are used to schedule maintenance and inspections.

The four methods discussed above cover most design situations, but which of these is utilized depends on the design criteria. It is typical for more than one (sometimes all) of the strategies to be utilized in a single design. For instance, in the design of an aircraft, the fail-safe approach is routinely applied to wings, fuselages, and control surfaces. However, a landing gear and a rotor in the jet engine are designed for finite life.

To provide some size scale to the issue of fatigue crack development, refer to Fig. 5.8.

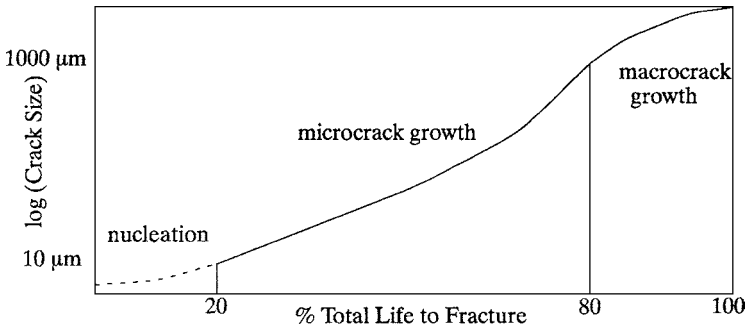


FIG. 5.8 Size scale associated with fatigue crack development.

Crack development can be divided into three separate regimes: nucleation, microcrack growth, and macrocrack growth. The first two regimes are often referred to together as Region I, or *crack initiation*. This is still a very unclear area. Although numerous theories exist, experimental verification is difficult. Obtaining repeatable data in this region has proven difficult and active research is underway. The macrocrack growth regime is referred to as Region II. This region is associated with linear elastic fracture mechanics (LEFM).

Region I: This region involves the formation of surface cracks of the order of 1 mm in length. It is considered to be controlled by the maximum shear stress fluctuation, $\Delta\tau_{\max}$, since cracks on this small scale tend to originate on planes experiencing maximum shear stress. Two kinds of maximum shear planes are shown in Fig. 5.9. One intersects the surface at 45° (Sec. A-A) and the other at 90° (Sec. B-B). Note that both are inclined 45° to the applied stress axis. The enlarged views in Fig. 5.9 represent the intersection of slip bands with the free surface. “Slip bands” refer to multiple parallel planes, each accommodating massive dislocation movement, and associated plastic slip. The cross sections depict discontinuities (called intrusions and extrusions) created on the free surface that eventually lead to a macroscopic crack.

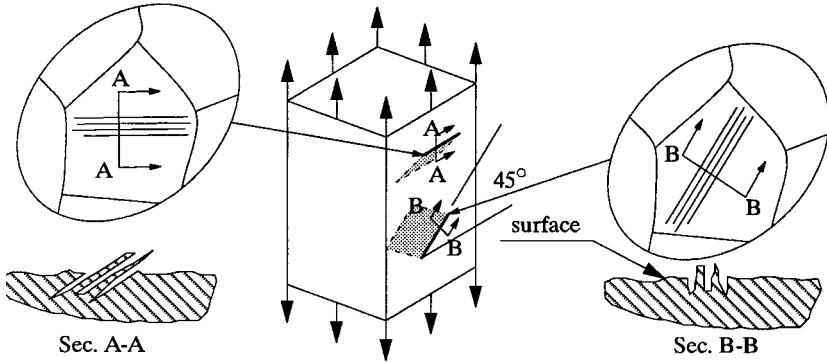


FIG. 5.9 Schematic microscopic shear cracks intersecting the surface at 45° (Sec. A-A) and 90° (Sec. B-B).

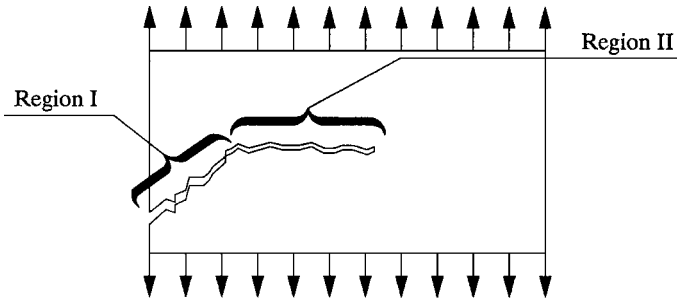


FIG. 5.10 Macroscopic cracks typically propagate perpendicular to maximum principal stress.

Region II: The surface steps created by the slip-band intersection are forced open and decohesion of slip planes forms small cracks oriented 45° to the loading axis. Upon growth, cracks typically turn to become oriented 90° to the principal stress direction. This is illustrated in Fig. 5.10. The crack is forced open and the crack tip blunts. This causes *striations* to form, which result in the *beach marks* that characterize fatigue fracture surfaces. This region is controlled by the range of principal stress ($\Delta\sigma_1$) acting normal to the plane of the crack. Generally, once this stage is reached, fracture mechanics are used to describe subsequent behavior.

5.4 STATIC STRENGTH ANALYSIS

In this section, a state of stress such as that depicted in Fig. 5.1b, is considered to be known. Based on this state of stress, the structural integrity of a component is assessed by comparing the stress state to the strength of the material. Although the methodology shown here is applicable to any three-dimensional stress state, surface stress states are emphasized since these comprise the vast majority of engineering design situations. Approaches are described in only a cursory manner, with more detailed references given. Emphasis is given to the application of the approaches to design situations.

5.4.1 Monotonic Tensile Data

The tensile test provides the input data for conducting static strength analysis. A sample of material (usually round or rectangular in cross section) is pulled apart under a monotonically increasing tensile load until failure occurs. Guidelines for conducting tensile tests are found in the American Society for Testing and Materials (ASTM) Specification E-8, "Standard Test Methods of Tension Testing of Metallic Materials."²⁷ A stress-strain curve from a tensile test is illustrated in Fig. 5.11, with a list of important points corresponding to "properties" measured by the test.

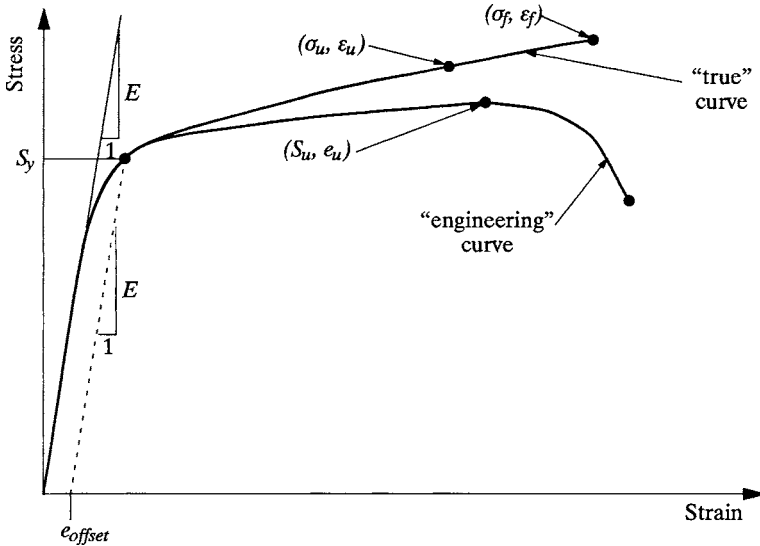


FIG. 5.11 Schematic engineering and true stress-strain curves, with list of properties.

Another important parameter is the *reduction in area*. It is determined from a measurement of the minimum diameter of the broken specimen, and the relation

$$RA = \frac{A_o - A_f}{A_o} = \frac{d_o^2 - d_f^2}{d_o^2} \tag{5.24}$$

where A_o and d_o are the initial specimen cross-sectional area and diameter, respectively, and the f subscript refers to those dimensions at fracture.

The engineering stress is computed by dividing the applied load by the original gauge section cross-sectional area A_o . Engineering strain is computed by dividing the change in gauge-section length by the initial gauge-section length. The calculation of "true" stress and strain quantities accounts for the fact that, as the loading increases, the cross-sectional area decreases and the gauge length increases. However, the need to distinguish between the two is rare, for everyday engineering design. The two curves are virtually identical up to plastic strains on the order of 10 percent.

A relation was developed by Ramberg and Osgood²⁸ to describe the stress-strain curve for many metallic engineering alloys. This relation is usually expressed as

$$\epsilon = \frac{\sigma}{E} + \left(\frac{\sigma}{K}\right)^{1/n} \tag{5.25}$$

where K = strength coefficient
 n = strain-hardening exponent

For situations involving large plasticity (such as forming operations) the approximate log-log linear (power log) relation between stress and plastic strain can sometimes be quite inaccurate over a wide range of plastic strains. Therefore, it can be important to specify the plastic strain range over which n is defined. A designer interested in moderate plastic strain in a notch might be concerned with the range 0.002 to 0.02. However, a manufacturing engineer interested in a forming operation might need more accurate stress-strain information over a range from 0.05 to 0.15. The ASTM Specification E-646, "Tensile Strain-Hardening Exponents (n -Values) of Metallic Sheet Materials,"²⁹ deals with this issue specifically.

Data from compression tests for engineering materials can be equally important for conducting a static strength assessment. ASTM Specification E-9, "Standard Test Methods of Compression Testing of Metallic Materials at Room Temperature,"³⁰ describes this type of testing. Data from such a test can be important when attempting to classify a material as ductile or brittle. Failure of "brittle" materials in tension is usually associated with internal stress risers, such as voids or inclusions. Under compression such stress concentrations are less influential and the strength of a brittle material can considerably exceed its own tensile strength (for instance, by a factor of over 4 for some cast irons).

5.4.2 Multiaxial Yielding Theories (Ductile Materials)

Ductile materials are considered to be able to exhibit notable plasticity in a tensile test prior to fracture. No rigorous definition of "ductile" exists. Generally, however, a material is considered ductile if the percent reduction in area is greater than 15 to 20 percent, and the ultimate tensile strength exceeds the yield strength by a notable amount. Another important indicator used to classify a material as ductile is the relation between magnitudes of the tensile and compressive yield strengths. Ductile materials tend to yield in compression at nearly the same stress level as they do in tension, whereas brittle materials are typically quite a bit stronger in compression.

For the design of ductile machine components, two theories are typically utilized: (1) the Tresca criterion (maximum shear stress) and (2) von Mises' criterion (equivalently, the octahedral shear-stress or distortion-energy theory). These approaches can be depicted as safe operating envelopes on axes of minimum versus maximum principal stress (Fig. 5.12). Notice that the Tresca approach is smaller and therefore more conservative than the von Mises.

The Tresca (Maximum Shear-Stress Theory) Criterion. This approach is based on the premise that yielding will occur when the maximum shear stress under multiaxial loading, τ_{\max} , is equal to the maximum shear stress imposed during a tensile test at yield. In other words, yielding occurs when

$$\tau_{\max} = \frac{\sigma_A - \sigma_B}{2} = \frac{S_y}{2} \tag{5.26}$$

where σ_A and σ_B are the maximum and minimum principal stresses, respectively. This approach can be restated in terms of an "equivalent stress,"

$$\sigma_{\text{eq,Tr}} = \sigma_A - \sigma_B \tag{5.27}$$

which is directly comparable to the axial yield strength of the material. In this way,

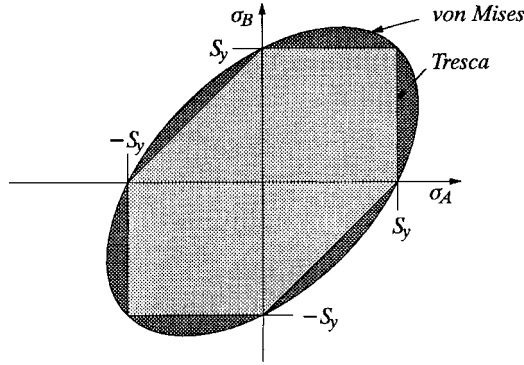


FIG. 5.12 Safe operating regions for von Mises (octahedral shear stress) and Tresca (maximum shear stress) criteria.

the “factor of safety” for the stress state is straightforwardly defined from the Tresca criterion by

$$FS_{Tr} = \frac{S_y}{\sigma_{eq,Tr}} \tag{5.28}$$

The von Mises Criterion. The von Mises criterion refers to any of several approaches shown to be essentially identical. These include the distortion energy, octahedral shear stress, and the Mises-Hencky theories. In terms of an equivalent stress, the von Mises approach is given by

$$\sigma_{eq,vM} = \frac{1}{\sqrt{2}} \sqrt{(\sigma_1 - \sigma_2)^2 + (\sigma_2 - \sigma_3)^2 + (\sigma_3 - \sigma_1)^2} \tag{5.29}$$

Conceptually, the approach can be considered a root-mean-square average of the principal shear stresses, with a scaling factor to assure that the equivalent stress is equal to σ_1 for a uniaxial stress state.

The factor of safety for the von Mises approach is thus given by

$$FS_{vM} = \frac{S_y}{\sigma_{eq,vM}} \tag{5.30}$$

Experiments have shown that the von Mises criterion is more accurate in terms of describing data trends, but the Tresca approach is a more conservative design option.¹³

5.4.3 Multiaxial Failure Theories (Brittle Materials)

In this section, the use of three design criteria is demonstrated. These approaches are referred to (in order of decreasing conservatism) as the Coulomb-Mohr, modified Mohr, and the maximum normal fracture criteria.¹³ Each can be considered to define safe operating envelopes on axes of minimum versus maximum principal stress (Fig. 5.13). The most notable difference between Figs. 5.12 and 5.13 is the typically greater compressive strength S_{uc} exhibited by a brittle material relative to its tensile strength S_{ut} . Also,

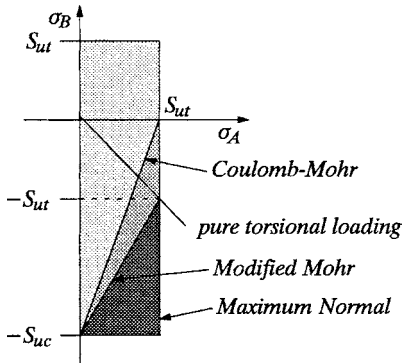


FIG. 5.13 Safe operating regions for the Coulomb-Mohr, modified Mohr, and maximum normal failure theories for brittle materials.

notice how only the first and fourth quadrants of principal stress space are depicted in Fig. 5.13. This is because the vast majority of all engineering stress states of concern to mechanical designers lie in these quadrants, with the vast majority located in the fourth. (With the exception of the deepest points in the ocean, it is difficult to imagine practical engineering states of surface stress that do not reside in or along the fourth quadrant.)

The three theories are described below, followed by the presentation of a static strength design algorithm. For all three theories, the factor of safety for a state of stress is defined as the ratio of the radial distance to the boundary (through the state of stress) to the radial distance defined by the state of stress. This is depicted in Fig. 5.14.

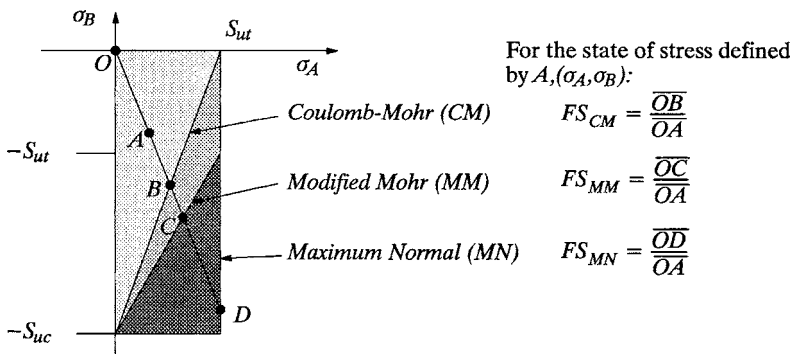


FIG. 5.14 Definition of factor of safety based on the Coulomb-Mohr, modified Mohr, and maximum normal failure theories for brittle materials.

The Coulomb-Mohr Fracture Theory. The Coulomb-Mohr theory is based on the concept that certain combinations of shear stress and stress normal to the plane of maximum shear are responsible for failure. This is manifested in the fourth quadrant of principal stress space by the line from S_{ut} on the tensile stress axis to $-S_{uc}$ on the compressive strength axis.

As is apparent from Figs. 5.13 and 5.14, the Coulomb-Mohr theory is the most conservative design approach. Experimental results have indicated that the approach is typically conservative for design applications.

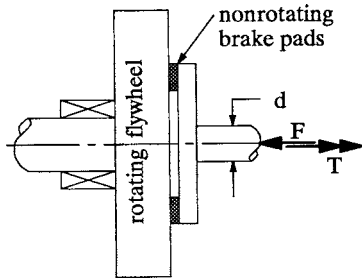
The Modified Mohr Fracture Theory. This theory is based on empirical observations that the maximum principal stress tends to define failure under torsional loading (or along a line 45° through the fourth quadrant of principal stress space). However, when significant compression accompanies torsion (stress states below the 45° torsion line), the maximum normal stress theory becomes nonconservative. Therefore, the line in the fourth quadrant defined by $(S_{ur} - S_{ut})$ and $(0, -S_{uc})$ is used as the boundary for

the modified Mohr theory. Since the approach is formulated from empirical observations, it tends to correlate well with data.

The Maximum Normal Fracture Theory. Conceptually, this is the simplest of the theories in this section. If the magnitude of the maximum (or minimum) principal stress in the material exceeds the material’s tensile (or compressive) strength, failure is predicted. Unfortunately, experiments have shown it to be nonconservative for situations involving substantial compression (states of stress in the fourth quadrant, below the line of pure torsion).

5.4.4 Summary Design Algorithm

In practice, the designation of a material as ductile or brittle and the selection of an appropriate failure criterion can be subjective. Major factors include whether or not compressive strength data are available, and whether or not compression constitutes a major portion of the loading. In situations where the choices are not clear, it is advisable to conduct analyses based on limiting assumptions, implementing all potential approaches to bound a solution. To assist in this, an algorithm is presented in the form of a flowchart in Table 5.1 that can be easily coded into a computer program or applied using a computer spreadsheet. The design engineer is responsible for supplying the correct input information (including the classification of the material as ductile or brittle) and for interpreting the output. Several techniques are used to evaluate strength and the designer must decide which is the most appropriate. Output from such a routine is presented in Example 4.



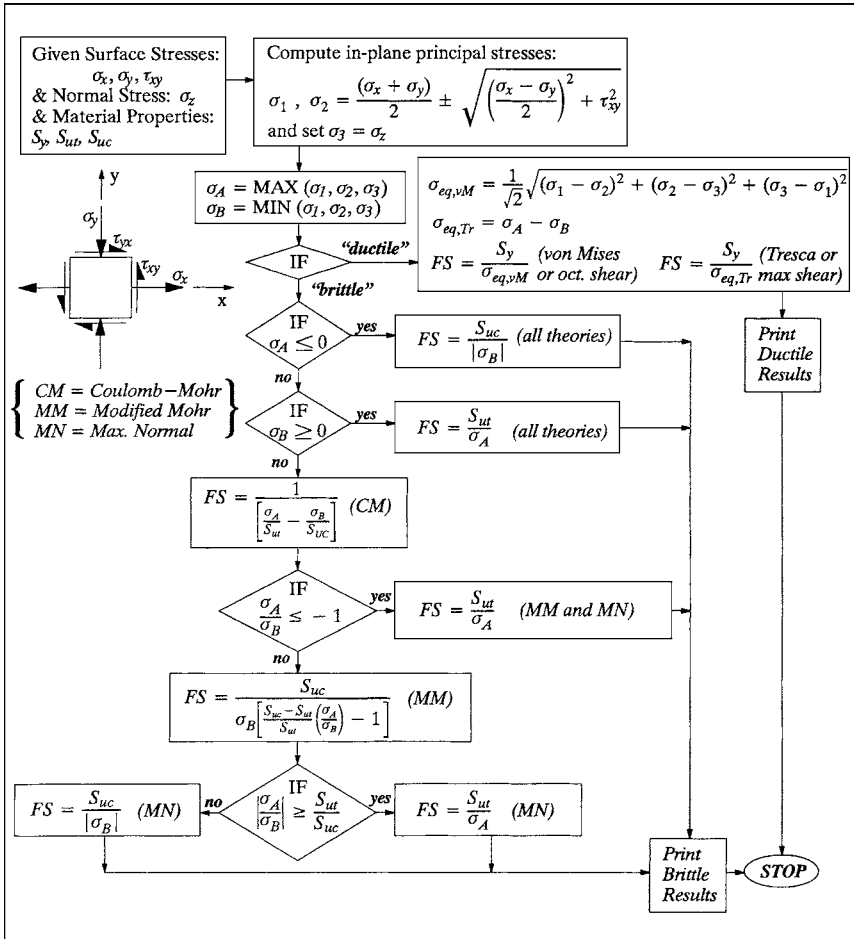
EXAMPLE 4 A round shaft is to be used to apply brake pads to the side of a large flywheel. The shaft is to experience a compressive load of $F = 22,000$ lb, and corresponding torsional load of $T = 23,100$ in·lb. Specify the diameter of the shaft d (to the nearest one-eighth inch) for a safety factor of at least 2.0 using the following materials:

1. ASTM #40 cast iron ($S_{ur} = 42.5$ ksi, $S_{uc} = 140$ ksi)
2. 1020 steel ($S_y = 65$ ksi)
3. Q&T 4340 steel ($S_y = 240$ ksi)

solution For each material, the three failure theories were used from Table 5.1. Diameters (in inches) and safety factors (in parentheses) estimated for each material are presented in tabular form, below.

	1. #40 iron	2. 1020	3. 4340
Tr	N/A	2.0 (2.15)	1.375 (2.62)
vM	N/A	1.875 (2.04)	1.25 (2.27)
CM	1.875 (2.02)	N/A	N/A
MM	1.75 (2.06)	N/A	N/A
MN	1.75 (2.38)	N/A	N/A

TABLE 5.1 Static Strength Analysis



5.5 FATIGUE STRENGTH ANALYSIS

The subject of fatigue analysis is considered in this section from the point of view of an engineering designer. Although this subject is still actively researched, a great deal of solid engineering methodology has been developed. The fatigue design strategy to be described in this section is outlined below.

Crack initiation is defined as the occurrence of a crack of engineering size, usually 1 to 2 mm in surface length. The basis of this definition is illustrated in Fig. 5.15. To obtain baseline fatigue data (stress-life or strain-life), tests are usually conducted on small specimens, 0.25 in (6 mm) in diameter. Usually, "failure" in these tests can be associated with complete fracture of the specimen. It is assumed that a component experiencing a localized stress-strain history equivalent to the axial specimen will develop a crack of approximately the same size in approximately the same number of cycles. This concept is often referred to as the local strain approach.^{13,23,31,32}

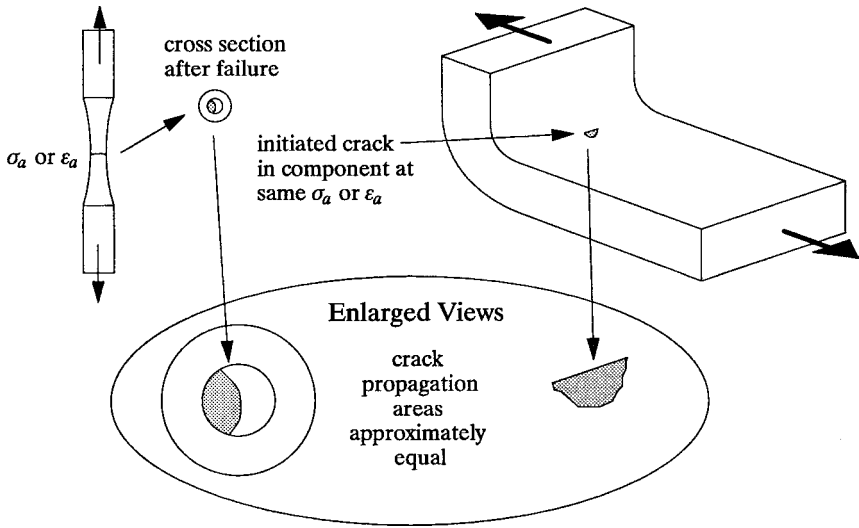


FIG. 5.15 Similitude between failure in a baseline test specimen and crack initiation in an actual engineering component.

In the remainder of this chapter, “failure” will refer to the occurrence of an engineering-sized crack, roughly the same size as that found in an axial specimen upon its failure in a standard fatigue test. The propagation of the crack due to subsequent fatigue loading is considered separately using fracture-mechanics techniques for damage-tolerant design.

5.5.1 Stress-Life Approaches (Constant-Amplitude Loading)

In this section, the *stress-life (S-N) approach* to fatigue design is overviewed. This is one of the earliest fatigue design approaches to be developed and can still be a useful tool. Its success is based on the fact that, for predominantly elastic loading, the state of stress in a component can often be characterized quite accurately. *As long as the state of fluctuating stress can be accurately estimated, the S-N approach can do a good job of predicting fatigue.* However, fatigue cracks usually develop at structural discontinuities, or notches. In these regions, localized cyclic plastic strains can develop and the task of estimating the state of stress becomes far more difficult. Without a reliable knowledge of the stress state, the utility of the *S-N* approach becomes limited and a strain-based approach (described later) becomes more useful.

Stress-Life Curve. Baseline data are generated by imposing fully reversed fluctuating stress in a standard specimen, as shown below in Fig. 5.16. This can be done via axial loading or rotating-bending.

Fully reversed loading refers to the fact that $\sigma_{\max} = -\sigma_{\min}$ (or, the alternating stress, $\sigma_a = \sigma_{\max}$). Tests are conducted by applying loading as shown in Fig. 5.16 until the specimen “fails,” usually by fracturing into two separate pieces. Typically, the gauge section ranges in size from 0.25 to 0.5 inch in diameter (6 to 12 mm). To generate *S-N* data for fatigue design purposes, a number of specimens must be tested at varying stress levels. Applicable ASTM guidelines are listed below.

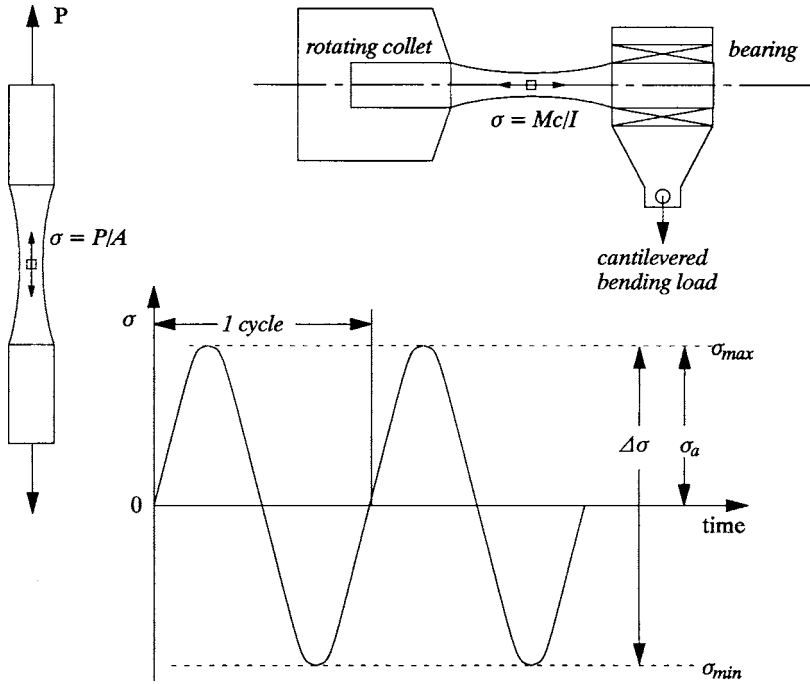


FIG. 5.16 Baseline $S-N$ fatigue testing.

- Details for conducting $S-N$ tests are presented in the ASTM E-466-82, “Standard Practice for Conducting Constant Amplitude Axial Stress-Life Tests of Metallic Materials.”³³
- Data from fatigue tests are analyzed according to the ASTM E-739, “Standard Practice for Statistical Analysis of Linear or Linearized Stress-Life ($S-N$) and Strain Life ($\epsilon-N$) Fatigue Data.”³⁴
- Data are typically presented according to ASTM E-468-82, “Standard Practice for Presentation of Constant Amplitude Fatigue Test Results for Metallic Materials.”³⁵

There are some fundamental differences between baseline data obtained from rotating-bending and axial testing. The stress amplitude for rotating-bending is computed elastically, even though severe plastic deformation occurs at higher load levels. Therefore, the quantity

$$S = \frac{Mc}{I} \tag{5.31}$$

is actually only a parameter with units of stress, indicating the severity of bending. A plasticity analysis would be required to estimate the actual stress at the specimen surface. And even for high-cycle tests (lower load levels), there is a bending-stress gradient as depicted in Fig. 5.17. For this reason, bending tests are less severe than axial tests and can make the material *appear* stronger. This is due to two factors, both related to the bending versus axial stress distribution: (1) Physically, more of the gauge section is subjected to the maximum stress in an axial test than in a bending test. This

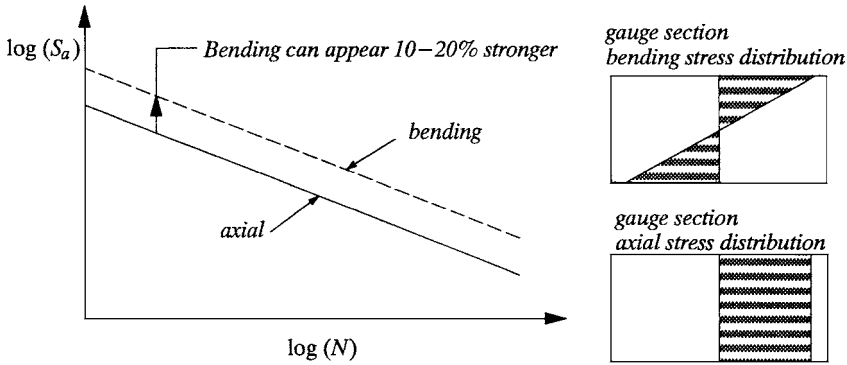


FIG. 5.17 Comparison of stress-life data from axial and rotating-bending test.

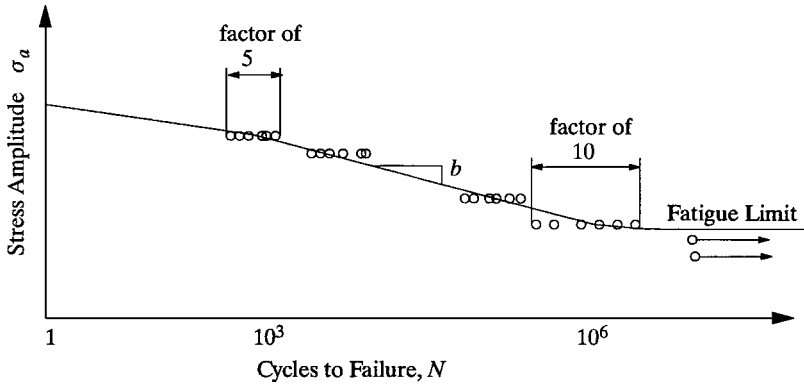


FIG. 5.18 Stress-life fatigue data.

increases the likelihood that a critically sized material defect or properly oriented slip system will experience the most severe stress fluctuation. (2) The bending stress distribution is less severe from the standpoint of crack propagation during microcrack development.

A major benefit to the use of a rotating-bending machine is speed. Motors are used to drive the specimen at a very high rpm, generating data very quickly (e.g., 10,000 rpm). A schematic set of $S-N$ data from such a machine is shown in Fig. 5.18 to illustrate some more fatigue data trends. In Fig. 5.18 and all subsequent $S-N$ plots, axes are logarithmic.

Scatter can plague fatigue data. Factors of 10 or more are not unusual in the high-cycle regime. Scatter is very dependent on cleanliness of material (pores, inclusions, and other microstructural defects). Statistical guidelines from ASTM E-739³⁴ can be very useful in understanding and utilizing fatigue data.

One of the most utilized features of the $S-N$ curve limit is the fatigue limit. It is important to remember that aluminum and other nonferrous metals do not exhibit a fatigue limit. (Fatigue limits are quoted in the literature for aluminum as the stress amplitude corresponding to a very large number of cycles, such as $5 \cdot 10^7$ to $5 \cdot 10^8$.) For ferrous alloys, fatigue limits can be affected by many factors, as outlined below.

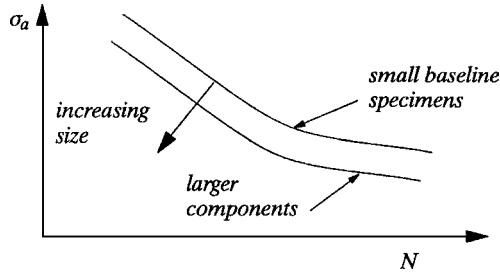


FIG. 5.19 Increasing component size decreases fatigue strength, relative to data generated with small specimens.

- *Size effects.* When a component is considerably larger than the specimen used to generate the baseline fatigue data, a greater volume of material is subjected to a particular stress amplitude. This increases the statistical probability that a microscopic flaw, defect, or slip system will exist that is susceptible to fatigue-crack development. For this reason larger components often fail sooner than smaller specimens, as depicted in Fig. 5.19. This discrepancy is affected by other factors, such as inhomogeneity of microstructure.
- *Type of loading.* Differences between bending and axial loading have already been discussed (Fig. 5.17).
- *Surface processing.* Besides surface roughness in general, plating, nitriding, induction hardening, rolling, shot peening, or any other surface modification can drastically affect the fatigue behavior of a part. Generally, processes improve fatigue resistance if they increase hardness, impose residual compressive surface stresses, and/or reduce surface roughness.
- *Grain size.* This is particularly important for high-cycle fatigue. Typically, smaller grain size means longer fatigue lives. (This is not surprising, since smaller grain size usually means higher yield strength.)
- *Material processing.* The “cleaner” the material, the better its fatigue resistance. For instance, vacuum-melt steel exhibits fatigue lives longer by 50 percent relative to furnace-melt steels. Wrought metals show better fatigue resistance than cast metals (Fig. 5.20). Crack nucleation and microcrack propagation time is avoided since microscopic defects such as inclusions or pores act as instant crack growth sites. (The same can be true for powdered-metal parts.)

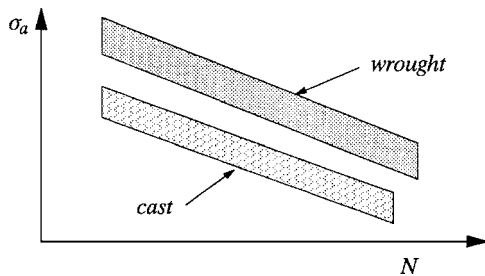


FIG. 5.20 Wrought material is generally more fatigue resistant than cast material.

- *Temperature and environment.* Both of these factors can exhibit profound negative synergism with fatigue mechanisms. (The sum of the two effects can be more than a simple superposition.) When these variables are important, loading frequency and waveform must be considered influential. This is not the case ordinarily (when environmental concerns are not considered influential).
- *Intermittent overloads.* Suppose a component operates in service at a stress level below the fatigue limit, but experiences occasional overloads. Even though the overloads are infrequent and cause no macroscopic plasticity, they can serve to reduce or eliminate the endurance limit.¹³

Numerous attempts have been made to quantify the effects just described.^{1-3,31,32} These are generally presented as empirical factors used to reduce the endurance limit. These factors tend to reduce the high-cycle, finite portion of the $S-N$ curve as well.

Finally, designers are frequently forced to evaluate the endurance of a part for which $S-N$ data are not available. Therefore, several textbooks have suggested empirical approaches to estimate the $S-N$ curve from monotonic tensile data.^{1,3,12} A comprehensive overview of many of these can be found in Dowling.¹³ For example, data have suggested the following relation between the endurance limit and ultimate tensile strength:¹ For wrought steels,

$$\begin{aligned}
 S_e &= 0.5 S_u && \text{for } S_u \leq 200 \text{ ksi} \\
 S_e &= 100 \text{ ksi} && \text{for } S_u > 200 \text{ ksi}
 \end{aligned}
 \tag{5.32}$$

For cast iron,

$$\begin{aligned}
 S_e &= 0.45 S_u && \text{for } S_u \leq 88 \text{ ksi} \\
 S_e &= 40 \text{ ksi} && \text{for } S_u > 88 \text{ ksi}
 \end{aligned}
 \tag{5.33}$$

S-N Finite-Life Prediction. Many factors have caused infinite-life design to become impractical, weight and cost being the primary motivators. It has become more common for designers to anticipate typical service-load histories and design for adequate service lives, building in a reasonable allowance for occasional abusive loading. This can result in components without unreasonably high safety factors that are therefore lighter and less expensive. The methodology to be presented here is intended primarily for use in high-cycle fatigue situations ($N > 10^5$ cycles), although it can be useful in other situations so long as stresses can be accurately determined.

For fatigue design based on finite life, the sloping portion of the curve from $10^3 \leq N \leq 10^6$ in Fig. 5.18 must be known from testing or estimated. If data are available, the log-log linear portion of the curve can be characterized by a power law relation,

$$S_a = C'(N)^{b'}
 \tag{5.34}$$

where C' and b' are curve-fit parameters used to relate the stress amplitude S_a and number of cycles to failure N . In the absence of fatigue data, the following procedure can be used to estimate these parameters:

- Assume the fatigue limit occurs at a life of 10^6 cycles. [If no fatigue limit data are available, estimate S_e from Eq. (5.32) or (5.33).]
- Assume a stress amplitude of $0.9S_u$ corresponding to a life of 1000 cycles, S_{1000} .

This results in a curve as shown in Fig. 5.21. The coefficient and exponent in Eq. (5.34) are therefore given by

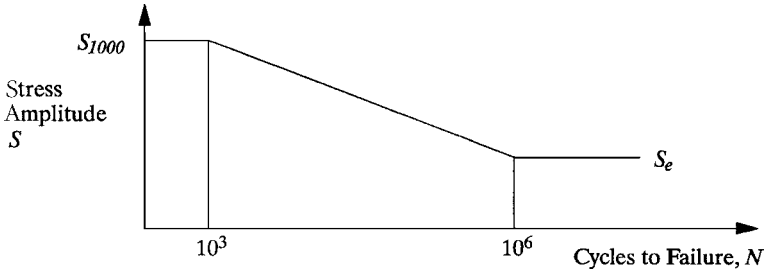


FIG. 5.21 Curve used to approximate $S-N$ data.

$$C' = \frac{(S_{1000})^2}{S_e} \tag{5.35}$$

$$b' = -\frac{1}{2} \log\left(\frac{S_{1000}}{S_e}\right) \tag{5.36}$$

If S_{1000} is assumed to be $0.9S_u$ and S_e to be $0.5S_u$, then $C' = 1.62S_u$ and $b' = -0.0851$.

An equivalent way to express an $S-N$ relation is through the use of the following axial fatigue parameters:

$$S = \sigma_f' (2N)^b \tag{5.37}$$

where σ_f' = fatigue strength coefficient
 b = fatigue strength exponent

This relation is referred to in the literature as the Basquin relation, and its parameters will be discussed in Sec. 5.5.2.

Notice the factor of two that appears in Eq. (5.37). The quantity $2N$ is considered the number of *stress reversals* to failure, since there are two reversals for every cycle (see Fig. 5.22). This is a consequence of some early work on variable-amplitude loading that was taking place while the concept of a “fatigue strength coefficient and exponent” was being developed to characterize fatigue data. At the time, it was felt that considering stress reversals instead of cycles could expedite cumulative fatigue damage analysis. This later proved not to be the case, and consequently, the factor of two must now be accounted for somewhat meaninglessly. This situation is discussed further in Bannantine.³²

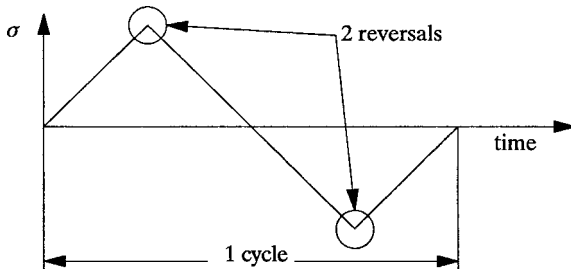


FIG. 5.22 Number of reversals = 2 (number of cycles).

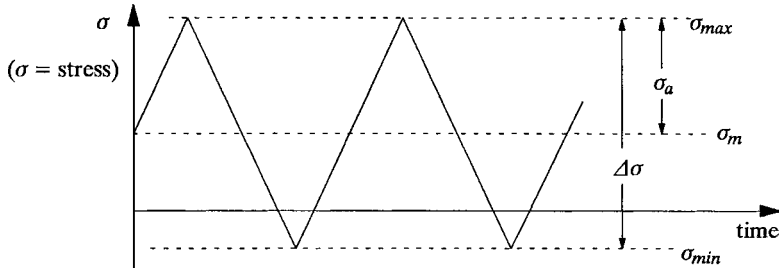


FIG. 5.23 Constant-amplitude loading with a mean stress.

The remainder of this section will be devoted to specifying how to use experimental or estimated baseline $S-N$ data (from constant-amplitude, fully reversed specimen loading) on more complex uniaxial stress histories.

Mean Stress Effects. Baseline data are fully reversed ($R = -1$) but actual engineering components are often subjected to loading with *nonzero* mean stress as depicted in Fig. 5.23. From this figure, several parameters are defined, including the stress ratio,

$$R = \frac{\sigma_{\min}}{\sigma_{\max}} \tag{5.38}$$

stress range,
$$\Delta\sigma = \sigma_{\max} - \sigma_{\min} \tag{5.39}$$

stress amplitude,
$$\sigma_a = \frac{\sigma_{\max} - \sigma_{\min}}{2} \tag{5.40}$$

and mean stress,
$$\sigma_m = \frac{\sigma_{\max} + \sigma_{\min}}{2} \tag{5.41}$$

Mean stresses can act to shorten or lengthen fatigue life, depending on (1) whether the mean stress is positive or negative and (2) whether the loading is predominantly elastic or plastic. This is depicted schematically in Fig. 5.24.

Tensile mean stresses superimpose with applied loading to decrease fatigue life while compressive mean stress decreases the applied loading to increase fatigue life.

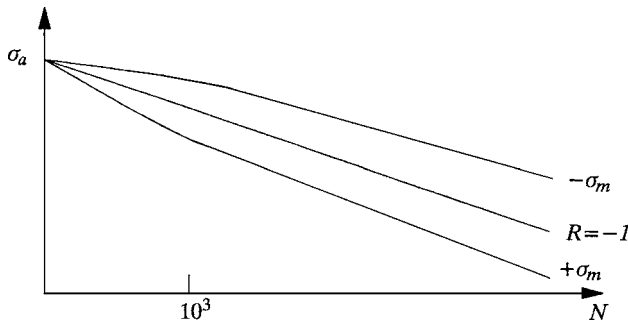


FIG. 5.24 Mean stress effect on $S-N$ curve.

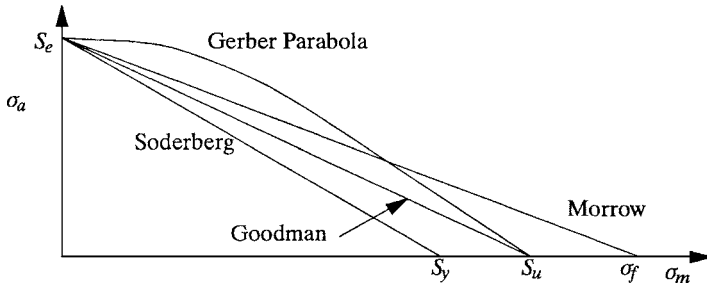


FIG. 5.25 Mean stress constant-life plots (endurance limit).

Mean stress relaxation can occur at higher load levels, diminishing the effect of mean stress at lower lives. This is particularly true when a component has a notch, as discussed later.

Mean stress data are often presented as plots of stress amplitude versus mean stress, corresponding to a particular life. For instance, Fig. 5.25 shows plots of several empirical relations to account for mean stress that have been suggested from testing at endurance-limit load levels. The curves represent combinations of mean stress and stress amplitude (σ_m and σ_a) that correspond to the fatigue limit S_e . Data sets have indeed been shown to lie in the vicinity of these lines and occasionally suggest that particular relations do a better job than others. However, in practice, none of these has been universally agreed upon as superior. In general, the Soderberg line has been determined to be too conservative for practical design use. The Goodman line and Gerber parabola are often more accurate than the Morrow relation. Another popular parameter was proposed by Smith, Watson, and Topper (SWT).³⁶ This relation is shown schematically with a Goodman line in Fig. 5.26.

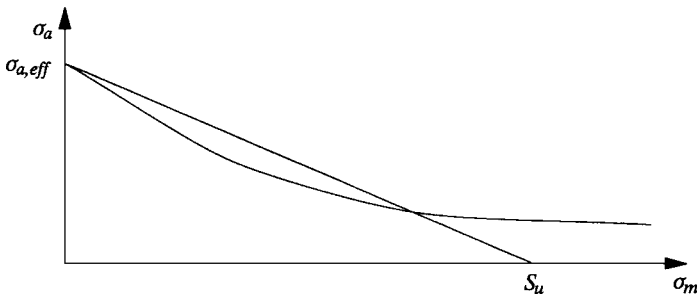


FIG. 5.26 Constant-life plots for Goodman and Smith-Watson-Topper relations.

The curves in Fig. 7.25, considered to describe the *fatigue limit*, can be extended to the finite-life regime by considering combinations of stress amplitude and mean stress that result in a particular life corresponding to a fully reversed test conducted at a stress amplitude of $\sigma_{a,eff}$. Schematically, this *effective, fully reversed stress amplitude* concept is depicted in Fig. 5.27. The effective stress amplitude, $\sigma_{a,eff}$, provides a conceptually straightforward approach to account for mean stress effect based on fully reversed baseline data. Relations for $\sigma_{a,eff}$ are given in Eqs. (5.42) to (5.46) for the criteria illustrated in Figs. 5.25 and 5.26:

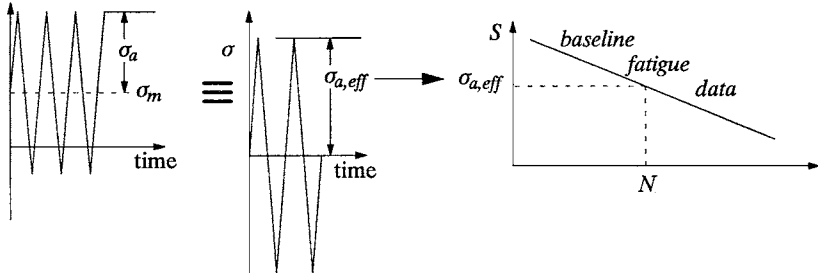


FIG. 5.27 Effective stress-amplitude concept.

Goodman:
$$\sigma_{a,eff} = \sigma_a \left(\frac{S_u}{S_u - \sigma_m} \right) \tag{5.42}$$

Soderberg:
$$\sigma_{a,eff} = \sigma_a \left(\frac{S_y}{S_y - \sigma_m} \right) \tag{5.43}$$

Morrow:
$$\sigma_{a,eff} = \sigma_a \left(\frac{\sigma_f}{\sigma_f - \sigma_m} \right) \tag{5.44}$$

Gerber:
$$\sigma_{a,eff} = \sigma_a \left(\frac{S_u^2}{S_u^2 - \sigma_m^2} \right) \tag{5.45}$$

Smith-Watson-Topper:
$$\sigma_{a,eff} = \sqrt{\sigma_a (\sigma_a + \sigma_m)} \tag{5.46}$$

Equations (5.42) to (5.45) are illustrated again in Fig. 5.28. These curves differ from those in Fig. 5.25. Each curve is based on the same input point, that is, the state of stress in the engineering component defined by σ_a and σ_m . But, each implies a different $\sigma_{a,eff}$ corresponding to the applied stress state. These curves make it apparent that Soderberg is the most conservative from a designer’s perspective, since it specifies the highest effective stress, and Gerber is the least conservative.

One final note should be made before leaving mean stress effects. The relations illustrated so far have been discussed primarily in the context of positive mean stress.

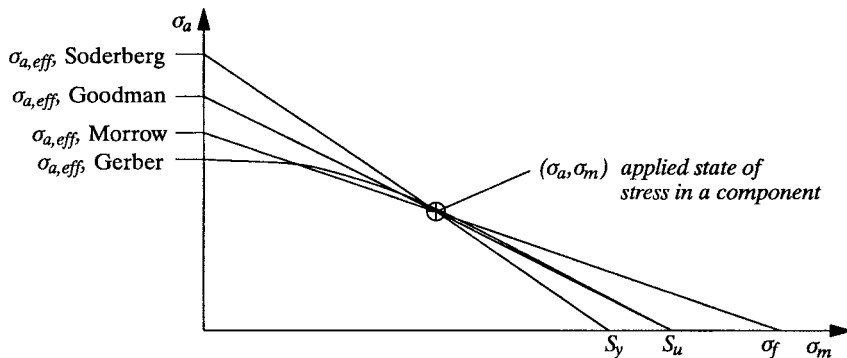


FIG. 5.28 Definition of $\sigma_{a,eff}$ from relations in Fig. 5.27.

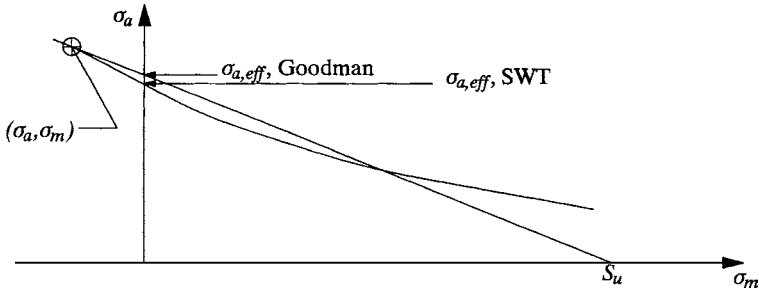


FIG. 5.29 Extension of Goodman and SWT relations into compressive mean stress regime.

The fact that tensile mean stresses have a deleterious effect on fatigue is modeled by the $\sigma_{a,eff}$ concept. (For example, increasing σ_m increases $\sigma_{a,eff}$ and decreases estimated life.) However, there are valuable data³⁷ that demonstrate the beneficial effect of compressive mean stress on fatigue. Therefore, a compressive mean stress should decrease $\sigma_{a,eff}$. (This is not the case for the Gerber parabola.) The Goodman and SWT relations have been shown to do a good job for small compressive stresses, as illustrated in Fig. 5.29. (“Small” is defined as having a magnitude of less than about $0.5S_y$. A more comprehensive treatment of compressive mean stress effects can be found in Ref. 31.)

The fact that compression can enhance fatigue life can be taken advantage of through material processes such as shot peening, proof loading, carburizing, nitriding, and induction hardening. All of these processes impose large compressive residual stresses at the surface of the material, reducing effective stress amplitudes and increasing fatigue life. (The latter three also considerably harden the surface layer.) Thread rolling and hole stretching are other processes that enhance fatigue resistance by inducing residual surface compression.

Notches. Figure 5.6 illustrated the concept of an elastic stress-concentration factor K_t defined as the maximum elastic stress at the notch root, divided by the nominal stress (based on net section area). Since the notch stresses increase according to K_t , it would be convenient, analytically, if fatigue strengths were reduced proportionally. However, the effect that a notch has on fatigue is dependent on

- Notch severity (magnitude of K_t)
- Material strength and ductility
- The applied nominal stress magnitude

Figure 5.30 illustrates how a notch can affect a set of fatigue data, relative to smooth-specimen data. Stress-concentration factor effects tend to diminish at lower lives since localized plastic flow can reduce the stress amplitude at the notch root, as shown in Fig. 5.31. At longer lives, K_t does a better job describing notch fatigue strength, but tends to overestimate the effect. Several factors can explain the reduced effect of K_t on fatigue. These include (1) the fact that localized stresses are reduced by yielding, (2) the effect of subsurface stress gradient (microcracks growing into a decreasing stress field), and (3) the fact that only a small volume of material experiences the extreme localized concentrated stresses. From a design point of view, using the full value of a stress-concentration factor to compute notch stresses ($\sigma_{notch} = K_t S_{nom}$) is a very safe way to operate, since notch effects are overestimated.

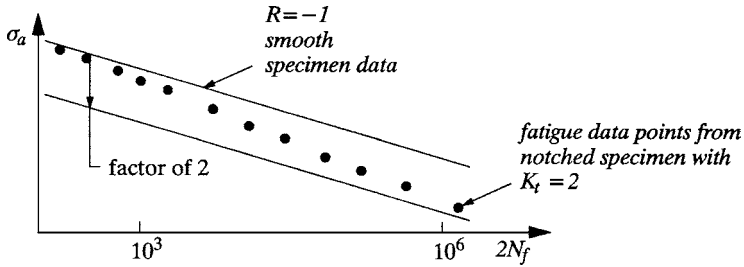


FIG. 5.30 Notch effect on $S-N$ behavior.

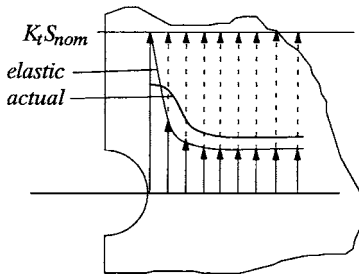


FIG. 5.31 Illustration explaining how elastically calculated K_t can overestimate the effect of a notch on fatigue behavior. Localized yielding and subsurface gradients are apparent.

Fatigue Notch Factors. Recognizing that K_t overestimates fatigue-strength reduction, the concept of an empirical fatigue notch factor (also called a fatigue-strength reduction factor) was developed. The fatigue notch factor K_f is defined from a comparison of fatigue data generated with smooth and notched specimens, as shown in Fig. 5.32.

Unfortunately, the use of fatigue notch factors in design is not straightforward. In many instances, K_f has been shown to vary with life, as is apparent in Fig. 5.32. Furthermore, it can only be reliably determined empirically (by experiment) for the material, geometry, and surface processing of interest.

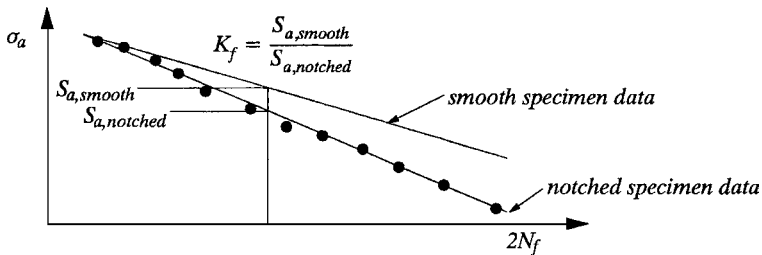


FIG. 5.32 Definition of fatigue notch factor.

To quantify the fatigue-strength reduction associated with a notch, a notch-sensitivity factor was developed as defined in Eq. (5.47):

$$q = \frac{K_f - 1}{K_t - 1} \tag{5.47}$$

where q varies from 0 to 1:

- $q = 0$ no notch effect ($K_f = 1$)
- $q = 1$ full elastic effect ($K_f = K_t$)

Some researchers have attempted to formulate empirical relations for K_f based on K_p for fatigue-limit load levels. One approach, proposed by Peterson, is given by

$$K_f = 1 + \frac{K_t - 1}{1 + (a/r)} \tag{5.48}$$

where r = the notch root radius

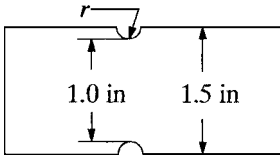
a = a “characteristic length” (empirical curve-fit parameter)

$$\alpha \cong \left(\frac{300}{S_u \text{ (ksi)}} \right)^{1.8} \times 10^{-3} \text{ in} \tag{5.49}$$

For steels, a rule of thumb assessment of the parameter α is often cited:

Annealed steel	Quenched and tempered	Highly hardened
$\alpha \approx 0.010 \text{ in}$	$\alpha \approx 0.0025 \text{ in}$	$\alpha \approx 0.001 \text{ in}$

Consistent with this is the general assessment that harder materials are more notch sensitive than softer materials. Example 5 uses Eq. (5.48) to illustrate this point. It should be remembered that no such empirical relations have been proposed for aluminum or other nonferrous materials.



EXAMPLE 5 This example illustrates the effects of tensile strength and notch severity on the estimated values of the fatigue notch factor. Use Eqs. (5.48) and (5.49) to compute K_f for the two different steels and three different notch root radii.

solution The values of K_f are tabulated below for two steels and three values of r :

Material A		Material B	
$S_u = 68 \text{ ksi}$		$S_u = 180 \text{ ksi}$	
$\alpha = 0.015 \text{ in}$		$\alpha = 0.0025 \text{ in}$	
$r \text{ (in)}$	K_t	Material A	Material B
		$K_f (S_u = 68)$	$K_f (S_u = 180)$
0.2	2.05	1.98	2.03
0.05	3.5	2.92	3.38
0.01	6.0	3.0	5.0

The K_f relations and the example shown above are valid only for fully reversed loading ($R = -1$). Mean stresses can affect notched components differently than smooth ones. To accurately analyze a particular situation, empirical data are usually necessary.

A great deal of data have been generated in the aerospace industry and are published in the form of plots^{38,39} such as the one shown in Fig. 5.33. These plots provide direct information on the combined effects of the mean stress and the stress-concentration factor.

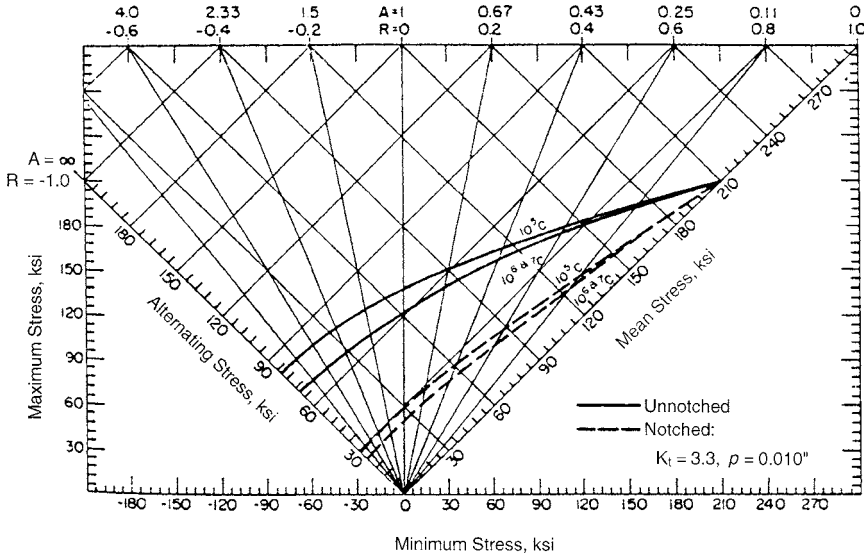


FIG. 5.33 Constant-life plots from MIL Handbook 5 (AISI 4340); $S_u = 208$ ksi.

A final important trend is noted by those who have studied fatigue notch factors: there appears to be an upper limit to K_f of about 5 or 6 for very sharp notches.³² Two possible explanations for this are: (1) the notch tip blunts, reducing K_f , or (2) the notch constitutes a crack and removes the initiation life of the component.

A safe, recommended approach suitable for design is outlined in Table 5.2 for uniaxial loading situations. If more detailed data are available, they can be incorporated into the approach as outlined below:

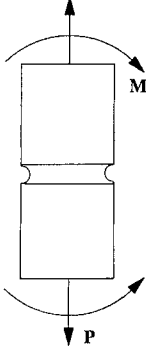
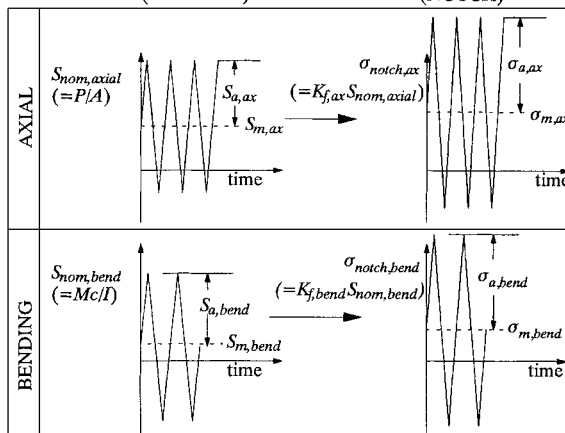
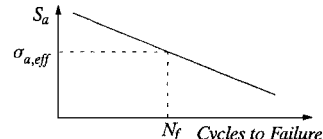
- Use a measured rather than estimated K_f over the entire range of life.
- Estimate the variation of K_f with life experimentally, or from a source such as that found in “MIL Handbook 5,” Fig. 5.33.
- If estimates are unduly conservative, use only the nominal mean stresses ($\sigma_{m,notch} = S_{m,ax} + S_{m,bend}$) to compute the notch mean stress.
- Use only nominal stress amplitudes, and modify baseline $S-N$ data using approaches detailed in Refs. 13 and 32.

5.5.2 Strain-Life Approaches (Constant-Amplitude Loading)

Cyclic Stress-Strain Relation. A standard, low-cycle fatigue specimen is fabricated and tested according to ASTM E-606, “Standard Recommended Practice for Constant-Amplitude Low-Cycle Fatigue Testing,”⁴⁰ in strain control. A typical specimen is depicted in Fig. 5.34, along with a stabilized cyclic stress-strain loop.

When fatigue testing is conducted, several specimens (ideally, at least 20) are tested at varying strain amplitudes. At each strain amplitude, a different stabilized loop forms, as depicted in Fig. 5.35. From these loops, the cyclic stress-strain curve may be

TABLE 5.2 Elastic Uniaxial Stress-Life Design Approach

(1) Obtain or otherwise estimate fully-reversed S-N data for material of interest using $S_a = C'(N)^{b'}$ OR $S_a = \sigma_f'(2N)^b$	
(2) Use K_f to estimate stresses at notch from in-phase bending and axial loading.	
<p>$K_{f,ax}$ = axial K_f (estimated from axial K_f) $K_{f,bend}$ = bending K_f (estimated from bending K_f)</p> 	<p>(NOMINAL) → (NOTCH)</p> 
(3) Combine axial and bending notch stresses into uniaxial notch stress history. NOTCH STRESS AMPLITUDE: $\sigma_{a,notch} = \sigma_{a,ax} + \sigma_{a,bend}$ NOTCH MEAN STRESS: $\sigma_{m,notch} = \sigma_{m,ax} + \sigma_{m,bend}$	
(4) Compute <i>effective fully-reversed notch stress amplitude</i> , using appropriate mean stress relation.	
(Goodman)	(SWT)
$\sigma_{a,eff} = \sigma_{a,notch} \left(\frac{S_u}{S_u - \sigma_{m,notch}} \right)$	OR $\sigma_{a,eff} = \sqrt{\sigma_{a,notch}(\sigma_{a,notch} + \sigma_{m,notch})}$
(5) Use effective notch stress amplitude to enter baseline S-N data to predict life $N_f = \left(\frac{\sigma_{a,eff}}{C'} \right)^{1/b'}$ OR $N_f = \frac{1}{2} \left(\frac{\sigma_{a,eff}}{\sigma_f'} \right)^{1/b}$	

defined from the locus of the tips of the stabilized hysteresis loops, and expressed using a Ramberg-Osgood²⁸ relation:

$$\epsilon_a = \frac{\sigma_a}{E} + \left(\frac{\sigma_a}{K'} \right)^{1/n'} \tag{5.50}$$

where K' = cyclic strength coefficient
 n' = cyclic strain-hardening exponent

In this relation, ϵ_a and σ_a represent strain and stress *amplitudes*, respectively. The curve therefore represents a relation between stress and elastic-plastic strain amplitudes that form during fully reversed strain-controlled testing.

The formation of the stabilized hysteresis loops depicted in Figs. 5.34 and 5.35 usually requires a substantial number of cycles, during which transient softening or hardening may occur. Such behavior is depicted in Fig. 5.36. This can cause the cyclic stress-strain relation to lie below or above the monotonic curve. If the cyclic curve is

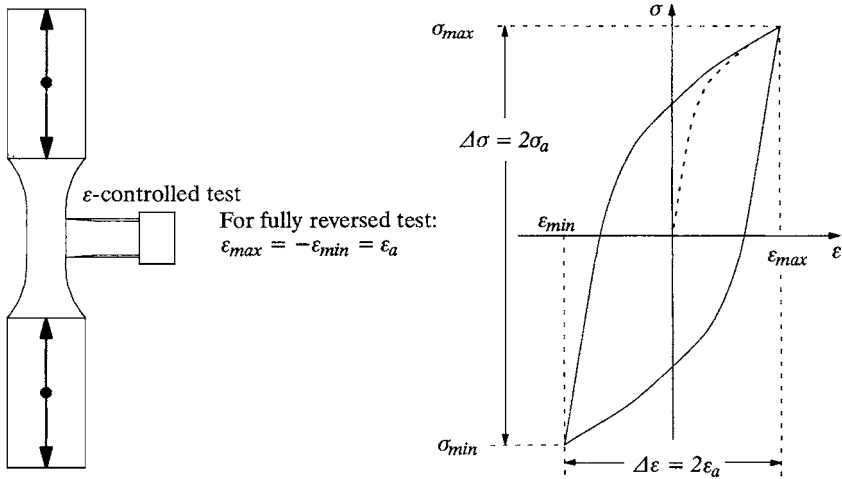


FIG. 5.34 Stabilized stress-strain hysteresis loop from typical ASTM E-606 fatigue test.

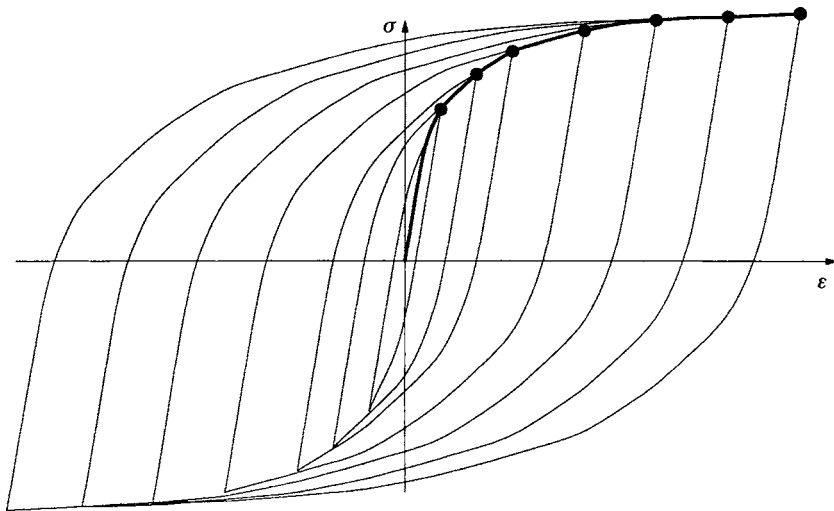


FIG. 5.35 Cyclic stress-strain curve from stable hysteresis loops.

below the monotonic curve, the material can be called a “cyclic softening material.” If the cyclic curve is above the monotonic curve, the material “cyclically hardens.” Mixed behavior is also observed, depending on the strain amplitude. Examples of each situation are shown in Fig. 5.37.

The transient stress behavior during a typical strain-controlled test is depicted differently in Fig. 5.38 for a cyclically softening material. This figure is a plot of peak and valley stress components at each reversal point throughout the life of the material. There are several noteworthy features to this plot. First, cyclic stabilization is shown to occur within about 10–20 percent of the total life. This depends on the material

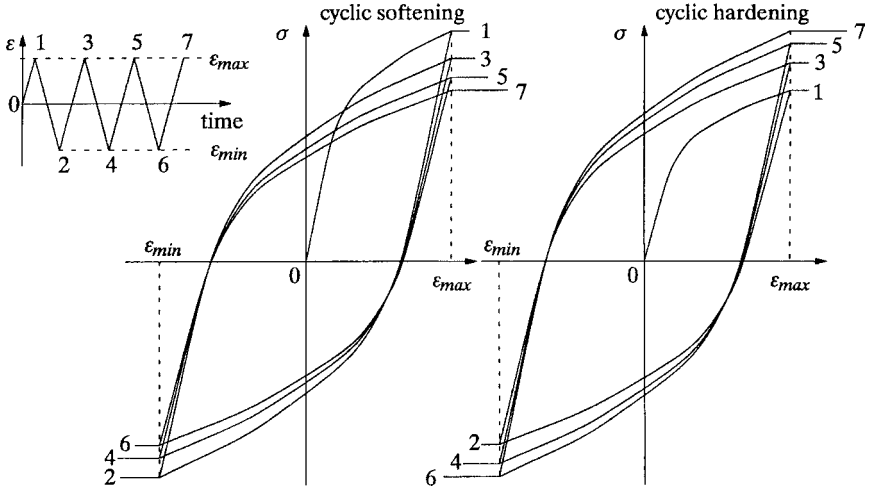


FIG. 5.36 Transient softening and hardening occurring on the first few cycles.

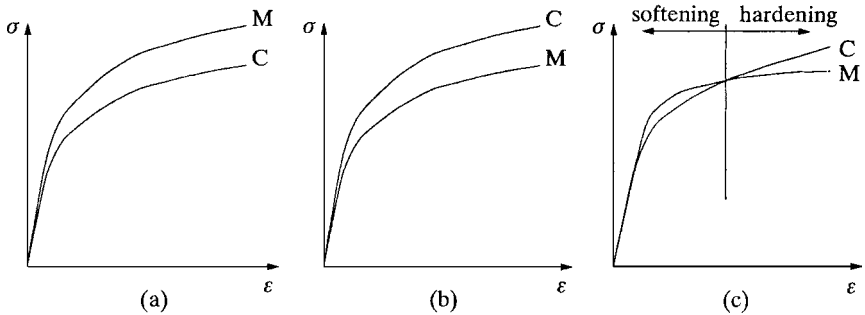


FIG. 5.37 Monotonic (*M*) and cyclic (*C*) stress-strain curves for (a) cyclic softening material, (b) cyclic hardening material, and (c) mixed transient behavior.

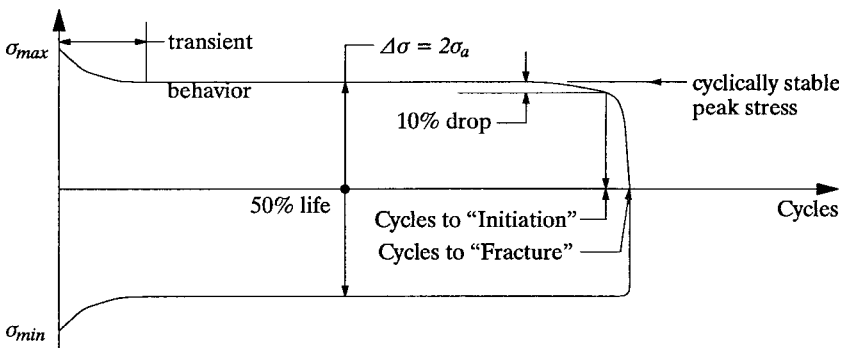


FIG. 5.38 Typical peak and valley stresses versus cycle for a strain-controlled test.

being tested, and the strain amplitude. At larger applied strains (lower lives), stabilization can be less pronounced (that is, the maximum stress can change gradually over the entire test). For this reason, the stabilized stress amplitude is usually defined as the stress amplitude at the “half-life” of the specimen (at near 50 percent of its total life). Near the end of the life of the specimen, notice in Fig. 5.38 how the peak tensile stress drops just prior to final fracture. This results from the decrease in specimen stiffness associated with crack formation. Therefore, this drop in the maximum stress is typically used to define the “crack initiation life” of the specimen, as opposed to the total number of cycles to fracture. (Notice how the compressive valley stress is maintained throughout the test, since the crack faces can sustain the compressive loading.) Some testing laboratories use a peak load drop of 10 percent from the half-life value to define initiation, others use a larger value, such as 50 percent, while others simply use the life to fracture. The discrepancy this causes is usually considered negligible, since the life of a specimen after a discernable crack (“engineering-sized,” on the order of 1 to 2 mm in surface length) has formed is generally a small percentage of the life to fracture. However, the subjectivity associated with reducing low-cycle fatigue data is apparent, especially in the low-cycle regime. It is advised that stress-versus-time data be obtained and reviewed by the engineer when low-cycle fatigue testing is conducted.

The definition of the cyclic stress-strain curve requires the testing of several specimens. This is referred to as “companion specimen” testing. Attempts have been made to define the curve from a single test called the “incremental step test.”⁴¹ It should be noted that this technique can only approximate the curve and not enough data exist to assess its general reliability.

Refer again to Fig. 5.35, and recall that the dark cyclic stress-strain curve [Eq. (5.50)] is defined by the tips of the hysteresis loops. The light curves (referred to as hysteresis curves) can be approximated well by scaling the dark curve, geometrically, by a factor of two. This is referred to as Massing’s hypothesis.⁴² To demonstrate this, refer to Fig. 5.39.

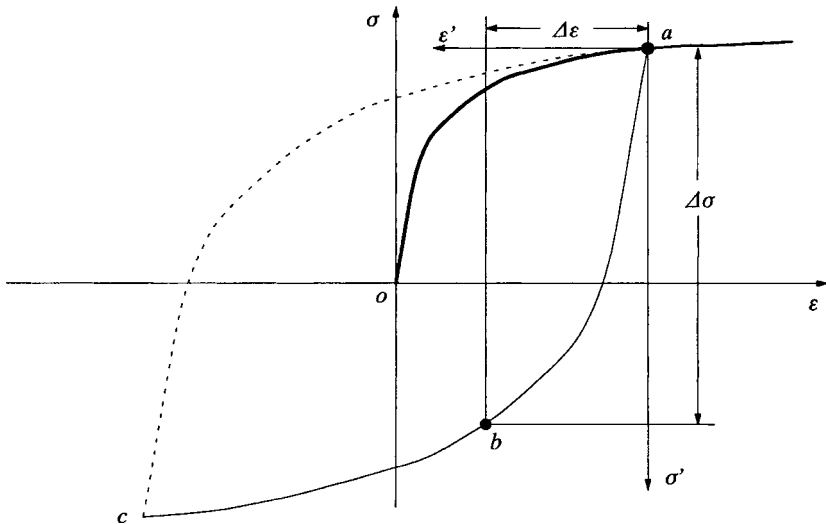


FIG. 5.39 Demonstration of Massing’s hypothesis: Solid curve $a-b-c$ is equal to dark curve $o-a$, geometrically doubled by a factor of two. The dashed curve $c-a$ is obtained by rotating the solid curve, $a-b-c$, by 180° .

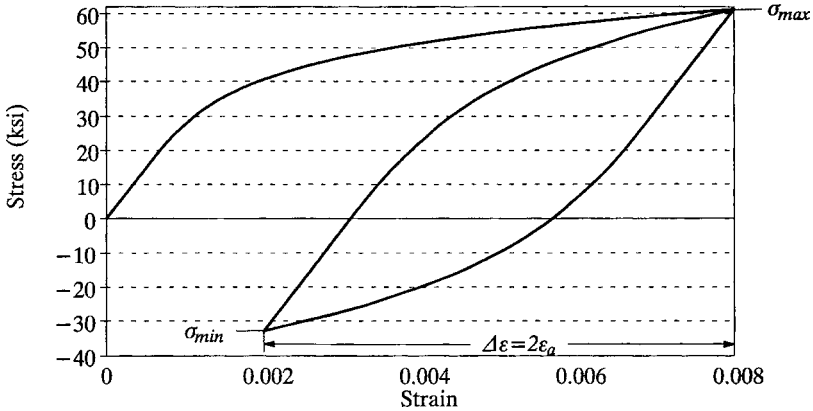


FIG. 5.40 Cyclically stable hysteresis loop computed for Example 6.

In Fig. 5.39, the dark curve from *o* to *a* is the cyclic stress-strain curve. The light curve from *a* to *b* to *c* is the reverse-loading hysteresis curve. The expression for the hysteresis curve on σ - ϵ axes is given by

$$\Delta\epsilon = \frac{\Delta\sigma}{E} + 2\left(\frac{\Delta\sigma}{2K'}\right)^{1/n'} \tag{5.51}$$

Notice that Eq. (5.51) is given in terms of stress and strain *ranges* (denoted by “ Δ ”). This is illustrated for point *b* along the curve *a-b-c* in Fig. 5.40. For fully reversed loading, the reversal at *c* would be followed by a stress-strain path along the dashed line from *c* back to *a*.

This is important, since it can be used to reveal the location (on σ - ϵ axes) where a stable hysteresis loop will form during constant-amplitude strain-controlled loading that is *not* fully reversed. The ability to estimate the form of the hysteresis curve provides a mechanism to estimate the path-dependent plasticity behavior of the material under axial loading. The use of this approach is demonstrated in Example 6 for constant-amplitude loading. Life prediction for this example will be discussed later (as will the use of this approach with variable-amplitude loading).

EXAMPLE 6 Consider an axial specimen with the following properties:

$$\begin{aligned} E &= 30,000 \text{ ksi} \\ K' &= 156.88 \text{ ksi} \\ n' &= 0.184 \end{aligned}$$

The specimen is to be subjected to strain-controlled cyclic loading between maximum and minimum values of 0.008 and 0.002. Compute the corresponding maximum and minimum stress and plot the cyclically stable hysteresis loop.

solution Using Eq. (5.50), the stress amplitude is computed that would correspond to a strain amplitude of 0.008, if the loading were fully reversed. By trial and error, this value is found to be 61.13 ksi:

$$0.008 = \frac{61.13 \text{ ksi}}{E} + \left(\frac{61.13 \text{ ksi}}{K'}\right)^{1/n'}$$

Now, the stress range $\Delta\sigma$ corresponding to a strain range, $\Delta\varepsilon$, of 0.006 is computed. This corresponds to $\varepsilon_{\max} - \varepsilon_{\min} = 0.008 - 0.002 = 0.006$. Equation (5.51) is used to define a value of $\Delta\sigma = 94.05$ ksi:

$$0.006 = \frac{94.05 \text{ ksi}}{E} + 2\left(\frac{94.05 \text{ ksi}}{2K'}\right)^{1/n'}$$

From these values, the stress is estimated to fluctuate from a maximum of 61.13 ksi to a minimum of $(61.13 - 94.05 =) -32.92$ ksi. The corresponding stable hysteresis loop is shown in Fig. 5.40.

Strain-Life Relation. As discussed in the preceding section, strain-controlled companion specimen fatigue testing per ASTM E-606⁴⁰ results in strain-amplitude versus cycles-to-failure data (defined as complete specimen fracture or the formation of detectable cracks). As shown in Fig. 5.41, the cyclically stable total strain amplitude can be divided into elastic and plastic components. This can be expressed as

$$\varepsilon_a = \varepsilon_a^e + \varepsilon_a^p \tag{5.52}$$

where the superscripts *e* and *p* represent elastic and plastic components, respectively. In 1910 Basquin⁴³ is credited with the observation that log-log plots of stress amplitude (and, therefore, elastic strain amplitude) versus life data behaved linearly. Manson⁴⁴ and Coffin,⁴⁵ working independently, later observed that log-log plots of plastic strain versus life were also linear. These two observations were combined into the now familiar form

$$\varepsilon_a = \frac{\sigma_f'}{E}(2N_f)^b + \varepsilon_f'(2N_f)^c \tag{5.53}$$

$$\varepsilon_a = \varepsilon_a^e + \varepsilon_a^p$$

where σ_f' = fatigue strength coefficient
b = fatigue strength exponent

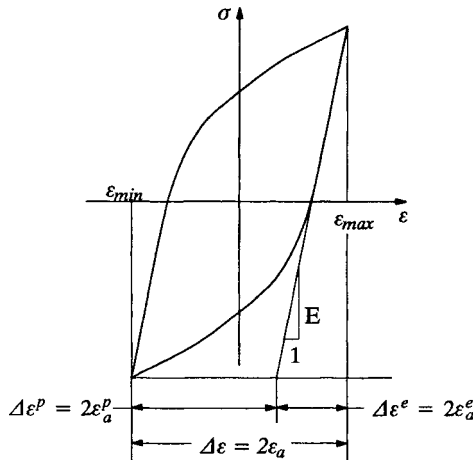


FIG. 5.41 Definition of elastic and plastic strain amplitude from total strain amplitude.

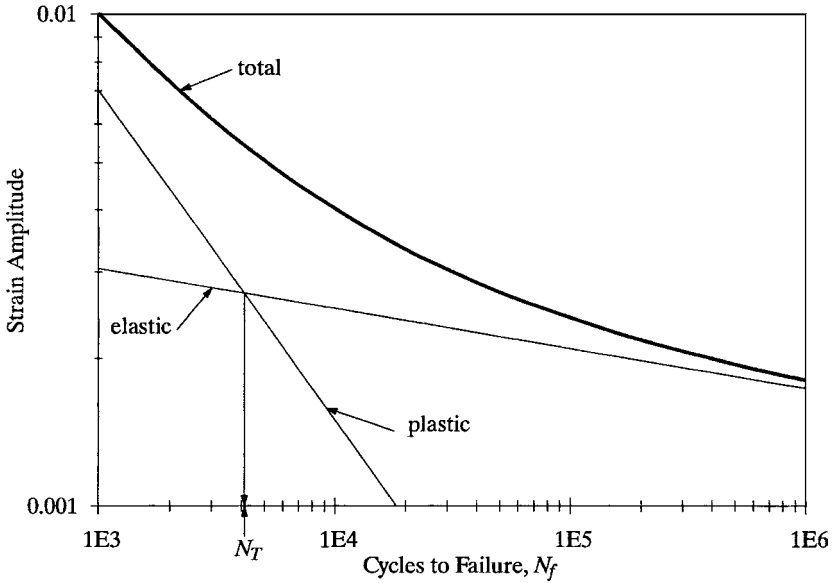


FIG. 5.42 Strain-life relation for a medium-strength steel.⁴⁹

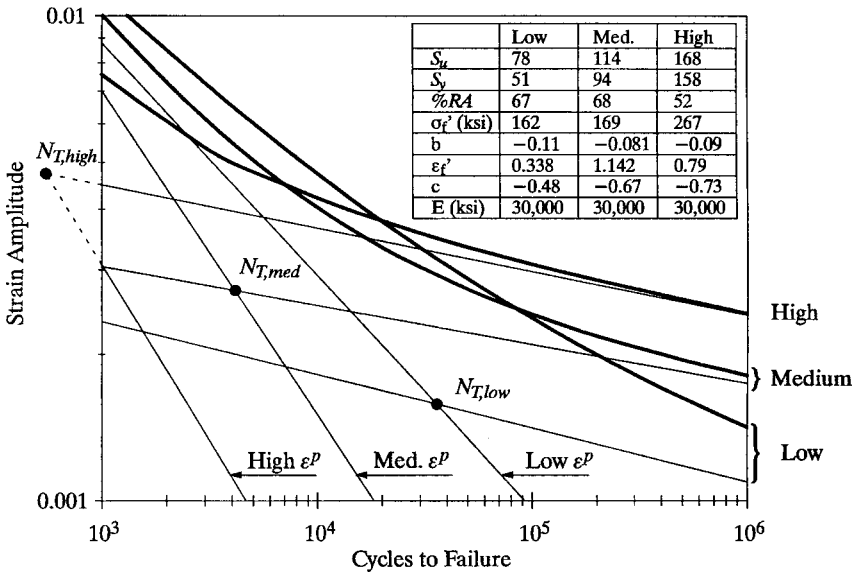


FIG. 5.43 Strain-life relation for a low-strength,⁵⁰ medium-strength,⁴⁹ and high-strength⁵¹ steel.

- ϵ_f' = fatigue ductility coefficient
- c = fatigue ductility exponent
- E = modulus of elasticity
- N_f = number of cycles to failure

Equation (5.53) serves as the foundation of local strain-based fatigue analysis.^{13,23,31,32,46-48} It is plotted in Fig. 5.42 for a medium-strength steel.⁴⁹ The “transition life,” N_p is also depicted in Fig. 5.42, as the life at which the elastic and plastic strain amplitudes are equal. The transition life can provide an indication of whether straining over a life regime of interest is more elastic or plastic. In general, the higher the tensile strength of the materials, the lower the transition life, and elastic strains tend to dominate for a greater portion of the overall life regime. To demonstrate this, Fig. 5.43 shows the same strain-life curve from Fig. 5.42, replotted with curves for a low-strength steel⁵⁰ and a high-strength steel.⁵¹

Inspection of Fig. 5.43 is interesting from the standpoint of selecting a material for maximum fatigue resistance. For example, in the higher-cycle life regime ($>10^5$ cycles) the higher-strength material provides the greatest fatigue strength. But for a component that must operate in the lower life regime ($<10^4$ cycles) the selection of the lowest-strength steel might be warranted. The medium-strength material could represent a more suitable selection if a combination of high strength and fatigue resistance is required.

As a consequence of Eqs. (5.52) and (5.53), and the Ramberg-Osgood formulation of the cyclic stress-strain curve [Eq. (5.50)], it is apparent that the cyclic strength coefficient and cyclic strain-hardening exponent may be expressed in terms of the fatigue strength and ductility coefficients and exponents as follows:

$$K' = \frac{\sigma_f'}{(\epsilon_f')^{n'}} \tag{5.54}$$

$$n' = \frac{b}{c} \tag{5.55}$$

However, experience has shown that parameters formed this way can result in a stress-strain curve that *does not* correlate well with actual stress versus strain-amplitude data points. For this reason, use of Eqs. (5.54) and (5.55) is not recommended if K' and n' may be fit directly to data.

Values for cyclic stress-strain and fatigue parameters can be found in Refs. 52 through 54. Unfortunately, tabulated data are available for only a fraction of available engineering alloys and heat treatments. Although such data are becoming more and more available, situations routinely arise where a designer must estimate fatigue properties without the availability of fatigue testing data.

Several attempts have been made to correlate fatigue parameters with monotonic tensile properties,^{46,55-57} but no clearly superior approach has been identified. Table 5.3 summarizes several approaches.

These relations should be used *only with a great deal of caution*. The universal slopes⁵⁵ approach, the Socie et al.⁵⁷ approach, and a more complicated four-point correlation approach were compared to data in Ref. 58. The four-point correlation method provided the best approximation but requires the true fracture stress, a quantity not generally reported during tensile testing. The potential for any of the approaches to provide poor life estimates is great. Considering the differences in deformation and failure mechanisms (on a microscopic level) between monotonic and cyclic loading, limited correlation is not surprising.

Some final notes about the limitations of strain-life data are in order. Equation (5.53) is based on data generated with polished specimens. (ASTM E-606 recommends

TABLE 5.3 Approximate Relations between Tensile Properties and Fatigue Parameters

	Universal slopes ⁵⁵	Modified universal slopes ⁵⁶	Socie et al. ⁵⁷
σ'_f	$1.9018 S_u$	$0.6227E \left[\frac{S_u}{E} \right]^{0.832}$	$S_u + 345 \text{ MPa}$
b	-0.12	-0.09	$-\frac{1}{6} \log \left(\frac{2(S_u + 345 \text{ MPa})}{S_u} \right)$
ϵ'_f	$0.7579 \left[\ln \left(\frac{1}{1-RA} \right) \right]^{0.6}$	$0.01961 \left[\ln \left(\frac{1}{1-RA} \right) \right]^{0.155} \left[\frac{S_u}{E} \right]^{-0.53}$	$\ln \left(\frac{1}{1-RA} \right)$
c	-0.6	-0.56	-0.6

that specimens be ground and longitudinally lapped to a surface finish of $8 \mu\text{in}$ or better, with no circumferential grinding marks observable at $20 \times$ magnification.) In the higher life regime, strain-controlled fatigue data are affected by the same factors that can affect stress-life data (surface finish, inclusions, defects, size, etc.). Although it is recognized in the literature that adjustments are necessary to account for surface effects, no accepted methodology to accomplish this exists. It is suggested²³ that the elastic portion of Eq. (5.53) can be modified, by adjusting the fatigue strength exponent b . However, this often affects the total strain-life curve into the lower-cycle regime as well, as is apparent in Fig. 5.44.

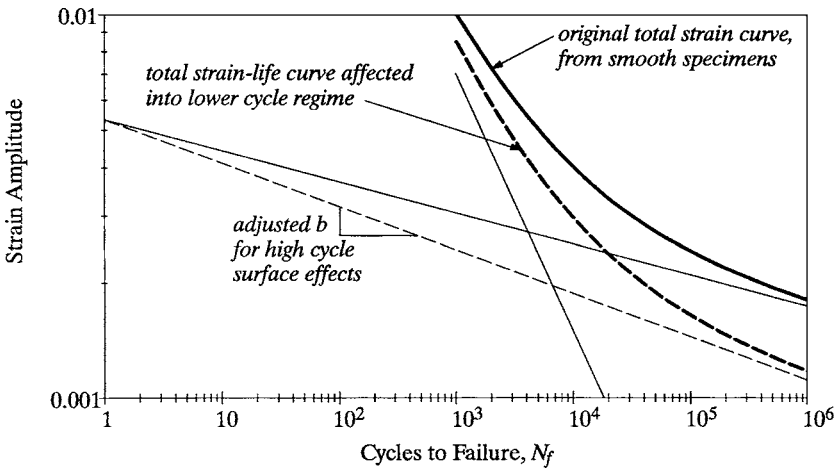


FIG. 5.44 Modifying the strain-life relation by adjusting b to account for surface roughness effects can influence the curve over the entire life regime.

Along these same lines, the strain-life equation itself has no mechanism to incorporate a fatigue limit. When lives in the vicinity of the endurance limit are being considered ($\geq 10^6$ – 10^7 cycles), the use of stress-based approaches should be considered.

Finally, it can be useful to obtain as much information about a particular data set as possible. Recall that “failure” in strain-controlled tests can be defined as complete fracture, or a drop in the cyclically stable maximum stress (typically 10 to 50 percent). This can be significant, especially if there is a substantial difference between the size of the component being analyzed and the size of the specimens used to generate the

data. Published data sets are often based on a very small number of data, generated over a fairly narrow range. There is scatter associated with all fatigue data, and generating more data could change associated strain-life curves drastically. Furthermore, additional uncertainty is associated with utilizing the strain-life relation outside the range over which data were collected. Knowing the range of experimental lives could be very worthwhile toward assessing the reliability of a fatigue life estimate.

Mean Stress Effects. The standard strain-life relation, Eq. (5.53), is formulated from fully reversed ($R = -1$) strain-controlled test data. However, engineering components are often subjected to loading that induces mean stresses (strains). Although the effect of mean stress on fatigue has been discussed, mean strain, in general, has little effect. For example, consider the stress-strain response during a mean strain axial fatigue test as depicted in Fig. 5.45. The mean stress in the specimen is shown to relax to a cyclically stable response by the seventh reversal. (This response is somewhat exaggerated, as many more cycles are usually required.) This should not be confused with cyclic softening, since cyclically stable materials can exhibit relaxation.

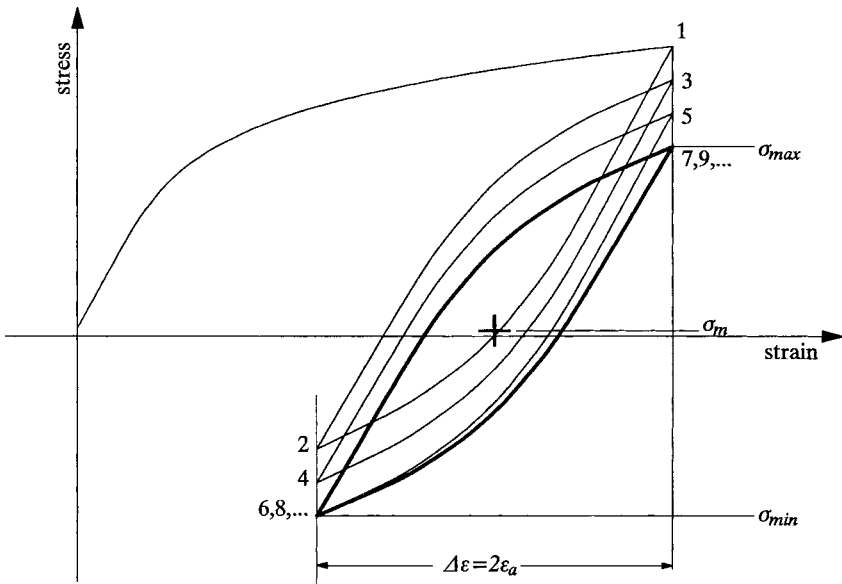


FIG. 5.45 Stress relaxation during a mean strain axial fatigue test.

Mean stress relaxation is the main reason that mean stresses tend to have more of an effect on high-cycle fatigue than on low-cycle fatigue. For high-cycle situations, loading is typically elastic and mean stresses relax little (if any).

Several approaches have been proposed to account for mean stresses with strain-based analysis.^{13,31,32} The most effective of these is the Smith-Watson-Topper³⁶ relation, already discussed in terms of stresses. This approach is based on empirical observations that the product of the stabilized maximum stress and the strain range (or amplitude) during a cycle is proportional to life [Eq. (5.56)]. From fully reversed data, the maximum stress can be approximated in terms of life as Eq. (5.57).

$$\sigma_{\max} \epsilon_a \propto N_f \tag{5.56}$$

$$\sigma_{\max} = \sigma'_f (2N_f)^b \tag{5.57}$$

Equations (5.53), (5.56), and (5.57) are combined to form the local-strain-based expression for the SWT relation,

$$\sigma_{\max} \epsilon_a = \frac{(\sigma'_f)^2}{E} (2N_f)^{2b} + \sigma'_f \epsilon'_f (2N_f)^{b+c} \tag{5.58}$$

It should be kept in mind that this expression is strictly empirically based. For extreme cases (e.g., high mean stress) outside the range of data for which the expression was established, the validity of this approach has not been assessed. For purposes of bounding a life estimate, an approximation may be made based on the strain amplitude only, neglecting the mean stress effect [i.e., using Eq. (5.53)]. This is demonstrated in Example 7.

EXAMPLE 7 Compute the life corresponding to the stable hysteresis loop from Example 6 (Fig. 5.40). The low-cycle fatigue parameters for the specimen are given as

$$\begin{aligned} \sigma'_f &= 110 \text{ ksi} & b &= -0.105 \\ \epsilon'_f &= 0.55 & c &= -0.625 \end{aligned}$$

solution The cyclically stable hysteresis loop fluctuated between maximum and minimum strain values of 0.008 and 0.002, with stresses ranging between $\sigma_{\max} = 61.13$ ksi and $\sigma_{\min} = -32.92$ ksi.

For the strain amplitude of $\epsilon_a = 0.003$ [= (0.008 - 0.002)/2], and maximum stress of $\sigma_{\max} = 61.13$ ksi, Eq. (5.58) appears as

$$(61.13)(0.003) = \frac{(\sigma'_f)^2}{E} (2N_f)^{2b} + \sigma'_f \epsilon'_f (2N_f)^{b+c}$$

This equation is solved iteratively for a life of $N_f = 2618$ cycles. If Eq. (5.53) is solved with no mean stress effect, an upper-bound life estimate of $N_f = 5590$ results.

Notches. Many mechanical components operate with elastically calculated stresses that exceed the yield strength of the material at a notch. However, once yielding occurs the elastic stress concentration factor K_t cannot be expected to accurately predict localized stresses. Since the material has yielded, local stress values are less than the elastically computed quantities. Similarly, strains computed elastically are exceeded in notches. This situation is depicted in Fig. 5.46. Equations (5.59) and (5.60) define notch stress- and strain-concentration factors, where σ_n and ϵ_n are the actual notch stress and strain, respectively, and S and e are elastically calculated nominal notch stress and strain, respectively.

$$K_\sigma = \frac{\sigma_n}{S} \tag{5.59}$$

$$K_\epsilon = \frac{\epsilon_n}{e} \tag{5.60}$$

To conduct a strain-based fatigue life estimate of a notch, the state of stress and strain at the notch root must be estimated. To achieve this, three approaches could be considered:

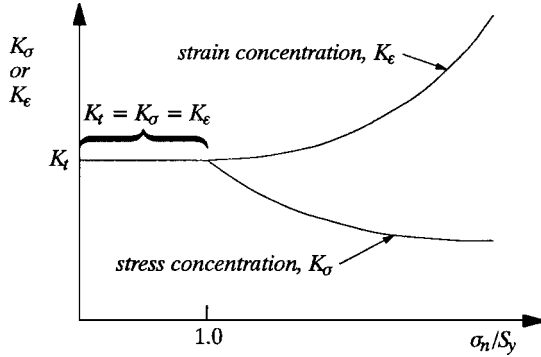


FIG. 5.46 Stress and strain concentration at a notch.

1. Place a strain gauge in the notch root.
2. Conduct elastic-plastic finite-element analysis.
3. Estimate notch root stress-strain from nominal, elastically calculated values.

The first two approaches sound straightforward enough, but both are extremely time consuming and complex. Notch geometries do not usually facilitate the placement of a strain gauge. Furthermore, a part must exist. This is not usually the case early in the design process. The application of finite-element analysis is getting easier for elastic situations, but is still a formidable task for elastic-plastic situations, especially under cyclic loading.²² Mesh density requirements are great and codes are simply not set up to easily accept cyclic input loading.

For this reason, item 3 in the above list is emphasized here. Specifically, the application of Neuber's rule⁵⁹ is discussed. Neuber originally noticed that the geometric mean of the stress- and strain-concentration factors remains approximately constant as plasticity occurs in a notch. This means that the product of notch root stress and strain can be determined from elastically calculated quantities. From this observation, Neuber's rule is stated as

$$K_t^2 S_e = \sigma_n \epsilon_n \tag{5.61}$$

If nominal stress is elastic, the left-hand side of the equation above can be restated as

$$\frac{(K_t S)^2}{E} = \sigma_n \epsilon_n \tag{5.62}$$

Notice that the left-hand side of this equation represents the applied loading (S) and notch geometry (K_t). The right-hand side is simply the product of the actual stress and strain in the notch root. If the left side is considered as known input, one more relation is needed to solve for the two unknowns. This relation is the cyclic stress-strain curve:

$$\epsilon_n = \frac{\sigma_n}{E} + \left(\frac{\sigma_n}{K'} \right)^{1/n'} \tag{5.63}$$

Figure 5.47 illustrates the approach for elastic nominal stress-strain. Neuber's rule is represented by the hyperbola. The product of stress and strain is a constant, defined by the geometry and applied loading. The cyclic stress-strain curve provides the second

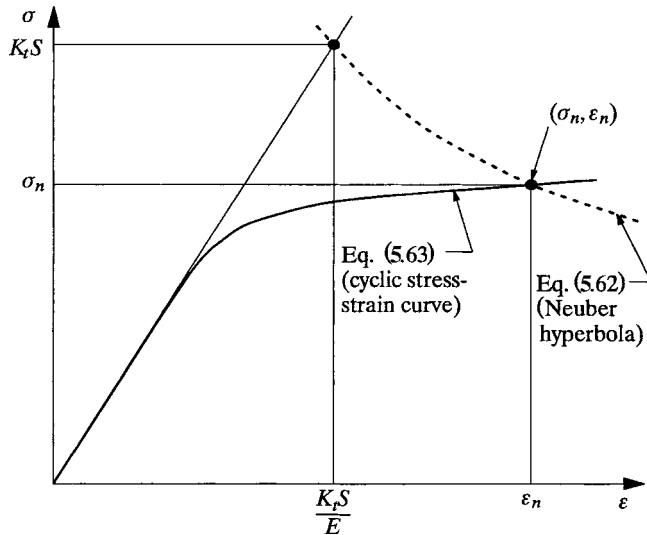


FIG. 5.47 Neuber’s rule specifies the point on the cyclic stress-strain curve corresponding to the notch root.

relation necessary to obtain the two unknowns, the stress and strain in the notch root, represented by the intersection of the two curves in Fig. 5.47.

In some instances, a component can be loaded such that the nominal stress S or nominal stress range ΔS is itself large enough to cause plastic straining. In this instance, the material’s cyclic stress-strain curve should be used to compute the nominal strain, e , according to

$$e = \frac{S}{E} + \left(\frac{S}{K'} \right)^{1/n'} \tag{5.64}$$

This is demonstrated in Example 8 for applied loading with a mean stress.

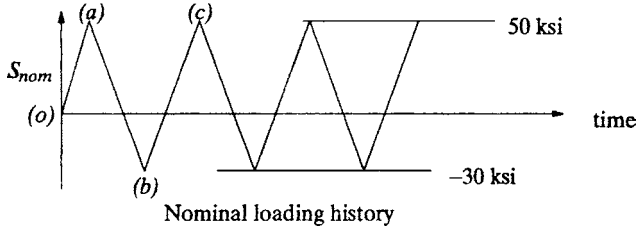
EXAMPLE 8 A notched steel bar has an elastic stress-concentration factor of $K_t = 2.42$. The material properties for the steel are given by

$$\begin{aligned} E &= 30,000 \text{ ksi} & K' &= 154 \text{ ksi} & n' &= 0.123 \\ \sigma_f' &= 169 \text{ ksi} & \epsilon_f' &= 1.14 \\ b &= -0.081 & c &= -0.67 \end{aligned}$$

For applied loading represented by the nominal stress history depicted on page 5.53, compute the cycles to crack initiation for constant-amplitude loading from 50 ksi to -30 ksi.

solution To conduct the analysis, consider loading from (o) to (a) , (a) to (b) , and finally (b) to (c) . Subsequent loadings are repeated (a) - (b) - (c) cycles. First, consider loading from (o) to (a) : The nominal stress changes from 0 to 50 ksi, or $\Delta S = 50 - 0$ ksi. For this initial loading segment, Neuber’s rule is expressed as

$$K_t^2 \Delta S \Delta e = \Delta \sigma \Delta \epsilon$$



On the left side of the Neuber equation, the nominal stress and strain ranges are related by

$$\Delta e = \frac{\Delta S}{E} + \left(\frac{\Delta S}{K'}\right)^{1/n'}$$

On the right side of the Neuber equation, the notch strain and stress ranges are related by

$$\Delta \epsilon = \frac{\Delta \sigma}{E} + \left(\frac{\Delta \sigma}{K'}\right)^{1/n'}$$

Combining these relations,

$$K_t^2(\Delta S) \left[\frac{\Delta S}{E} + \left(\frac{\Delta S}{K'}\right)^{1/n'} \right] = \Delta \sigma \left[\frac{\Delta \sigma}{E} + \left(\frac{\Delta \sigma}{K'}\right)^{1/n'} \right]$$

$$(2.42)^2(50)(0.001773) = \Delta \sigma \left[\frac{\Delta \sigma}{E} + \left(\frac{\Delta \sigma}{K'}\right)^{1/n'} \right]$$

Solving iteratively, $\Delta \sigma = 78.19$ ksi. This corresponds to a strain of

$$\Delta \epsilon = \frac{78.19}{E} + \left(\frac{78.19}{K'}\right)^{1/n'} = 0.00665$$

Therefore, at point (a), the notch root stress and strain are defined (78.19 ksi, 0.00665).

Next, to get from (a) to (b) the approach is similar, but the stress and strain changes occur along the hysteresis curve, Eq. (5.51), rather than along the cyclic stress-strain curve, Eq. (5.50). The nominal stress changes from 50 to -30 ksi: $\Delta S = 50 - (-30) = 80$ ksi. For this segment, Neuber's rule is expressed as

$$K_t^2 \Delta S \Delta e = \Delta \sigma \Delta \epsilon$$

On the left side of the Neuber equation, the nominal strain change is related to the nominal stress change by

$$\Delta e = \frac{\Delta S}{E} + 2 \left(\frac{\Delta S}{2K'}\right)^{1/n'}$$

On the right side of the Neuber equation, the notch strain range is related to the notch stress by

$$\Delta \epsilon = \frac{\Delta \sigma}{E} + 2 \left(\frac{\Delta \sigma}{2K'}\right)^{1/n'}$$

Combining these relations,

$$K_t^2(\Delta S) \left[\frac{\Delta S}{E} + 2 \left(\frac{\Delta S}{2K'}\right)^{1/n'} \right] = \Delta \sigma \left[\frac{\Delta \sigma}{E} + 2 \left(\frac{\Delta \sigma}{2K'}\right)^{1/n'} \right]$$

$$(2.42)^2(80)(0.002701) = \Delta\sigma \left[\frac{\Delta\sigma}{E} + \left(\frac{\Delta\sigma}{2K'} \right)^{1/m'} \right]$$

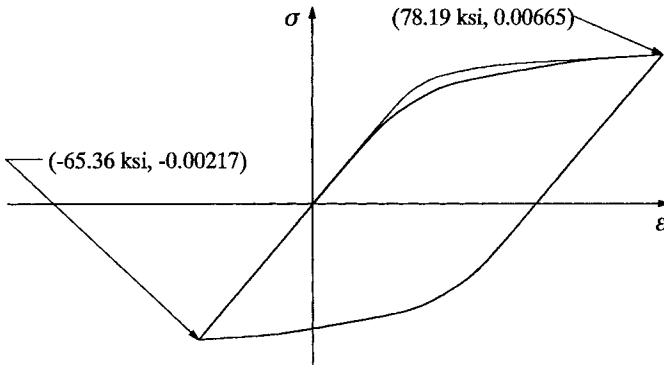
Solving iteratively, $\Delta\sigma = 143.55$ ksi.

The strain change corresponding to this stress change is given by

$$\Delta\epsilon = \frac{143.55}{E} + 2 \left(\frac{143.55}{2K'} \right)^{1/m'} = 0.008817$$

Therefore, at point (b), the stress is given by $78.19 - 143.55 = -65.36$ ksi, and the strain is given by $0.00665 - 0.008817 = -0.00217$.

Finally, to get from (b) to (c), notice that the nominal stress change is the same as in the proceeding step. The hysteresis loop for the cycle is shown below.



From this, the strain amplitude is given by $\Delta\epsilon/2 = 0.004409$ and the maximum stress is 78.19 ksi. The SWT estimation of life for this notch root stress-strain response is 7318 cycles (14,636 reversals):

$$(78.19)(0.004409) = \frac{(\sigma_f')^2}{E} [2(7318)]^{2b} + \sigma_f' \epsilon_f' [2(7318)]^{b+c}$$

5.5.3 Variable-Amplitude Loading

Thus far, the fatigue-life prediction approaches presented in this section have only been discussed in the context of constant-amplitude loading. However, engineering components are seldom subjected to constant-amplitude loading for their entire life. More often, load fluctuations occur with means and amplitudes that vary. In this section, a methodology is presented for applying the approaches presented earlier to variable-amplitude fatigue-life prediction.

Cumulative Damage. In order to compute the life of a component subjected to irregular loading, the concept of “fatigue damage” was developed, whereby each cycle is considered to expend a finite fraction of the overall life. The most widely utilized damage concept is that of linear damage (also called Miner’s rule or the Palmgren-Miner rule).

Linear damage is best explained by considering a single “cycle” of loading (from a minimum to maximum and back to a minimum). If this cycle were applied under constant amplitude to a new component, the techniques described previously in this chapter

could be used to compute the number of times N that cycle could be applied before a crack could be expected to develop. With the linear damage concept, each cycle of loading is considered to impose an amount of fatigue “damage” equal to $1/N$. (Equivalently, each cycle is considered to expend $1/N$ th of the component life.) If this damage is counted for each cycle of loading, then failure would occur when the cumulative damage reached a value of unity. At this point, 100 percent of the fatigue life has been expended. In other words, damage imposed by the i th cycle of loading DAM_i is expressed by

$$DAM_i = \frac{1}{N_i} \tag{5.65}$$

where N_i is the number of cycles a new component would be computed to sustain under constant-amplitude loading. Failure is considered to occur when

$$\sum_{i=1}^{N_f} DAM_i = 1 \tag{5.66}$$

Other, more sophisticated nonlinear cumulative-damage approaches have been proposed.¹² Also, several effects, such as sequence of loading or overloads, have been shown to bias linear damage summation in either the conservative or nonconservative directions. However, given all the uncertainties associated with fatigue-life estimation, linear damage theory has been successfully applied to a wide range of engineering design situations, especially when loading is highly irregular and in the absence of major overloads.

Cycle Counting. In order to sum damage for variable-amplitude load histories, it is necessary to define “cycles” from those histories. For certain situations, this can be a fairly straightforward problem. For instance, consider that n_1 cycles of constant-amplitude loading at an effective stress amplitude of $(\sigma_a)_1$ are applied to a component (Fig. 5.48). Following this, the peak and valley (maximum and minimum) values of stress change, such that an effective stress amplitude of $(\sigma_a)_2$ is now being applied. If this loading continues for n_2 cycles, how many cycles (n_3) could a third range of loading

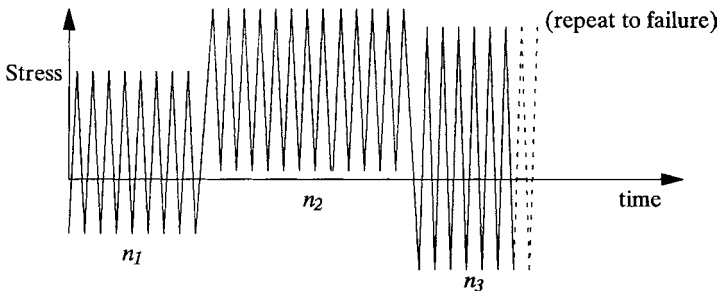


FIG. 5.48 Block loading problem.

be applied until failure is expected? For each effective stress amplitude, a corresponding fatigue life of N_1 , N_2 , and N_3 can be calculated. Therefore, n_3 can be computed from Eq. (5.66), written for this problem as

$$\sum DAM_i = \frac{n_1}{N_1} + \frac{n_2}{N_2} + \frac{n_3}{N_3} = 1 \tag{5.67}$$

For situations where loading is more irregular, numerous cycle-counting procedures have been proposed. Several approaches are presented in ASTM E-1049, "Recommended Practices for Cycle Counting in Fatigue Analysis."⁶⁰ Of these, rainflow cycle counting is the most popular and widely used approach.

Rainflow Cycle Counting. The concept of rainflow cycle counting has been described by two completely different approaches (referred to as the "falling rain" and "ASTM" approaches) that yield the same results. In each of these, it is necessary to define a "block" of irregular loading. This block could correspond to measurements or estimates over a representative period of service operation (one day, one job, one proving-ground lap, etc.). Furthermore, the block must be reorganized such that the largest peak in the history occurs as the first reversal. Cycles occurring prior to this are simply moved to the end such that the overall peak-valley content of the block remains the same. The "falling rain" approach is described first by considering the stress history, shown in Fig. 5.49. It must be visualized that "gravity" acts along the time axis, as shown in the figure. With this basis, the approach is described below.

1. Define a block (or history) with the highest peak occurring first.
2. Assuming "gravity" acts along the time axis, start a "flow of water droplets" at each peak and valley, *in succession*. The droplets flow along the profile and over the edge.
3. Flow originating at a peak (or valley) stops (-) if it "sees" a higher peak (or a deeper valley) than the one from which it started.
4. Flow also stops (>) to avoid collision with rain from a previous flow.

Stress "ranges" (valley-to-peak) are defined by the amount of vertical travel incurred by a particular flow. For instance, the rainflows in Fig. 5.49 define the eight ranges shown at the top of page 5.57.

To predict life, damage imposed by each of the four rainflow counted ranges is computed appropriately. This is demonstrated in Example 9.

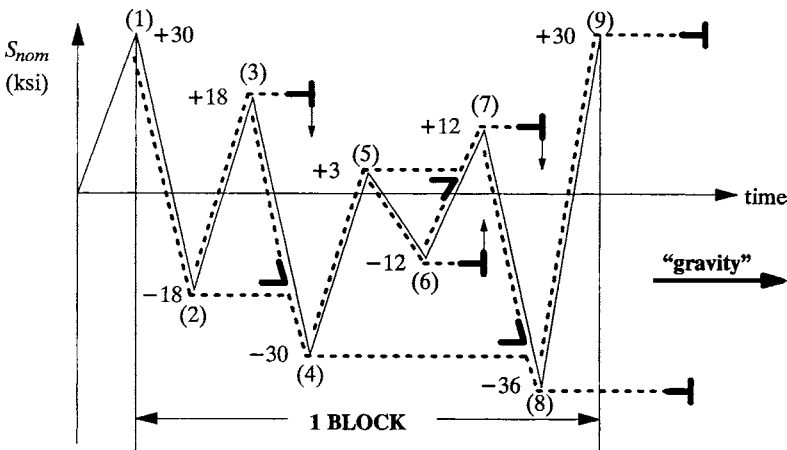
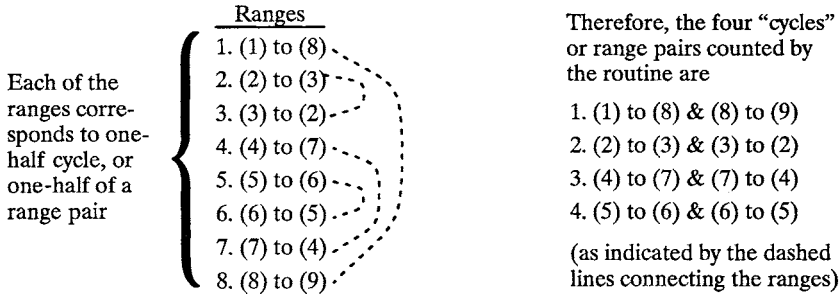


FIG. 5.49 Rainflow cycle counting ("falling rain" analogy).



EXAMPLE 9 For a forged 1040 steel component with a stress concentration factor of 1.8, conduct an elastic analysis and compute the number of times the nominal stress-loading block shown in Fig. 5.49 can be sustained by the component. The material properties for the material are given by

$$\sigma'_f = 223 \text{ ksi}$$

$$b = -0.14$$

solution The rainflow-cycle-counted nominal and notch stresses are tabulated below. The effective stress amplitude is based on the SWT parameter [Eq. (5.46)].

Range pair	S_{\max} (ksi)	S_{\min} (ksi)	σ_{\max} (ksi)	σ_{\min} (ksi)	σ_a (ksi)	$\sigma_{\text{eff},a}$ (ksi)	N (cycles)	D (cyc ⁻¹)
(1–8)(8–9)	30	–36	54	–64.8	59.4	56.64	8922	1.12E–4
(2–3)(3–2)	18	–18	32.4	–32.4	32.4	4.82E5	2.08E–6	
(4–7)(7–4)	12	–30	21.6	–54	37.8	28.57	1.18E6	8.46E–7
(5–6)(6–5)	3	–12	5.4	–21.6	13.5	8.54	6.61E9	1.5E–10

$$\Sigma D = 0.000115$$

The life of the component, in number of blocks to failure, is computed as shown below:

$$\text{Life} = \frac{1}{\Sigma D} = 8696 \text{ blocks}$$

The ASTM rainflow approach is conceptually quite different from the falling rain approach, but both give identical answers. The ASTM procedure is extremely beneficial analytically, since it can be implemented using a few lines of computer code. A BASIC listing to implement rainflow cycle counting is presented below, as Table 5.4.

Notch Strain Analysis. The estimated life in Example 9 is somewhat low and likely not in the elastic regime, indicating that cyclic plasticity may be occurring in the notch root. To analyze such a situation, a computer program can be written to implement a Neuber analysis (similar to Example 8) for every nominal stress range in the block (RANGE in Table 5.4). This is demonstrated in Example 10.

EXAMPLE 10 The nominal stress history from Fig. 5.49 is to be applied to a forged 1045 steel shaft with a K_t value of 1.8 and again for a K_t value of 3.0. Compute the notch stress-strain response. Rainflow-cycle-count the strain history and estimate the life of each component. The properties are given below.

TABLE 5.4 BASIC Computer Listing for ASTM Rainflow Approach

Nominal stress reversals are stored in an array, Stress(NPTS), where NPTS=number of reversals in the history. Since the history must begin and end with the maximum peak, NPTS will always be an odd integer.

```

Event(1) = Stress(1)
N = 1 : 'Counter N initialized
J = 1 : 'Counter J initialized
1 N = N + 1
  J = J + 1
  IF (J = NPTS + 1) THEN GOTO 3
  Event(N) = Stress(J)
2 IF (N < 3) GOTO 1
  X = ABS(Event(N) - Event(N-1))
  Y = ABS(Event(N-1) - Event(N-2))
  IF (X < Y) THEN GOTO 1
  RANGE = Y
  Xmean = (Event(N-1) + Event(N-2)) / 2
  Xamplitude = RANGE / 2
  N=N-2
  Event(N)=Event(N+2)
  GOTO 2
3 'Finished
  END
    
```

$$\begin{aligned}
 K' &= 171.4 \text{ ksi} & \sigma'_f &= 223 \text{ ksi} \\
 n' &= 0.18 & b &= -0.14 \\
 E &= 30,000 \text{ ksi} & \epsilon'_f &= 0.61 \\
 & & c &= -0.57
 \end{aligned}$$

solution The rainflow-cycle-counted strain amplitude and maximum stress for each range pair in the stress history are tabulated below for each shaft. The estimated number of cycles corresponding to each range pair are computed using the SWT parameter, Eq. (5.58).

Range pair	For $K_t = 1.8$			For $K_t = 3.0$		
	ϵ_a	σ_{\max} (ksi)	N (cycles)	ϵ_a	σ_{\max} (ksi)	N (cycles)
(1-8)(8-9)	0.002619	46.25	35,760	0.005737	59.60	4,018
(2-3)(3-2)	0.001352	25.08	9.31E5	0.002149	43.87	6.75E4
(4-7)(7-4)	0.001124	29.80	9.66E5	0.002693	39.88	3.19E4
(5-6)(6-5)	0.00045	11.74	4.39E8	0.000756	26.59	9.40E6

The life in number of blocks for each shaft is computed as shown below. For $K_t = 1.8$,

$$\text{Life} = \frac{1}{\sum 1/N} = 33,248 \text{ blocks}$$

For $K_t = 3.0$,

$$\text{Life} = \frac{1}{\sum 1/N} = 3842 \text{ blocks}$$

The mean stress effect on life predictions can be assessed by assuming the strain range to be fully reversed (neglecting mean stress). To do this, the N for each range pair is

computed using Eq. (5.53). This results in life predictions of 31,230 blocks for $K_t = 1.8$ and 3387 blocks for $K_t = 3.0$.

In Example 9, life predictions are based on notch root stresses and strains estimated from the applied nominal stress ranges and Neuber's rule. The estimated notch root stress-strain history can be plotted as a set of repeating hysteresis loops, such as presented in Fig. 5.50. This illustrates an important physical feature associated with rainflow

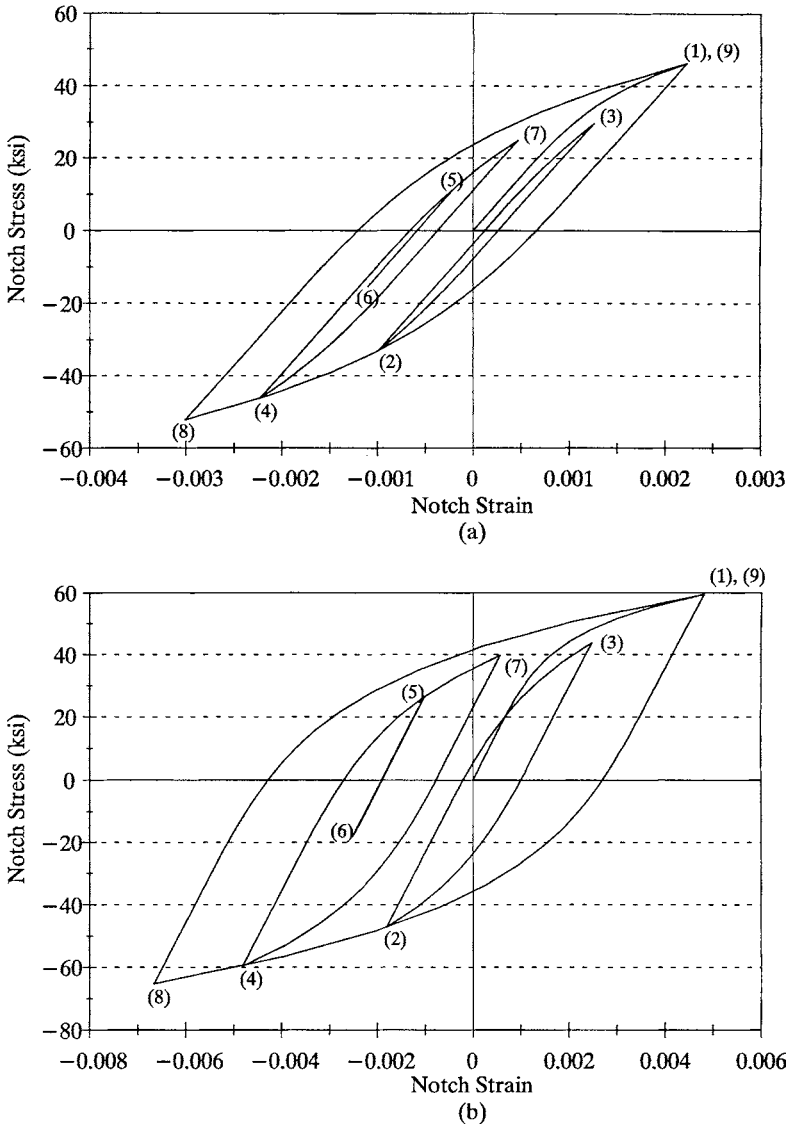


FIG. 5.50 Closed hysteresis loops from Example 10 for (a) $K_t = 1.8$ and (b) $K_t = 3.0$.

cycle counting, in that each event defined by the routine corresponds to a closed hysteresis loop shown in the figure. Comparing Fig. 5.50 and the nominal stress history, Fig. 5.49, notice that each closed hysteresis loop can be directly identified with each rainflow-cycle-counted range pair. Also note that, for this example load history, the largest strain range imposes the vast majority of damage. In general, this may not be the case.

5.6 DAMAGE-TOLERANT DESIGN

The structural integrity assessment methodologies presented in preceding sections of this chapter assume the material to be free of substantial flaws or defects. Stresses and strains are computed and compared to the strength of homogeneous engineering material. Damage-tolerant design recognizes that flaws, specifically cracks, can and do exist, even before a component is placed into service. Therefore, the focus of this design philosophy is on estimating behavior of a crack in an engineering material under service loading, and *fracture mechanics* provide the analytical tools.

Macroscopic cracks are assumed to exist in regions where detection may be difficult or impossible (e.g., under a flange or rivet head), and the behavior of the crack is predicted under anticipated service loading. The estimated behavior is used to schedule inspection and maintenance in order to assure that defects do not propagate to a catastrophic size.

Only a brief overview is presented in this section. This important method, used extensively in the aerospace industry, is covered comprehensively with example applications in several references.^{9,13,31,32,61-65} The discussion here is limited to linear elastic approaches, although research on elastic-plastic fracture mechanics is very active, particularly regarding the behavior of very small cracks in locally plastic strain fields.⁶⁶⁻⁶⁸

5.6.1 Stress-Intensity Factor

An “ideal” crack in an engineering structure has been modeled analytically as a notch with a root radius of zero (Fig. 5.51). When a stress is applied perpendicular to the

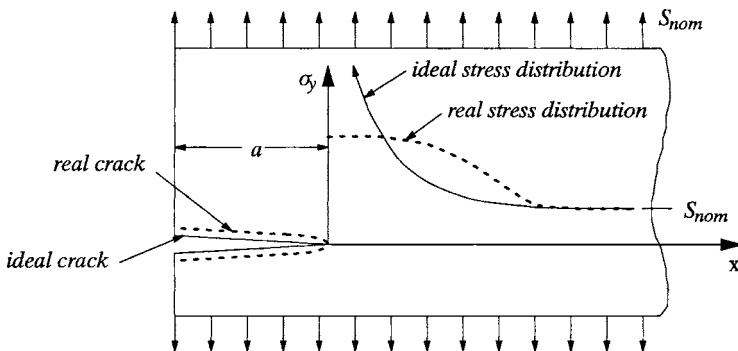


FIG. 5.51 Schematic crack opening and stress distribution from the tip of an edge crack of length a , in a theoretical and real engineering material.

ideal crack, stresses approach infinity at the crack tip. This is evident in Fig. 5.51 and Eq. (5.68) for the stress along the x axis:

$$\sigma_y = \frac{K_I}{\sqrt{2\pi x}} \tag{5.68}$$

The parameter K_I is referred to as the “stress-intensity factor” and it lies at the center of all fracture mechanics analyses.

The stress-intensity factor can be considered a quantitative measure of the severity of a crack in material attempting to sustain a particular state of stress. It also can be thought of as the rate at which the stresses approach infinity at the tip of a theoretical crack. Since real material cannot sustain infinite stress, intense localized deformation occurs, causing the crack tip to blunt and stresses to redistribute, as depicted in Fig. 5.51. Even though crack-tip deformation is plastic, as long as the size of the plastic zone at the crack tip is small relative to crack dimensions, the elastically calculated K_I has been successfully used to describe the strength of an engineering component. Therefore, the term “linear elastic fracture mechanics” (LEFM) is typically applied to analyses based on K_I .

The significance of the subscript I is shown in Fig. 5.52. Since cracks are considered analytically as planar defects, the subscript refers to the mode in which the two crack faces are displaced. Mode I is the normal loading mode (crack faces are pulled apart) while II and III are shear loading modes (crack faces slide relative to each other). The discussion in the remainder of this section is directly in terms of mode I analyses. However, the extension of the approaches to the shear modes is straightforward.

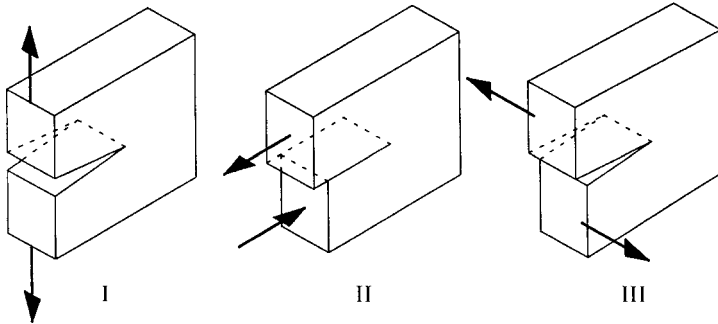


FIG. 5.52 Crack loading modes: (left) I, normal; (center) II, sliding; (right) III, tearing.

Stress-intensity factors can be computed for any geometry and loading combination using finite-element analysis, but not without considerable analytical effort. More typically in design, stress-intensity factors are found from a tabulated reference.^{69–72} They are usually expressed as in Eq. (5.69), in terms of the gross nominal stress S_{nom} , crack length, and geometry for a particular type of loading (e.g., bending or tension). Since they are elastically calculated, they can be superimposed.

$$K_I = f(a, \text{geometry}) S_{nom} \sqrt{a} \tag{5.69}$$

5.6.2 Static Loading

The premise of damage-tolerant design is that engineering materials with macroscopic cracks can sustain stresses without failure, up to a point. Obviously, the larger a crack

in a component, the less load it can sustain. One of the important features of K_I is its ability to characterize combinations of loading and crack size that correspond to unstable crack propagation (or the strength of the cracked component). Experiments have shown that cracks in engineering materials propagate catastrophically at a certain critical value of the stress-intensity factor, K_c . The critical value is referred to as the *fracture toughness* (not directly associated with the impact strength or area under a stress-strain curve) and is considered a property of the material. In other words, failure is predicted when

$$K_I = f(a, \text{geometry}) S_{\text{nom}} \sqrt{a} = K_c \tag{5.70}$$

Like other “material properties,” K_c is influenced by numerous factors including environment, rate of loading, etc. But an important distinction for K_c arises from its observed dependence on specimen size. As the thickness t of the specimen increases along the dimension of the crack front, increasing constraint develops, making plastic deformation more difficult and causing the material to behave in a more brittle manner. Therefore, as shown in Fig. 5.53, as the thickness increases, K_c decreases asymptotically to a value referred to as K_{IC} , the *plane-strain fracture toughness*. Specifications for the experimental determination of K_{IC} are found in ASTM E-399, “Standard Test Method for Plane-Strain Fracture Toughness of Metallic Materials,”⁷¹ and tabulated values can be found in Refs. 73 through 80 for many engineering alloys.

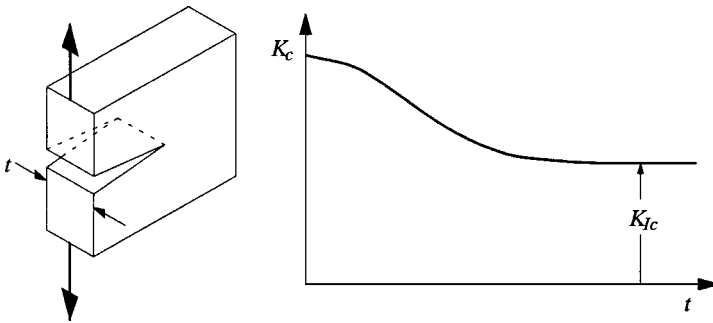


FIG. 5.53 As specimen thickness increases, fracture toughness K_c decreases asymptotically to the value K_{IC} , the plane-strain fracture toughness.

5.6.3 Fatigue Loading

Cracks in engineering components tend to propagate progressively under fatigue loading. The damage-tolerant design philosophy takes advantage of this phenomenon to schedule periodic inspection and maintenance of components to assure against the growth of a crack to the catastrophic size associated with Eq. (5.70).

Paris and Erdogan⁸¹ are credited with first making the observation that the stress-intensity factor range can be used effectively to correlate crack propagation rates for a particular material under a wide variety of crack geometry and loading combinations. As shown schematically in Fig. 5.54a, suppose three separate specimens are subjected to the $R = 0$ loading at different applied loading levels. A stress-intensity factor range is computed from each nominal stress range. Cracks grow through each specimen at different rates, as shown in Fig. 5.54b. However, if the crack propagation rate, da/dN , is plotted versus stress-intensity factor range ΔK_I , (on log-log coordinates), then the data from all three tests collapse to the single curve, Fig. 5.54c. This curve is considered to

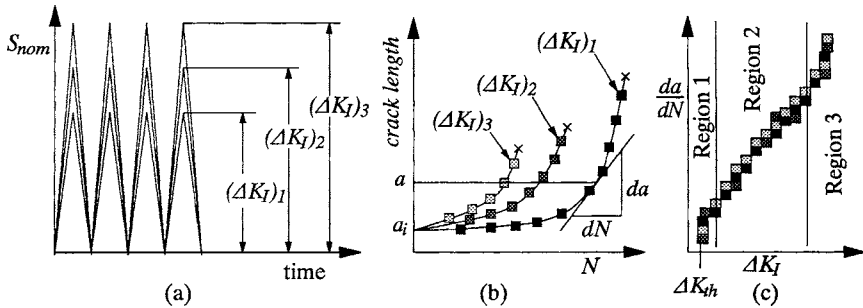


FIG. 5.54 Schematic data from three separate specimens: (a) Different nominal stress ranges lead to three different ΔK ranges for a given crack length; (b) crack length versus cycles of applied loading; (c) crack growth rate versus ΔK for all three tests.

be a characteristic of the material. Guidelines for conducting this type of testing are specified in ASTM E-647, “Standard Test Method for Measurement of Fatigue Crack Growth Rates.”⁸²

The shape associated with the crack growth rate curve (Fig. 5.54c) has been referred to as *sigmoidal*, having three distinct regions. Region 1 is associated with another property called the threshold stress-intensity factor range, ΔK_{th} . This is analogous to the endurance limit for local stress-based fatigue design. Applied loading cycles below ΔK_{th} are considered not to result in any crack advancement. Values of ΔK_{th} for various materials can be found in Refs. 73 through 80. At the upper region of the curve (called Region 3), peak values of K_I are approaching K_c . At this point crack propagation is rapid and growing beyond the limits of LEFM validity. The middle portion of the curve, Region 2, is important since it encompasses a substantial portion of the propagation life. Data in this regime usually appear somewhat linear on logarithmic coordinates, leading to the Paris relation,

$$\frac{da}{dN} = A_p (\Delta K)^{n_p} \tag{5.71}$$

Life prediction based on LEFM is based upon the integration of Eq. (5.71), or any other relation describing the data in Fig. 5.54c. This is illustrated in Eq. (5.72) for constant-amplitude loading:

$$N = \int_0^N dN = \int_{a_i}^{a_f} \frac{da}{\Delta K} = \int_{a_i}^{a_f} \frac{da}{f(\text{geometry}, a) \sqrt{a}} \tag{5.72}$$

As implied in Eq. (5.72) and Fig. 5.54b, a fracture mechanics analysis of crack propagation must begin with the assumption of an initial crack of length a_i . [The final crack length, a_f in Eq. (5.72), can be directly calculated from the maximum anticipated loading and K_c .] The definition of the initial crack size for testing purposes is well defined (ASTM E-647, Ref. 82) but for design purposes can be less objective. Sometimes, cracks are considered to exist where they may be difficult to detect, such as underneath a seam. However, for macroscopically smooth surfaces, the assumption of very small initial crack lengths (cracks that would be difficult to detect without the aid of a microscope, on the order of 0.001 in) can significantly affect the analysis, since small cracks can result in extremely low estimated propagation rates. Very small crack lengths, on the order of typical surface roughness values or surface scratches, are not considered to lie within the valid domain of LEFM.^{66–68} The threshold stress intensity factor can be used to define valid initial crack lengths.

Mean stress effects on crack propagation are accounted for with empirical relations usually defined in terms of the stress ratio R [Eq. (5.38)]. Two widely referenced equations were developed by Foreman,⁸³

$$\frac{da}{dN} = \frac{A_f(\Delta K)^{n_f}}{(1 - R)K_c - \Delta K} \quad (5.73)$$

and Walker,⁸⁴

$$\frac{da}{dN} = A_w \left(\frac{\Delta K}{(1 - R)^{1-m_w}} \right)^{n_w} \quad (5.74)$$

Constants in Eqs. (5.73) and (5.74) are empirically defined by comparison to constant-amplitude data generated over a range of load ratios. The relations can then be used to estimate crack growth during variable-amplitude load histories, usually by assuming that only certain segments in the history will result in incremental crack advancements. For example, damaging segments can be defined as only those that are both *tensile* and *increasing*. Maximum and minimum stresses for a particular segment are used to compute ΔK and R for use in Eq. (5.73) or (5.74), which is thus considered to compute the amount of crack growth resulting from that segment. References 9, 13, 31, 32, and 61 through 65 provide more detailed explanations of the implementation and use of fracture mechanics, including coverage of more advanced topics such as crack closure and sequence effects.

5.7 MULTIAXIAL LOADING

Fatigue under multiaxial loading is an extremely complex phenomenon. Evidence of this is the fact that even though the topic has been actively researched for more than a century, new theories on multiaxial fatigue are still emerging.⁸⁵ However, recent work has led to advances in understanding of the mechanisms of multiaxial fatigue and addressed some of the problems associated with implementing those advances for practical design problems.

In this section, only multiaxial fatigue-life prediction approaches are presented that are considered somewhat established. Although such approaches only exist for fairly simplistic multiaxial loading (e.g., constant amplitude, proportional loading, high-cycle regime), they still cover a substantial number of design situations.

5.7.1 Proportional Loading

Loading is defined as proportional when the ratios of principal stresses remains fixed with time. A consequence of this is that principal stress directions do not rotate. The simplest example would be a situation where the three components of surface stress are in phase and fully reversed, as shown in Fig. 5.55a. Figure 5.55b depicts a situation where stresses fluctuate in phase about mean values. In this case, whether or not the loading is purely proportional depends on the ratios of the mean stresses. The mean stresses can cause a slight oscillation of the principal stress axes over a cycle. In either case, a modified Sines approach has been successfully applied to this type of loading in the high-cycle regime.

Sines³⁷ observed that *mean torsional stresses do not influence fatigue behavior*, while mean tensile stresses decrease life and mean compression improves life. Sines' approach can be summarized as follows:

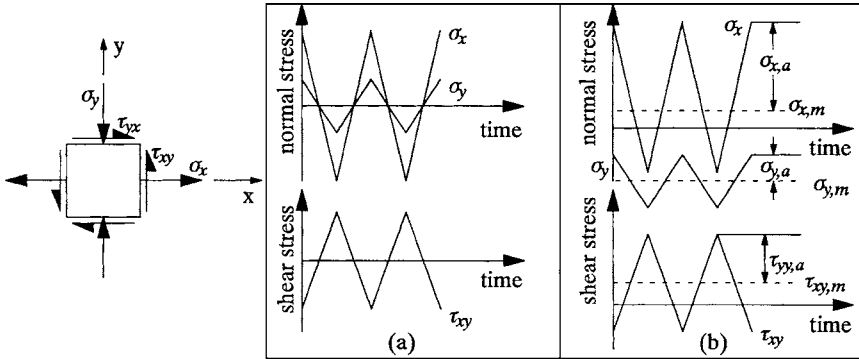


FIG. 5.55 (a) Pure proportional loading, fully reversed stress components. (b) Proportional stress amplitudes, with mean stresses.

- Compute the amplitude and mean of each normal stress:

$$\sigma_{x,a} = (\sigma_{x,max} - \sigma_{x,min})/2$$

$$\sigma_{x,m} = (\sigma_{x,max} + \sigma_{x,min})/2$$

$$\sigma_{y,a} = (\sigma_{y,max} - \sigma_{y,min})/2$$

$$\sigma_{y,m} = (\sigma_{y,max} + \sigma_{y,min})/2$$

$$\sigma_{z,a} = (\sigma_{z,max} - \sigma_{z,min})/2$$

$$\sigma_{z,m} = (\sigma_{z,max} + \sigma_{z,min})/2$$

- Compute the amplitude of the shear stress:

$$\tau_{xy,a} = (\tau_{xy,max} - \tau_{xy,min})/2$$

- Compute the principal stress amplitude from the amplitudes of the normal and shear applied stresses:

$$\sigma_{1,a} = \left(\frac{\sigma_{x,a} + \sigma_{y,a}}{2} \right) + \sqrt{\left(\frac{\sigma_{x,a} - \sigma_{y,a}}{2} \right)^2 + \tau_{xy,a}^2} \tag{5.75}$$

$$\sigma_{2,a} = \left(\frac{\sigma_{x,a} + \sigma_{y,a}}{2} \right) - \sqrt{\left(\frac{\sigma_{x,a} - \sigma_{y,a}}{2} \right)^2 + \tau_{xy,a}^2} \tag{5.76}$$

$$\sigma_{3,a} = \sigma_{z,a} \tag{5.77}$$

- Calculate the equivalent stress amplitude according to a von Mises and an equivalent mean stress as given by

$$S_{eq,a} = \frac{1}{\sqrt{2}} \sqrt{(\sigma_{1,a} - \sigma_{2,a})^2 + (\sigma_{2,a} - \sigma_{3,a})^2 + (\sigma_{3,a} - \sigma_{1,a})^2} \tag{5.78}$$

$$S_{eq,m} = \sigma_{x,m} + \sigma_{y,m} + \sigma_{z,m} \tag{5.79}$$

- Use $S_{eq,a}$ and $S_{eq,m}$ as an amplitude and mean stress (in place of σ_a and σ_{mean}) to form an effective, fully reversed stress amplitude, such as described in Fig. 5.27 or given in Eqs. (5.42) to (5.46).

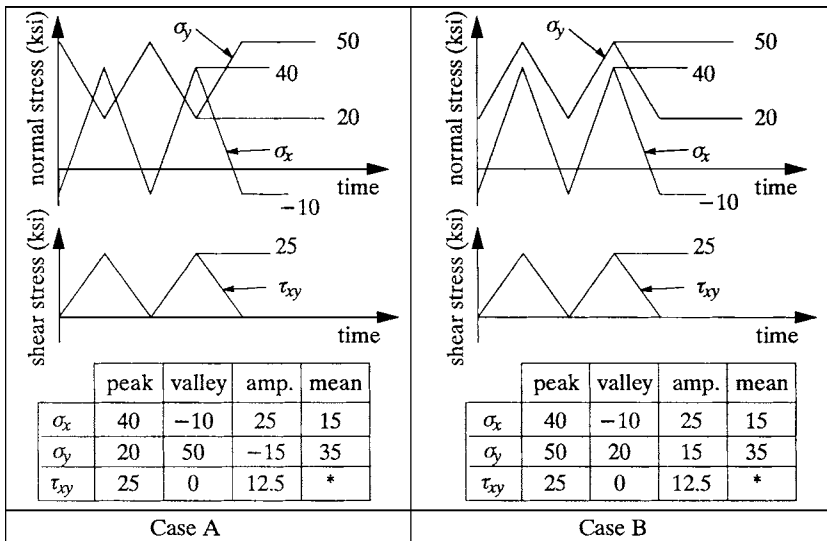
Note that $\tau_{xy,a}$ influences neither $S_{eq,a}$ nor $S_{eq,m}$, and thus does not affect the life estimate. If a pressure-free surface element is being considered, then $\sigma_{3,a} = 0$, and Eq. (5.77) can be simplified to

$$S_{eq,a} = \sqrt{\sigma_{x,a}^2 - (\sigma_{x,a})(\sigma_{y,a}) + \sigma_{y,a}^2 + 3\tau_{xy,a}^2} \tag{5.80}$$

eliminating the intermediate principal stress-amplitude calculations.

An important point must be kept in mind when implementing this approach: *it can be crucial to keep track of the algebraic sign of the amplitudes of the normal stress components $\sigma_{x,a}$, $\sigma_{y,a}$, and $\sigma_{z,a}$, as well as the principal stresses $S_{1,a}$ and $S_{2,a}$.* Generally, “amplitudes” are considered positive. However, considering amplitude as always positive here can lead to nonconservative life estimates! When two normal stresses *peak* at the same time, then both amplitudes should be considered positive (or the two should have the same algebraic sense). When one is at a *valley* while the other is at a *peak*, then the amplitude of the valley signal is negative while amplitude of the peak signal is positive (or the two should have the opposite algebraic sense). Example 11 serves to illustrate that point.

EXAMPLE 11 Estimate the fatigue life for two materials experiencing the Case A and B stress histories below. The only difference between the two stress histories is the phase relation of the normal stress in the y direction. Properties for the two materials (1045 steels) are as follows: (1) $S_u = 220$ ksi, $\sigma_f' = 843$ ksi, $b = -0.1538$; (2) $S_u = 137$ ksi, $\sigma_f' = 421$ ksi, $b = -0.1607$.



solution The peak, valley, amplitude, and mean stresses are tabulated above for each load history. For Case A, notice the negative amplitude for $\sigma_{y,a}$. For Case A, $S_{eq,a} = 41.16$ ksi. For Case B, $S_{eq,a} = 30.7$ ksi. For both cases, $S_{eq,m} = 50$ ksi.

Goodman:
$$\sigma_{a,eff} = S_{eq,a} \left(\frac{S_u}{S_u - S_{eq,m}} \right)$$

SWT:
$$\sigma_{a,eff} = \sqrt{S_{eq,a}(S_{eq,a} + S_{eq,m})}$$

Using the equivalent amplitude and mean stresses, the Goodman and SWT parameters were used to compute effective stress amplitudes and corresponding lives. Results are tabulated below.

	Case A		Case B	
	$\sigma_{a,eff}$ (ksi)	N (cycles)	$\sigma_{a,eff}$ (ksi)	N (cycles)
Material 1				
Goodman	53.26	31.4×10^6	39.76	211×10^6
SWT	61.25	12.7×10^6	49.80	48×10^6
Material 2				
Goodman	64.81	5.7×10^4	48.38	3.52×10^5
SWT	61.25	8.1×10^4	49.80	2.94×10^5

Several important observations can be made from Example 11. Estimated lives are significantly shorter for Case A relative to Case B. This is because the von Mises equivalent stress amplitude reflects the fact that principal shear stresses fluctuate more in Case A than they do in Case B. Also, whether or not the Goodman approach is more or less conservative than the SWT approach depends on the material and load history. For Case B, the SWT prediction is more conservative than Goodman for either material. But, for Case A, SWT is more conservative for the harder material (1), but less so for the softer material (2).

5.7.2 Nonproportional Loading

For nonproportional loading no consensus exists on the most suitable design approach. The ASME Boiler and Pressure Vessel Code⁸⁶ presents a generalized procedure, given in Table 5.5. Based on this procedure, an equivalent stress parameter, SEQA, has been derived⁸⁷ for combined, constant-amplitude, out-of-phase bending (or axial) and torsional stress:

$$SALT = \frac{\sigma_{x,a}}{\sqrt{2}} \sqrt{1 + C^2 + \sqrt{1 + 2C^2 \cos(2\phi) + C^4}} \tag{5.81}$$

where $\sigma_{x,a}$ and $\tau_{xy,a}$ = elastically calculated notch bending (or axial) and torsional shear-stress amplitudes, respectively, $C = 2\tau_{xy,a}/\sigma_{x,a}$, and ϕ = the phase angle between bending and torsion. This parameter reduces to the Tresca (maximum shear) equivalent stress amplitude for in-phase loading. A similar relation can be defined based on the von Mises criterion:⁸⁷

$$SEQA = \frac{\sigma}{\sqrt{2}} \sqrt{1 + \frac{3}{4}C^2 + \sqrt{1 + \frac{3}{2}C^2 \cos(2\phi) + \frac{9}{16}C^4}} \tag{5.82}$$

For bending-torsion cases, these relations can simplify analysis. For a more random load history, the applications of the ASME approach is demonstrated in Example 12.

EXAMPLE 12 Use the procedure outlined in ASME Code Case NB-3216.2 to compute the Tresca-based S_{alt} for the bending-torsion operating cycle shown on page 5.69. Also,

TABLE 5.5 Excerpt from ASME Boiler and Pressure Vessel Code, Sec. III: Multiaxial Fatigue Evaluation

NB-3216.1 Constant Principal Stress Direction.

For any case in which the directions of the principal stresses at the point being considered do not change during the cycle, the steps stipulated in the following subparagraphs shall be taken to determine the alternating stress intensity.

(a) Principal Stresses—Consider the values of the three principal stresses at the point versus time for the complete stress cycle taking into account both the gross and local structural discontinuities and the thermal effects which vary during the cycle. These are designated as σ_1 , σ_2 and σ_3 for later identification.

(b) Stress Differences—Determine the stress differences $S_{12} = \sigma_1 - \sigma_2$, $S_{23} = \sigma_2 - \sigma_3$ and $S_{31} = \sigma_3 - \sigma_1$ versus time for the complete cycle. In what follows, the symbol S_{ij} is used to represent any one of these stress differences.

(c) Alternating Stress Intensity—Determine the extremes of the range through which each stress difference (S_{ij}) fluctuates and find the absolute magnitude of this range for each S_{ij} . Call this magnitude $S_{r ij}$ and let $S_{alt ij} = 0.5 S_{r ij}$. The alternating stress intensity S_{alt} , is the largest of the $S_{alt ij}$'s.

NB-3216.2 Varying Principal Stress Direction.

For any case in which the directions of the principal stresses at the point being considered do change during the stress cycle, it is necessary to use the more general procedure of the following subparagraphs.

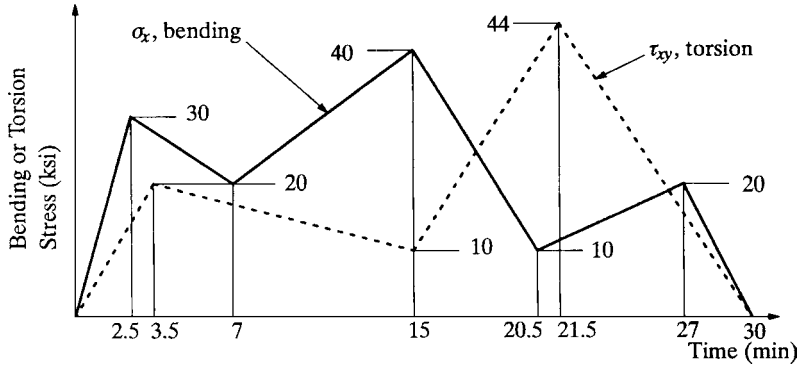
(a) Consider the values of the six stress components, σ_t , σ_l , σ_r , τ_{tl} , τ_{lr} , τ_{rt} versus time for the complete stress cycle, taking into account both the gross and local structural discontinuities and the thermal effects which vary during the cycle. (*The subscripts t, l and r represent the tangential, longitudinal and radial directions, respectively.*)

(b) Choose a point in time when the conditions are one of the extremes for the cycle (either maximum or minimum, algebraically) and identify the stress components at this time by the subscript i. In most cases, it will be possible to choose at least one time during the cycle when the conditions are known to be extreme. In some cases it may be necessary to try different points in time to find the one which results in the largest value of alternating stress intensity.

(c) Subtract each of the six stress components σ_{it} , σ_{il} , σ_{ir} , τ_{itl} , τ_{ilr} , τ_{irt} from the corresponding stress components σ_t , σ_l , σ_r , τ_{tl} , τ_{lr} , τ_{rt} at each point in time during the cycle and call the resulting components σ'_t , σ'_l , σ'_r , τ'_{tl} , τ'_{lr} , τ'_{rt} .

(d) At each point in time during the cycle, calculate the principal stresses, σ'_1 , σ'_2 and σ'_3 , derived from the six stress components, σ'_t , σ'_l , σ'_r , τ'_{tl} , τ'_{lr} , τ'_{rt} . Note that the directions of the principal stresses may change during the cycle but the principal stress retains its identity as it rotates.

(e) Determine the stress differences $S'_{12} = \sigma'_1 - \sigma'_2$, $S'_{23} = \sigma'_2 - \sigma'_3$ and $S'_{31} = \sigma'_3 - \sigma'_1$ versus time for the complete cycle and find the largest absolute magnitude of any stress difference at any tie. The alternating stress intensity, S_{alt} , is one-half of this magnitude.



modify the final step (e) of the approach to compute an equivalent stress amplitude based on the von Mises criterion and compute that quantity for the same load history.

solution The difficult step for implementing the procedure shown in Table 5.5 is step b, selecting the critical time in the load history. In this example, either $t = 0$ ($\sigma_{xi} = 0$ and $\tau_{xyi} = 0$) or $t = 21.5$ min ($\sigma_{xi} = 11.54$ ksi and $\tau_{xyi} = 44$ ksi) give identical results. The Tresca-based equivalent stress amplitude is given by

$$\text{SALT} = 44.38 \text{ ksi}$$

Step e in the procedure can be modified to define a von Mises equivalent stress amplitude:

$$\text{SEQA} = \frac{1}{\sqrt{2}} \sqrt{(\sigma_1' - \sigma_2')^2 + (\sigma_2' - \sigma_3')^2 + (\sigma_3' - \sigma_1')^2}$$

This results in

$$\text{SEQA} = 38.54 \text{ ksi}$$

Although the ASME approach demonstrated in Example 12 is straightforward in its implementation, it has the potential to make very nonconservative life estimates for long loading histories. In fact, predictions made by the approach have been shown to be nonconservative, even for relatively simple constant-amplitude, out-of-phase bending, and torsional loading.^{87,88} Active research in multiaxial fatigue-life prediction is still underway to address practical design concerns such as notches⁸⁹ and variable-amplitude loading.^{90,91}

REFERENCES

1. Shigley, J. E. and C. R. Mischke: "Mechanical Engineering Design," 5th ed., McGraw-Hill Book Company, New York, 1989.
2. Spotts, M. F.: "Design of Machine Elements," 6th ed., Prentice-Hall, Englewood Cliffs, N.J., 1985.
3. Juvinall, R. C.: "Fundamentals of Machine Component Design," John Wiley and Sons, New York, 1983.
4. Slocum, A. H.: "Precision Machine Design," Prentice-Hall, Englewood Cliffs, N.J., 1992.

5. Timoshenko, S. P., and J. N. Goodier: "Theory of Elasticity," 3d ed., McGraw-Hill Book Company, New York, 1970.
6. Boresi, A. P., and O. M. Sidebottom: "Advanced Mechanics of Materials," 4th ed., John Wiley and Sons, New York, 1985.
7. Landgraf, R. W., and R. A. Chernenkoff: "Residual Stress Effects on Fatigue of Surface Processed Steels," "Analytical and Experimental Methods for Residual Stress Effects in Fatigue," ASTM STP 1004, ASTM, Philadelphia, 1986.
8. Fung, Y. C.: "A First Course in Continuum Mechanics," 2d ed., Prentice-Hall, Englewood Cliffs, N.J., 1977.
9. Hertzberg, R. W.: "Deformation and Fracture Mechanics of Engineering Materials," 3d ed., John Wiley and Sons, New York, 1989.
10. Dieter, G. E.: "Mechanical Metallurgy," 3d ed., McGraw-Hill Book Company, New York, 1986.
11. Beer, F. P., and E. R. Johnson: "Mechanics of Materials," 2d ed., McGraw-Hill Book Company, New York, 1992.
12. Collins, J. A.: "Failure of Materials in Mechanical Design," John Wiley and Sons, New York, 1981.
13. Dowling, N. E.: "Mechanical Behavior of Materials," Prentice-Hall, Englewood Cliffs, N.J., 1993.
14. A. S. Cobayashi (ed.): "Manual on Experimental Stress Analysis," Prentice-Hall, Englewood Cliffs, N.J., 1987.
15. Dally, J. W., and W. F. Riley: "Experimental Stress Analysis," 3d ed., McGraw-Hill Book Company, New York, 1991.
16. Peterson, R. E.: "Stress Concentration Factors," John Wiley and Sons, New York, 1974.
17. Young, Y. C.: "Roark's Formulas for Stress and Strain," 6th ed., McGraw-Hill Book Company, New York, 1989.
18. Zienkiewicz, O. C.: "The Finite Element Method," 3d ed., McGraw-Hill Book Company, New York, 1987.
19. Cook, R. D., D. S. Malkus, and M. E. Plesha: "Concepts and Applications of Finite Element Analysis," 3d ed., John Wiley and Sons, New York, 1989.
20. Reddy, J. W.: "An Introduction to the Finite Element Method," McGraw-Hill Book Company, New York, 1984.
21. Bickford, W. B.: "A First Course in the Finite Element Analysis," Richard D. Irwin, Homewood, Ill., 1988.
22. Sorem, J. R., Jr., and S. M. Tipton: "The Use of Finite Element Codes for Cyclic Stress-Strain Analysis," "Fatigue Design," European Structural Integrity Society, vol. 16, J. Solin, G. Marquis, A. Siljander and S. Sipilä, eds., Mechanical Engineering Publications, London, 1993, pp. 187–200.
23. "Fatigue Design Handbook," Society of Automotive Engineers, Warrendale, Pa., 1990.
24. Tipton, S. M., and G. J. Shoup: "The Effect of Proof Loading on the Fatigue Behavior of Open Link Chain," *Trans. ASME, J. Fatigue and Fracture Eng. Mat. Technol.*, vol. 114, no. 1, pp. 27–33, January 1992.
25. Shoup, G. J., S. M. Tipton, and J. R. Sorem: "The Effect of Proof Loading on the Fatigue Behavior of Studded Chain," *Int. J. Fatigue*, vol. 14, no. 1, pp. 35–40, January 1992.
26. Tipton, S. M., and J. R. Sorem: "A Reversed Plasticity Criterion for Specifying Optimal Proof Load Levels," "Advances in Fatigue Lifetime Predictive Techniques," vol. 2, ASTM STP 1211, M. R. Mitchell and R. W. Landgraf, eds., American Society for Testing and Materials STP, Philadelphia, 1993, pp. 186–202.
27. "Standard Test Methods of Tension Testing of Metallic Materials," Specification E-8, American Society for Testing and Materials, Philadelphia.
28. Ramberg, W., and W. Osgood: "Description of Stress-Strain Curves by Three Parameters," NACA TN 902, 1943.

29. "Tensile Strain-Hardening Exponents (n -Values) of Metallic Sheet Materials," Specification E-646, American Society for Testing and Materials, Philadelphia.
30. "Standard Test Methods of Compression Testing of Metallic Materials at Room Temperature," Specification E-9, American Society for Testing and Materials, Philadelphia.
31. Fuchs, H. O., and R. I. Stephens: "Metal Fatigue in Engineering," John Wiley and Sons, New York, 1980.
32. Bannantine, J. A., J. J. Comer, and J. H. Handrock: "Fundamentals of Metal Fatigue Analysis," Prentice-Hall, Englewood Cliffs, N.J., 1990.
33. "Standard Practice for Conducting Constant Amplitude Axial Stress-Life Tests of Metallic Materials," Specification E-466, American Society for Testing and Materials, Philadelphia.
34. "Standard Practice for Statistical Analysis of Linear or Linearized Stress-Life (S - N) and Strain Life (ϵ - N) Fatigue Data," Specification E-739, American Society for Testing and Materials, Philadelphia.
35. "Standard Practice for Presentation of Constant Amplitude Fatigue Test Results for Metallic Materials," Specification E-468, American Society for Testing and Materials, Philadelphia.
36. Smith, K. N., P. Watson, and T. H. Topper: "A Stress-Strain Function for the Fatigue of Metals," *J. Materials*, vol. 5, no. 4, pp. 767–778, December 1970.
37. Sines, G.: "Failure of Metals under Combined Repeated Stresses with Superimposed Static Stresses," NACA Tech. Note 3495, 1955.
38. "MIL Handbook 5," Department of Defense, Washington, D.C.
39. Grover, H. J.: "Fatigue of Aircraft Structures," NAVAIR 01-1A-13, 1966.
40. "Standard Recommended Practice for Constant-Amplitude Low-Cycle Fatigue Testing," Specification E-606, American Society for Testing and Materials, Philadelphia.
41. Martin, J. F.: "Cyclic Stress-Strain Behavior and Fatigue Resistance of Two Structural Steels," Fracture Control Program Report No. 9, University of Illinois at Urbana-Champaign, 1973.
42. Massing, G.: "Eigenspannungen und Verfestigung beim Messing (Residual Stress and Strain Hardening of Brass)," *Proc. Second International Congress for Applied Mechanics*, Zurich, September 1926.
43. Basquin, O. H.: "The Exponential Law of Endurance Tests," *American Society for Testing and Materials Proceedings*, vol. 10, pp. 625–630, 1910.
44. Manson, S. S.: "Behavior of Materials under Conditions of Thermal Stress," *Heat Transfer Symposium*, University of Michigan Engineering Research Institute, pp. 9–75, 1953 (also published as NACA TN 2933, 1953).
45. Coffin, L. F.: "A Study of the Effects of Thermal Stresses on a Ductile Metal," *Trans. ASME*, vol. 76, pp. 931–950, 1954.
46. Mitchell, M. R.: "Fundamentals of Modern Fatigue Analysis for Design," "Fatigue and Microstructure," Society of Automotive Engineers, pp. 385–437, 1977.
47. Socie, D. F.: "Fatigue Life Prediction Using Local Stress-Strain Concepts," *Experimental Mechanics*, vol. 17, no. 2, 1977.
48. Socie, D. F.: "Fatigue Life Estimation Techniques," Electro General Corporation Technical Report 145A-579, Minnetonka, Minn.
49. Socie, D. F., N. E. Dowling, and P. Kurath: "Fatigue Life Estimation of a Notched Member," ASTM STP 833, *Fracture Mechanics; Fifteenth Symposium*, R. J. Sanford, ed., American Society for Testing and Materials, Philadelphia, 1984, pp. 274–289.
50. Sehitoglu, H.: "Fatigue of Low Carbon Steels as Influenced by Repeated Strain Aging," Fracture Control Program Report No. 40, University of Illinois at Urbana-Champaign, June 1981.
51. Kurath, P.: "Investigation into a Non-arbitrary Fatigue Crack Size Concept," Theoretical and Applied Mechanics, Report No. 429, University of Illinois at Urbana-Champaign, October 1978.
52. "Technical Report on Fatigue Properties—SAE J1099," SAE Informational Report, Society of Automotive Engineers, Warrendale, Pa., 1975.

53. Boller, C., and T. Seeger: "Materials Data for Cyclic Loading," Parts A to E, Elsevier Science Publishers B. V., 1987.
54. Boardman, B. E.: "Crack Initiation Fatigue—Data, Analysis, Trends, and Estimations," SAE Technical Paper 820682, 1982.
55. Manson, S. S.: "Fatigue: A Complex Subject—Some Simple Approximations," *Proc. Soc. Experimental Stress Analysis*, vol. 12, no. 2, 1965.
56. Muralidharan, U., and S. S. Manson: "A Modified Universal Slopes Equation for Estimation of Fatigue Characteristics of Metals," *Trans. ASME, J. Eng. Mat. Technol.*, vol. 110, pp. 55–58, January 1988.
57. Socie, D. F., M. R. Mitchell, and E. M. Caulfield: "Fundamentals of Modern Fatigue Analysis," Fracture Control Program Report No. 26, University of Illinois at Urbana-Champaign, 1977.
58. Ong, J. H.: "An Evaluation of Existing Methods for the Prediction of Axial Fatigue Life from Tensile Data," *Int. J. Fatigue*, vol. 15, no. 1, pp. 13–19, 1993.
59. Neuber, H.: "Theory of Stress Concentration for Shear Strained Prismatical Bodies with Arbitrary Stress-Strain Law," *Trans. ASME, J. Appl. Mech.*, vol. 12, pp. 544–550, 1961.
60. "Recommended Practices for Cycle Counting in Fatigue Analysis," Specification E-1049, American Society for Testing and Materials, Philadelphia.
61. Broek, D.: "Elementary Engineering Fracture Mechanics," 4th ed., Kluwer Academic Publishers, Dordrecht, The Netherlands, 1986.
62. Broek, D.: "The Practical Use of Fracture Mechanics," Kluwer Academic Publishers, Dordrecht, The Netherlands, 1988.
63. Barsom, J. M., and S. T. Rolfe: "Fracture and Fatigue Control in Structures," 2d ed., Prentice-Hall, Englewood Cliffs, N.J., 1987.
64. Anderson, T. L.: "Fracture Mechanics: Fundamentals and Applications," CRC Press, Boca Raton, Fla., 1991.
65. Ewalds, H. L., and R. J. H. Wanhill: "Fracture Mechanics," Edward Arnold Publishers, London, 1984.
66. Newman, J. C., Jr.: "A Review of Modelling Small-Crack Behavior and Fatigue Life Predictions for Aluminum Alloys," *Fatigue and Fracture Eng. Mat. Struct.*, vol. 17, no. 4, pp. 429–439, 1994.
67. Miller, K. J.: "Materials Science Perspective of Metal Fatigue Resistance," *Mat. Sci. Technol.*, vol. 9, no. 6, pp. 453–462, 1993.
68. Ahmad, H. Y., and J. R. Yates: "An Elastic-Plastic Model for Fatigue Crack Growth at Notches," *Fatigue and Fracture Eng. Mat. Struct.*, vol. 17, no. 4, pp. 439–447, 1994.
69. Y. Murakami (ed.): "Stress Intensity Factors Handbook," Pergamon Press, Oxford, 1987.
70. Rooke, D. P., and D. J. Cartwright: "Compendium of Stress Intensity Factors," Her Majesty's Stationery Office, London, 1976.
71. "Standard Test Method for Plane-Strain Fracture Toughness of Metallic Materials," Specification E-399, American Society for Testing and Materials, Philadelphia.
72. Tada, H., P. C. Paris, and G. R. Irwin: "The Stress Analysis of Cracks Handbook," 2d ed., Paris Productions, Inc., 226 Woodbourne Dr., St. Louis, Mo., 1985.
73. J. P. Gallagher (ed.): "Damage Tolerant Design Handbook." Metals and Ceramics Information Center, Battelle Columbus Laboratories, Columbus, Ohio, 1983.
74. "Aerospace Structural Metals Handbook," Metals and Ceramics Information Center, Battelle Columbus Laboratories, Columbus, Ohio, 1991.
75. Hudson, C. M., and S. K. Seward: "A Compendium of Sources of Fracture Toughness and Fatigue Crack Growth Rate Data for Metallic Alloys," *Int. J. Fracture*, vol. 14, pp. R151–R184, 1978.
76. Hudson, C. M., and S. K. Seward: "A Compendium of Sources of Fracture Toughness and Fatigue Crack Growth Data for Metallic Alloys—Part II," *Int. J. Fracture*, vol. 20, pp. R59–R117, 1982.

77. Hudson, C. M., and S. K. Seward: "A Compendium of Sources of Fracture Toughness and Fatigue Crack Growth Data for Metallic Alloys—Part III," *Int. J. Fracture*, vol. 39, pp. R43–R63, 1989.
78. Hudson, C. M., and J. J. Ferraino: "A Compendium of Sources of Fracture Toughness and Fatigue Crack Growth Data for Metallic Alloys—Part IV," *Int. J. Fracture*, vol. 48, no. 2, pp. R19–R43, March 1991.
79. Taylor, D.: "A Compendium of Fatigue Threshold and Growth Rates," EMAS, Great Britain, 1985.
80. "Data Book on Fatigue Growth Rates of Metallic Materials," JSMS, Japan, 1983.
81. Paris, P. C., and R. Erdogan: "A Critical Analysis of Crack Propagation Laws," *Trans. ASME, J. Basic Eng.*, vol. 85, p. 528, 1963.
82. "Standard Test Method for Measurement of Fatigue Crack Growth Rates," Specification E-647, American Society for Testing and Materials, Philadelphia.
83. Forman, R. G., V. E. Kearney, and R. M. Engle: "Numerical Analysis of Crack Propagation in Cyclic-Loaded Structures," *Trans. ASME, J. Basic Eng.*, ser. D., vol. 89, pp. 459–464, 1967.
84. Walker, K.: "The Effect of Stress Ratio during Crack Propagation and Fatigue for 2024-T3 and 7075-T6 Aluminum Alloy Specimens," NASA TN-D 5390, National Aeronautics and Space Administration, 1969.
85. Miller, K. J.: "Metal Fatigue—Past, Current and Future," *Proc. Institution of Mechanical Engineers*, vol. 205, 1991.
86. "ASME Boiler and Pressure Vessel Code," Sec. III, Div. I, Subsection NA, American Society of Mechanical Engineers, New York, 1974.
87. Tipton, S. M.: "Fatigue Behavior under Multiaxial Loading in the Presence of a Notch: Methodologies for the Prediction of Life to Crack Initiation and Life Spent in Crack Propagation," Ph.D. dissertation, Stanford University, Stanford, Calif., 1985.
88. Tipton, S. M., and D. V. Nelson: "Fatigue Life Predictions for a Notched Shaft in Combined Bending and Torsion," "Multiaxial Fatigue," ASTM STP 853, K. J. Miller and M. W. Brown, eds., American Society for Testing and Materials, Philadelphia, 1985, pp. 514–550.
89. Tipton, S. M., and D. V. Nelson: "Developments in Life Prediction of Notched Components Experiencing Multiaxial Fatigue," "Material Durability/Life Prediction Modelling," PVP-vol. 290, S. Y. Zamirk and G. R. Halford, eds., ASME, 1994, pp. 35–48.
90. Bannantine, J. A.: "A Variable Amplitude Multiaxial Fatigue Life Prediction Method," Ph.D. dissertation, The University of Illinois, Champaign, 1989.
91. Chu, C. C.: "Programming of a Multiaxial Stress-Strain Model for Fatigue Analysis," SAE Paper 920662, Society of Automotive Engineers, Warrendale, Pa., 1992.
92. "Failure Analysis and Prevention," "Metals Handbook," 8th ed., vol. 10, American Society for Metals, Metals Park, Ohio, 1978.

